T.C.
YEDİTEPE UNIVERSITY
INSTITUTE OF HEALTH SCIENCES
DEPARTMENT OF HISTOLOGY AND EMBRYOLOGY

EXPLORATION OF THE EFFECTS OF HYDROGEN SULFIDE ON STEROIDOGENESIS AND HISTOMORPHOLOGY IN THE DEHYDROEPIANDROSTERONE-INDUCED POLYCYSTIC OVARY SYNDROME RAT MODEL THROUGH HISTOLOGICAL AND BIOCHEMICAL METHODS

THE DOCTOR OF HISTOLOGY AND EMBRYOLOGY THESIS

AYSUN ÖZBAY ÖNAL

İSTANBUL-2024

APPROVAL

Institute: Yeditepe University Institute of Health Sciences

Programme: Doctoral Program in Histology and Embryology

Title of the Thesis: Exploration of the Effects of Hydrogen Sulfide on Steroidogenesis and Histomorphology in the Dehydroepiandrosterone-Induced Polycystic Ovary Syndrome Rat Model through Histological and Biochemical Methods

Owner of the Thesis : Aysun Özbay Önal

Examination Date: 20/02/2024

The Jury judges that the candidate named above has satisfactorily completed her thesis.

Supervisor:	Assoc. Prof. Alev Cumbul (Yeditepe University, Faculty of Medicine, Department of Histology and Embryology)
Member/Examiner:	Prof. Berrin Avcı (Bursa University, Faculty of Medicine, Department of Histology and Embryology)
Member/Examiner:	Prof. Rukset Attar (Yeditepe University, Faculty of Medicine, Department of Obstetrics and Gynecology)
Member/Examiner:	Assoc. Prof. Salime Pelin Ergüven (University of Health Sciences, Faculty of Medicine, Department of Histology and Embryology)
Member/Examiner:	Asst. Prof. Dr. Oya Alagöz (Yeditepe University, Faculty of Medicine, Department of Histology and Embryology)

APPROVAL

This thesis has been deemed by the jury in accordance with the relevant articles of Yeditepe University Graduate Education and Examinations Regulation and has been approved by Administrative Board of Institute with decision dated ..... and numbered .....

Prof. Dr. Bayram Yılmaz

Director of Institute of Health Sciences

DECLARATION

I hereby declare that this thesis is my own work and that, to the best of my knowledge and belief, it contains no material previously published or written by another person nor material which has been accepted for the award of any other degree except where due acknowledgement has been made in the text.

20/02/2024

Aysun Özbay Önal

DEDICATION

to challenging emotions and situations,

to not giving up,

to learning more…

to SERHAN…

ACKNOWLEDGEMENTS

To my esteemed mentor Prof. Dr. Berrin AVCI, whose vast knowledge and foresight have guided me academically and from whom I always felt the guiding hand on my shoulder. I am grateful for the valuable insights I gained and proud to have worked together.

To the esteemed faculty members of the Department of Histology and Embryology at Bursa Uludağ University Faculty of Medicine, who supported my education with patience and great dedication and whom I will always honor with respect.

To my dear mentor and thesis advisor Assoc. Prof. Dr. Alev CUMBUL, who instilled the love of science with her innovative style, supported my education and motivated me with her patient and tolerant attitude.

For the contributions throughout my education and the support provided, I express my gratitude to Prof. Dr. Aylin YABA UÇAR, the Head of the Department.

I thank Prof. Dr. Bayram YILMAZ, our institute secretary, esteemed Hasan KOÇ and Dr. Engin SÜMER with whom I greatly enjoyed working together, as well as the entire YÜDETAM team for their support and interest.

To my dear friend Dr. Cihan Süleyman ERDOĞAN, who answered all my questions and shared his extensive laboratory experiences with me, I express my happiness.

Assistant Prof. Dr. Kübra AÇIKALIN ÇOŞKUN, who graciously shared her scientific experience with me, I extend my sincere thanks.

To my beloved family, who has been with me in every circumstance throughout my life, providing both material and moral support and who played a crucial role in bringing me to where I am today, I express my heartfelt thanks.

To my dear husband, Op. Dr. Mustafa ÖNAL, I express my profound gratitude as someone who, throughout various phases of my life, particularly starting from my university years, has consistently encouraged me, stood by my side, and provided unwavering support in both good and bad times. Thanks to your strong shoulders and reassuring support, overcoming every challenge has become even more meaningful. Knowing that every moment we've shared has evolved into a more significant and powerful experience with your genuine kindness fills me with infinite happiness.

Lastly, I extend my infinite thanks to my son Serhan ÖNAL, whose love has embraced my heart since the moment I first learned of his existence and who continuously empowers me.

This work was has received support from a grant provided by the Scientific and Technological Research Council of Turkey (TUBITAK, Project number:222S748).

TABLE OF CONTENTS

LIST OF TABLES

LIST OF FIGURES

LIST OF SYMBOLS AND ABBREVIATIONS

PCOS: Polycystic Ovary Syndrome

H_2S: Hydrogen Sulfide

NO: Nitric Oxide

CO: Carbon Monoxide

NaHS: Sodium Hydrogen Sulfide

DHEA: Dehydroepiandrosterone

OMI: Oocyte Maturation Inhibitor

ZP: Zona Pellucida

ER: Endoplasmic Reticulum

hCG: Human Chorionic Gonadotropin

HPG: Hypothalamic-Pituitary-Gonadal Axis

KiSS1R: Kisspeptin Receptor

GnRH: Gonadotropin-releasing Hormone

FSH: Follicle-stimulating Hormone

LH: Luteinizing Hormone

StAR: Steroidogenic Acute Regulatory Protein

ATP: Adenosine Triphosphate

cAMP: Cyclic Adenosine Monophosphate

PKA: Protein Kinase A

CREB: cAMP Response Element Binding Protein

CYP17A1: 17-α-hydroxylase/17,20-lyase

3β-HSD: 3β-hydroxysteroid Dehydrogenase

CYP19A1: Aromatase

ESHRE: The European Society of Human Reproduction and Embryology

ASRM: The American Society for Reproductive Medicine

SHBG: Sex Hormone-binding Globulin

PCOM: Polycystic Ovarian Morphology

GDF-9: Growth Differentiation Factor-9

AMH: Anti-müllerian Hormone

TGF-β: Transforming Growth Factor-β

BMP: Bone Morphogenetic Proteins

IGFBP-1: Insulin-like Growth Factor-binding Protein-1

IGF-2: Insulin-like Growth Factor-2

VEGF: Vascular Endothelial Growth Factor

CSE, CTH: Cystathionine Gamma-lyase

CBS: Cystathionine Beta-synthase

3-MST: 3-Mercaptopyruvate Sulfurtransferase

CAT: Cysteine Aminotransferase

Trx: Thioredoxin

MTO: Methanethiol Oxidase

CARS2: Cysteinyl-tRNA Synthetase-2

Cysteine-SSH: Cysteine Persulfide

S2O3-2: Thiosulfate

TST: Thiosulfate Sulfurtransferase

SO_3^{-2}: Sulfite

SO_4^{-2}: Sulfate

H^+: Hydrogen Ion

HS^-: Hydrogen Sulfide Ion

Na_2S: Sodium Sulfide

DATS: Diallyl Trisulfide

NRF-2: Transcription Factor Nuclear Erythroid 2-related Factor-2

GV: Germinal Vesicle

MI: Metaphase-I

MII: Metaphase-II

qRT-PCR: Quantitative Real Time Polymerase Chain Reaction

E_2: Estradiol

H&E: Hematoxylin&Eosin

PBS: Phosphate Buffer Saline

PAS: Periodic Acid-Schiff

ART: Assisted Reproductive Technology

AREG: Amphiregulin

EREG: Epiregulin

PLAT: Plasminogen Activator

MMP: Matrix Metalloproteinase

TNF-α: Tumor Necrosis Factor-alpha

IL-1β: Interleukin-1Beta

NF-κB: Nuclear Factor KappaB

ABSTRACT

Özbay Önal, A. (2024). Investigation of the Effect of Hydrogen Sulfide on Steroidogenesis and Histomorphology in Dehydroepiandrosterone-Induced Polycystic Ovary Syndrome Rat Model with Histological and Biochemical Methods, Yeditepe University, Institute of Health Sciences, Department of Histology and Embryology, PhD thesis, İstanbul.

Polycystic ovary syndrome is a disease that affects the reproductive, endocrine and metabolic systems. Hydrogen Sulfide is an endogenous gas that possesses intracellular signaling, angiogenesis, vasodilation, anti-inflammatory responses, antioxidant activities and anti-apoptotic processes. Our study is designed to investigate the effect of the H_2S donor NaHS on anovulatory infertility, impaired follicular development and disrupted steroidogenesis mechanisms induced by DHEA. Thirty adult female rats were categorized into five groups: control, vehicle, PCOS, NaHS and PCOS+NaHS, respectively. The control group underwent no interventions. The vehicle group received a subcutaneous mixture of 0.01 ml 95% ethanol and 0.09 ml sesame oil. The PCOS model was created with subcutaneously administration of DHEA at a dose of 6 mg/100 g body weight. NaHS was administered intraperitoneally with a dose of 200 μg/kg/day. DHEA resulted in elevated serum E_2 and serum progesterone levels, disturbance in the estrus cycle, a decrease in primordial, primary, Graafian follicle and corpus luteum numbers and an increase in secondary, cystic and atretic follicle numbers. It also increased apoptosis in follicles in parallel with the increase in atretic follicle numbers. DHEA has led to an increase in the protein and mRNA expressions of StAR, 3β-HSD and CYP19A1, while causing a decrease in the protein and mRNA expressions of CBS and CTH. The localization of CBS and CTH proteins in granulosa cells and oocytes has been identified. NaHS has reversed the disrupted estrus cycle, follicular damage and apoptosis induced by DHEA. It has reduced the increased expressions of StAR, 3β-HSD and CYP19A1 at both protein and mRNA levels and increased the decreased expressions of CBS and CTH at both protein and mRNA levels. In our study, we believe that NaHS reinstates the hormonal balance, prevents ovarian damage and corrects disorders in steroidogenesis.

Key words: Hydrogen Sulfide, steroidogenesis, PCOS, rat

The study was supported by TUBITAK, Project No. 222S748.

ÖZET

Özbay Önal, A. (2024). Dehidroepiandrosteron ile İndüklenen Polikistik Over Sendromu Sıçan Modelinde Hidrojen Sülfid'in Steroidogenez ve Histomorfoloji Üzerine Etkisinin Histolojik ve Biyokimyasal Yöntemler ile Araştırılması, Yeditepe Üniversitesi, Sağlık Bilimleri Enstitüsü, Histoloji ve Anabilim Dalı, Doktora Tezi, İstanbul.

Polikistik over sendromu, üreme, endokrin, metabolik sistemleri etkileyen bir hastalıktır. Hidrojen Sülfid, hücre içi sinyal iletimi, anjiyogenez, vazodilatasyon, anti-inflamatuar yanıtlar, anti-oksidan ve anti-apoptotik fonksiyonlara sahip endojen bir gazdır. Çalışmamız, DHEA tarafından tetiklenen anovulatuvar infertilite, bozulmuş foliküler gelişim ve bozulmuş steroidogenez mekanizmaları üzerinde H_2S donörü NaHS'ün etkisini araştırmak için tasarlanmıştır. 30 adet yetişkin dişi sıçan; kontrol, çözgen, PCOS, NaHS ve PCOS+NaHS şeklinde 5 gruba ayrılmıştır. Kontrol grubuna herhangi bir işlem uygulanmamıştır. Çözgen grubuna 0.01 ml %95 etanol ve 0.09 ml susam yağı karışımı subkutan olarak verilmiştir. PCOS modeli, 6 mg/100 g vücut ağırlığı dozunda subkutan DHEA uygulamasıyla oluşturulmuştur. NaHS, 200 µg/kg/gün dozunda intraperitoneal olarak uygulanmıştır. DHEA, serum E_2 ve progesteron seviyelerinde artışa, östrus siklusunda bozulmaya, primordiyal, primer, Graaf folikül ve korpus luteum sayısında azalmaya, sekonder, kistik ve atretik folikül sayısında artışa neden olmuştur. Aynı zamanda atretik folikül sayısındaki artışa paralel olarak folikülerde apoptozu artırmıştır. DHEA, StAR, 3β-HSD ve CYP19A1 protein ve mRNA ekspresyonlarında artışa, CBS ve CTH protein ve mRNA ekspresyonlarında azalmaya yol açmıştır. CBS ve CTH proteinlerinin granüloza hücreleri ve oositlerin sitoplazmalarında lokalize olduğu belirlenmiştir. NaHS, DHEA kaynaklı bozulan östrus siklusunu, foliküler hasarı ve apoptozu tersine çevirmiştir. Artan StAR, 3β-HSD ve CYP19A1 protein ve mRNA ekspresyonlarını düşürmüş ve azalan CBS ve CTH protein ve mRNA ekspresyonlarını artırmıştır. Çalışmamızda NaHS'ün over fonksiyonlarını düzenleyen hormonal dengeyi yeniden kurduğunu, over hasarını önlediğini ve steroidogenez bozukluğunu düzelttiğini düşünüyoruz.

Anahtar kelimeler: Hidrojen Sülfid, steroidogenez, PCOS, sıçan

Bu çalışma TÜBİTAK tarafından desteklenmiştir. Proje no: 222S748.

1. INTRODUCTION AND PURPOSE

Polycystic Ovary Syndrome (PCOS) is an endocrine disorder, and in women with this condition, follicular growth halts at the early antral stage. Anovulation or a low ovulation rate is observed in PCOS, leading to an increase pregnancy loss in the early stages and contributing to fertility. In this condition, elevated androgen levels create a positive feedback effect on LH secretion and a negative feedback effect on FSH secretion. The increase in LH levels leads to hyperplasia in the stroma and theca cells. Androgen production in the ovary increases, sustaining chronic anovulation. Disruption occurs in folliculogenesis due to the adverse effects on various factors involved in follicle growth, influenced by androgens and other factors. Follicles experience arrest as dominant follicle development is impaired, resulting in ovulation disorders [1].

Gasotransmitters are endogenously produced intracellular signaling molecules. Gasotransmitters directly bind to their targets within the cell and exert their effects through protein synthesis. Hydrogen sulfide (H_2S), much like nitric oxide (NO) and carbon monoxide (CO), is another gasotransmitter [2]. H_2S is a colorless gas. H_2S smells like rotten eggs. The active production of this gas molecule by mammalian cells suggests its physiological significance. H_2S has a low molecular weight. It doesn't require a specific carrier to pass through the cell membrane. H_2S exhibits various effects in physiological and pathological conditions in the central nervous system, urinary, respiratory, cardiovascular, and digestive systems [3,4,5].

We formulated the hypothesis of our study as follows: ''In experimentally induced PCOS, Sodium Hydrogen Sulfide (NaHS) has a safeguarding effect on anovulatory infertility, impaired follicular development, and disrupted steroidogenesis''. In order to test this hypothesis in the thesis, the impact of this approach on the ovaries of rodent with experimentally induced PCOS using dehydroepiandrosterone (DHEA) were investigated histologically, immunohistochemically, and biochemically. The aim was to explore the potential impact of the H_2S donor NaHS on the mechanisms of possible damage.

2. LITERATURE REVIEW

2.1. The Female Reproductive System

The ovaries, fallopian tubes, uterus, cervix, vagina, and external genital organs are components of the female reproductive system. In the female reproductive system, oocytes are produced in the ovaries, and these produced oocytes are transported to the fallopian tubes. If they encounter sperm, the oocyte is fertilized in the fallopian tube. All these events occur under the responsibility of this system [6].

2.1.1. Embryology of the Ovaries

Germ cells originating from the epiblast layer emigrate along the primitive streak. By the third week, they settle among the endoderm cells near the wall of the yolk sac allantois. By the fourth week they progress along the dorsal aspect of the mesentery of the hindgut. At the 5th week, primordial germ cells reach the primitive gonads, and then, by the 6th week, they invade the genital ridges. If these cells don't reach the genital ridges the gonads can't develop. As primordial germ cells reach the primitive gonads the epithelial cells on the genital ridges proliferate and embed themselves into the underlying mesenchyme forming primitive sex cords. In female embryos with XX sex chromosomes primitive sex cords in the form of irregular cell clusters develop. These cell clusters contain primitive germ cell groups and are predominantly situated in the medulla of the ovary. Subsequently cell clusters disappear making way for vascular stroma (ovarian medulla). The surface epithelium of the female gonad proliferates, and by the 7th week, secondary germ cords develop. Cortical cords are embedded into the underlying mesenchyme in close proximity to the surface. In the third month, secondary germ cords separate into cell clusters and undergo proliferation. They enclose each oogonium with a layer of epithelial cells. Oogonia and the adjacent epithelial cells constitute the primordial follicle [7].

2.1.2. The Ovaries Anatomy

The ovaries are anatomically situated in the ovarian fossa on the lateral wall of the pelvis. The fossa ovarica lies amid the external iliac artery and the internal iliac artery. The ovaries are connected to the back surface of the broad ligament through the mesovarium which is a peritoneal fold. The suspensory ligament attaches the ovary to the pelvis. The blood vessels and nerves of the ovary are carried by the suspensory

ligament. The ovarian ligament connects the ovary to the uterus. The developing gonad is attached to the base of the pelvis through the ovarian ligament. This ligament is a remnant of the gubernaculum from the embryonic period (Figure 1) [8].

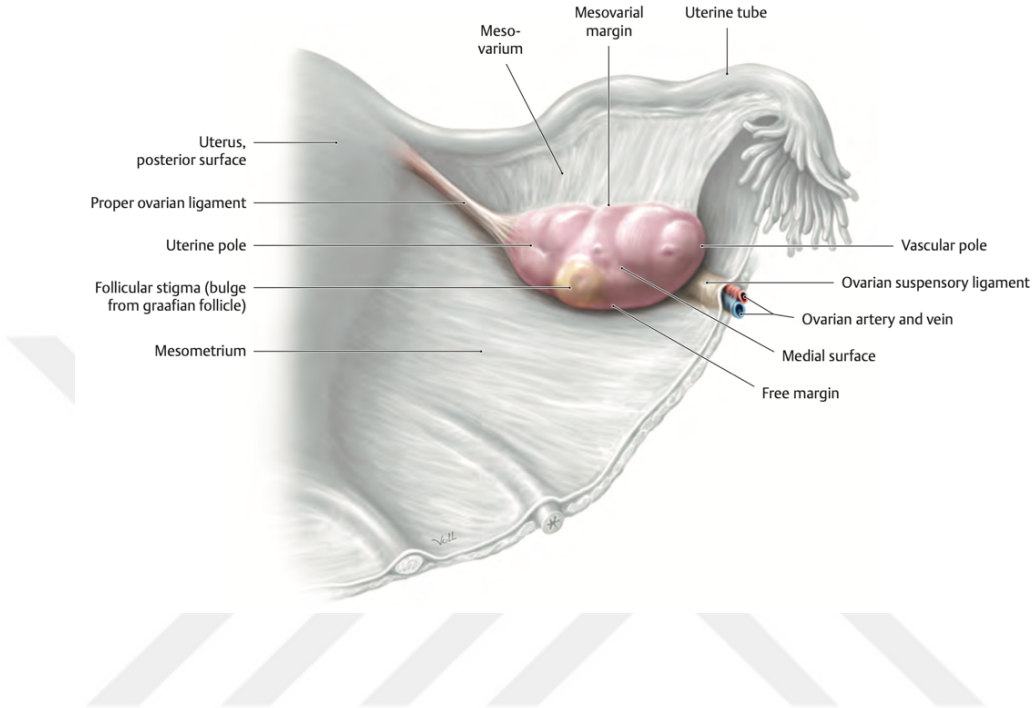

Figure 1. The anatomy of the ovaries [8].

2.1.3. Histology of the Ovaries

The exterior of the ovaries is lined with a single layer of cuboidal or simple squamous epithelium. This epithelium is referred to as the germinal epithelium. Just below the epithelium, the tunica albuginea is located. This structure is an irregular dense connective tissue. Histologically the ovaries can be distinguished into the cortex and medulla although the boundary between them is not well-defined. The medulla portion is situated at the center of the ovary. In the structure of the medulla, blood vessels, nerves, and lymph vessels are present within loose connective tissue. Surrounding the medulla, the cortex is located at the outer edge of the ovary. In the cortex, ovarian follicles at various maturation stages are found within a dense connective tissue stroma. Each follicle contains a single oocyte. Smooth muscle cells are dispersed in the stroma surrounding the follicle (Figure 2) [9,10].

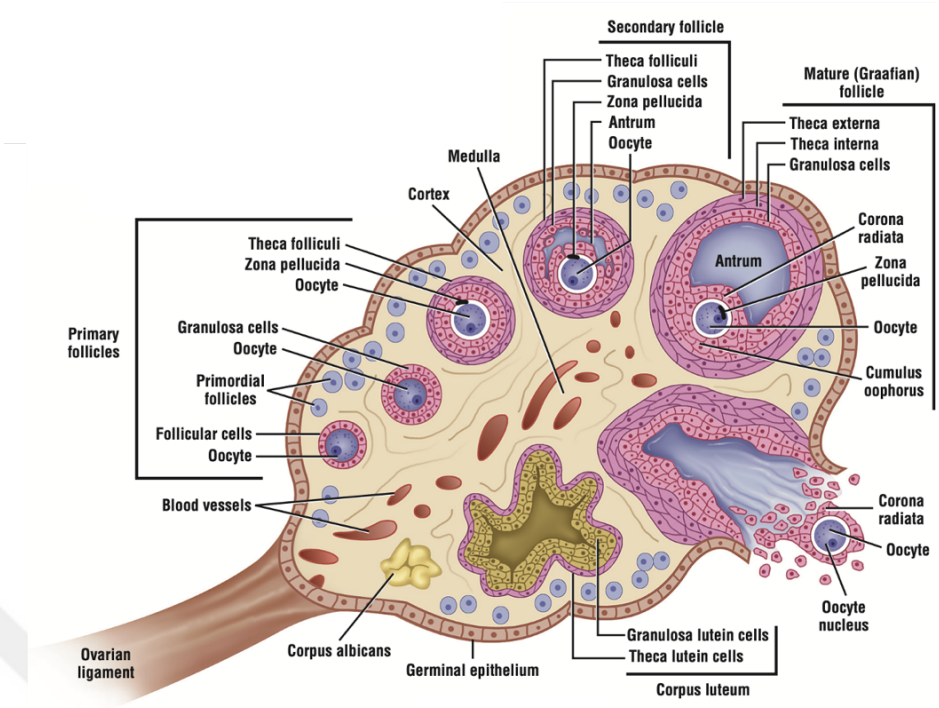

Figure 2. The general structure of the ovary [10].

Among the functions of the ovaries are the generation of mature oocytes developmentally (gametogenesis) and the synthesis of steroid hormones such as estrogen and progesterone (steroidogenesis). The generation of female gametes is termed oogenesis, with developing gametes referred to as oocytes and fully developed gametes as ovum. The estrogens secreted by the ovaries are responsible for the development of genital organs, the maturation of secondary sexual characteristics during puberty, and also have an impact on breast tissues. They stimulate ductal and stromal growth, support mammary development by fostering the accumulation of adipose tissue. Progesterone, conversely, prepares the uterus for a potential pregnancy. It also readies the mammary glands for lactation by supporting lobular proliferation [9].

2.1.4. Oogenesis

Oogenesis is a process in which oocyte formation takes place. This process relies on numerous interactions amid the developing oocyte, the granulosa cells surrounding the oocyte, and the cumulus cells. Oogenesis begins around the 12th week of fetal development. Upon reaching a female gonad, primordial germ cells transform into oogonia. Oogonia pass on successive mitotic cell divisions, and from 3rd month

onwards, the initial meiotic division begins in some oogonia. However, meiosis halts at the prophase stage without progressing, and oogonia transform into primary oocytes. As mitotic divisions continue, the amount of primary oocytes gets to seven million by the 5th month. Simultaneously, cell death begins, leading to the atresia of numerous oogonia and primary oocytes. Primary oocytes awaiting in the prophase stage of meiosis I, along with surrounding flattened follicular cells, form the primordial follicle. Primary oocytes don't complete their first meiotic divisions until puberty. They pause during the diplotene stage of prophase of the 1st meiotic division and remain quiescent in this state until the periovulatory phase. During this process, the maturation of the oocyte is suppressed by the oocyte maturation inhibitor (OMI) put out by the follicular cells. It is estimated that at birth, there are around 1 million primary oocytes in the ovaries, decreasing to 400.000 by the initiation of puberty. This number further decreases to 40.000 at the beginning of puberty. Throughout the reproductive period, about 500 oocytes mature and are expelled from the ovary through ovulation. The first meiotic division, which was paused in the diplotene stage during puberty, is completed immediately preceding ovulation. The primary oocyte, awaiting in the prophase stage, progresses towards the metaphase stage. During the completion of the first meiotic division, each resulting daughter cell has an equal number of chromosomes. However, cytoplasmic division doesn't occur equally. As the cell, which takes up the majority of the cytoplasm, forms the secondary oocyte, the cell with less cytoplasm transforms into a polar body. The resulting secondary oocyte enters the second meiotic division and pauses in the metaphase stage immediately preceding ovulation. If fertilization take place, the secondary oocyte goes through the second meiotic division. This results in the creation of a maternal pronucleus with 23 chromosomes and a second polar body. However, the second polar body isn't developmentally capable and undergoes apoptosis [7].

2.1.5. Folliculogenesis

The functional structures of female reproduction are the follicles in the ovary. Folliculogenesis supports not just oogenesis but also initiates the synthesis of hormones for female sexual characteristics and early pregnancy. The evolution phases of follicles are classified as primordial, primary (unilaminar and multilaminar), secondary, and Graafian follicle stages.

2.1.5.1. Primordial Follicle

Folliculogenesis kicks off with the formation of primordial follicles. In primordial follicles, there are single-layered flat follicle cells surrounding the primary oocyte. The outer surface of the follicular cells surrounding the primary oocyte is delimited by the basal lamina. Primordial follicles situated in the cortex layer of the ovary are just beneath the tunica albuginea. The diameter of the primary oocyte within the primordial follicle is approximately 30 µm. It contains a structure called the Balbiani body in the cytoplasm, which is composed of mitochondria, lysosomes, endoplasmic reticulum, Golgi membranes and vesicles (Figure 3) [9].

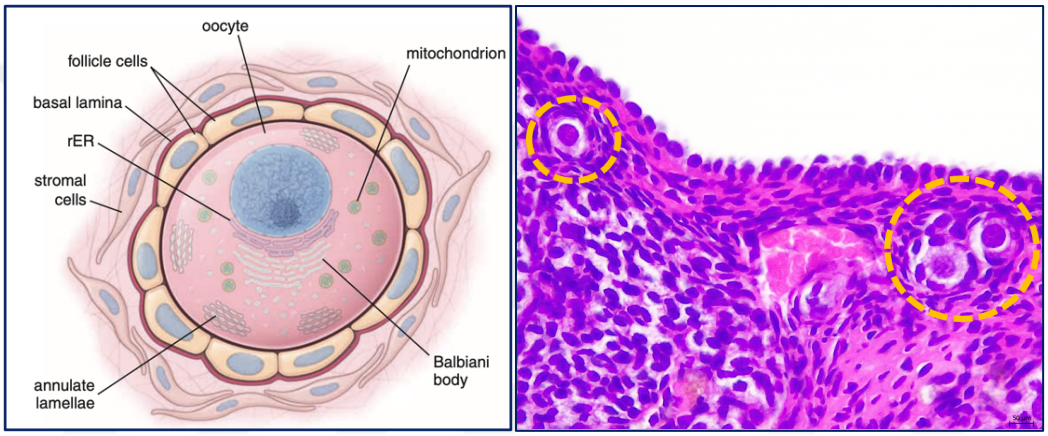

Figure 3. The Structure of the Primordial Follicle [9]. Yellow dashed circle: primordial follicle. The scale bar represents 50 µm for x40 magnification.

2.1.5.2. Primary Follicle

The primary oocyte in the primordial follicle grows, and the follicular cells proliferate. When the follicular cells transition from a flat to a cuboidal form, this follicle is now referred to as a primary follicle. As the oocyte continues to develop, specific proteins are secreted from the oocyte. These proteins (ZP-1, ZP-2, and ZP-3) come together to form the structure of the zona pellucida, situated amid the oocyte and follicular cells. The function of ZP-3 as a sperm-binding receptor and initiator of the acrosome reaction makes it distinctive. Primary follicles are of 2 types. It is termed a unilaminar primary follicle when the primary oocyte is enveloped by a sole layer of cuboidal follicular cells. Cuboidal follicular cells in the cubic form undergo mitosis to become multilayered, forming the membrana granulosa (stratum granulosum) layer. The follicle surrounded by multilayered cuboidal cells is called a multilaminar primary

follicle. The multilayered follicular cells are now defined as granulosa cells. As the granulosa cells multiply, the stromal cells around the follicle give rise to the theca folliculi. Theca folliculi gives rise to the theca interna and theca externa layers. Theca interna is the inner layer facing the granulosa cells. This layer consists of cuboidal secretory cells and is highly vascularized. Having LH receptors enables its involvement in androgen synthesis. Besides secretory cells, fibroblasts and collagen fibrils are present. It possesses a well-developed vascular network, similar to endocrine organs. A basal lamina is found amidst the theca interna and granulosa layers. This establishes a boundary between the two layers. Thus, the avascular granulosa layer and the rich capillary bed of the theca interna are separated from each other. In the theca externa, bundles of collagen fibers, smooth muscle cells are found (Figure 4) [9].

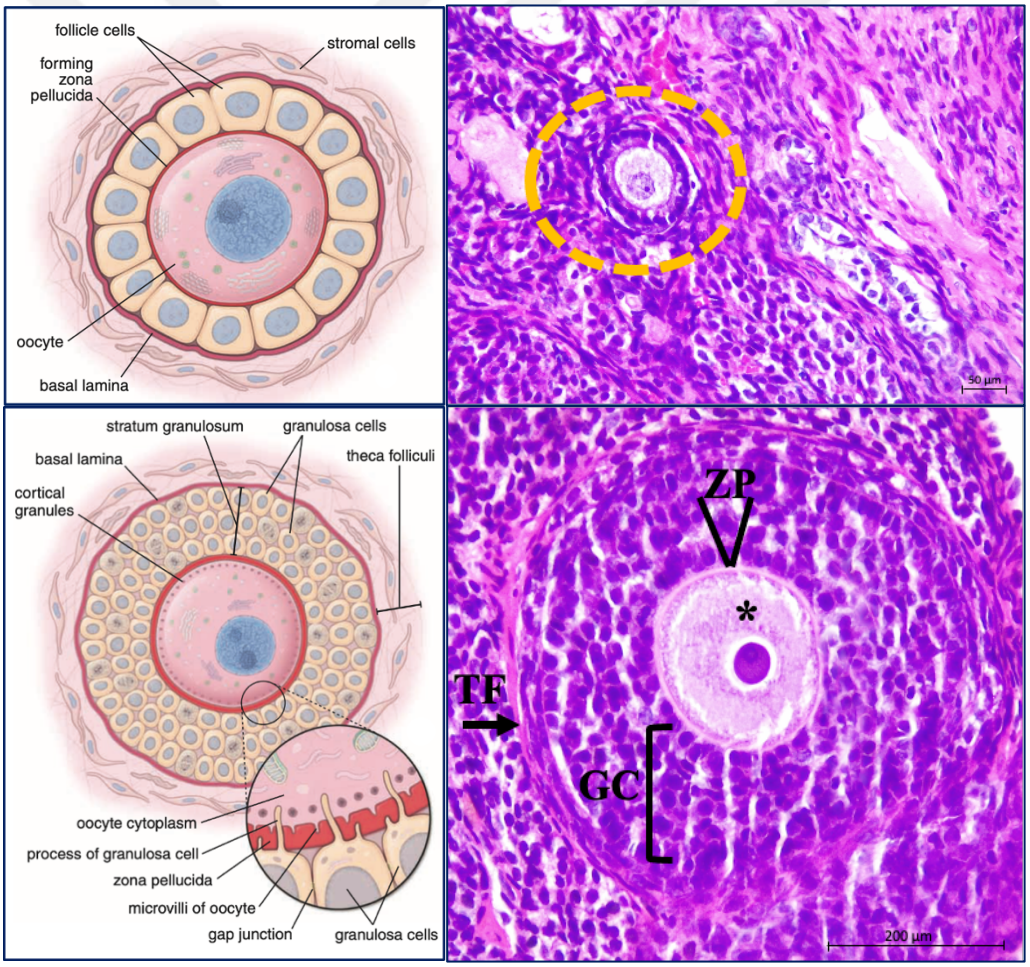

Figure 4. The Structure of Primary Follicles [9]. Yellow dashed circle: unilaminar primary follicle, ZP: zona pellucida, GC: granulosa cells, TF: theca folliculi, *: oocyte. The scale bar represents 200 µm for x10 and 50 µm for x40 magnification.

2.1.5.3. Secondary Follicle

When the stratum granulosum becomes a layer of 6-12 rows of cells, cavities start to form among the granulosa cells. These cavities fill with a fluid rich in hyaluronic acid, called follicular liquor, secreted by the granulosa cells. The merging of these cavities results in a single space known as the antrum. The follicle is termed as a secondary follicle or antral follicle. When the diameter of the oocyte reaches 125 µm, the growth of the oocyte is inhibited by the secretion of Oocyte Maturation Inhibitor (OMI) into the antral fluid by granulosa cells. OMI concentration are diminished in mature follicles but elevated in small-sized follicles (Figure 5) [9].

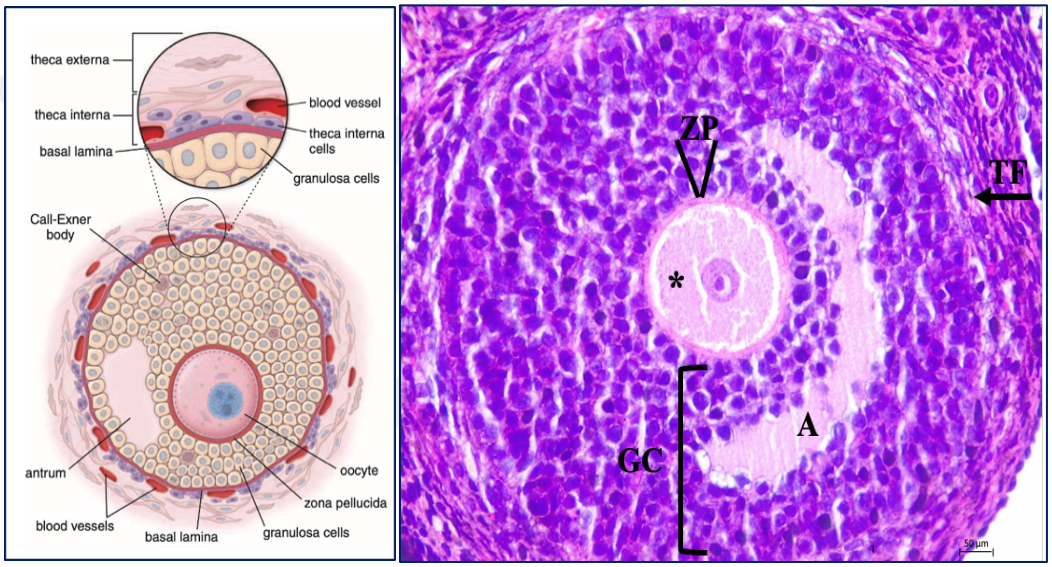

Figure 5. The Structure of the Secondary Follicle [9]. ZP: zona pellucida, GC: granulosa cells, TF: theca folliculi, *: oocyte, A: antrum. The scale bar represents 50 µm for x40 magnification.

2.1.5.4. Graafian (Mature) Follicle

As the diameter of the secondary follicle increases, expansion is observed in the antrum as well. The granulosa cells around the oocyte are cumulus oophorus, forming a mound towards the antrum. The cumulus oophorus cells encircling the oocyte, which are expelled with the oocyte during ovulation, are called the corona radiata. Due to the large size of the follicle, there is swelling on the surface of the ovary. When the follicle attains its full size, cut down in mitotic events of the granulosa cells is observed. While the size of the antrum increases, on the other hand stratum granulosum layer becomes

thinner. In preparation for ovulation, the connections among the oocyte, cumulus cells, the granulosa cells loosen. At this stage, the cytoplasm of teka interna cells is filled with lipid droplets. Theca interna cells are stimulated by LH to release androgens. Granulosa cells demonstrate an effect in transforming androgens into estrogens in response to FSH. Following a sudden increase in LH, the LH receptors on granulosa cells decrease, leading to a cessation of estrogen production by granulosa cells. 12-24 hours after the LH peak, the primary oocyte undergoes the 1st meiosis. The secondary oocyte and the first polar body come about. Granulosa cells become luteinized. Progesterone production commences (Figure 6) [9].

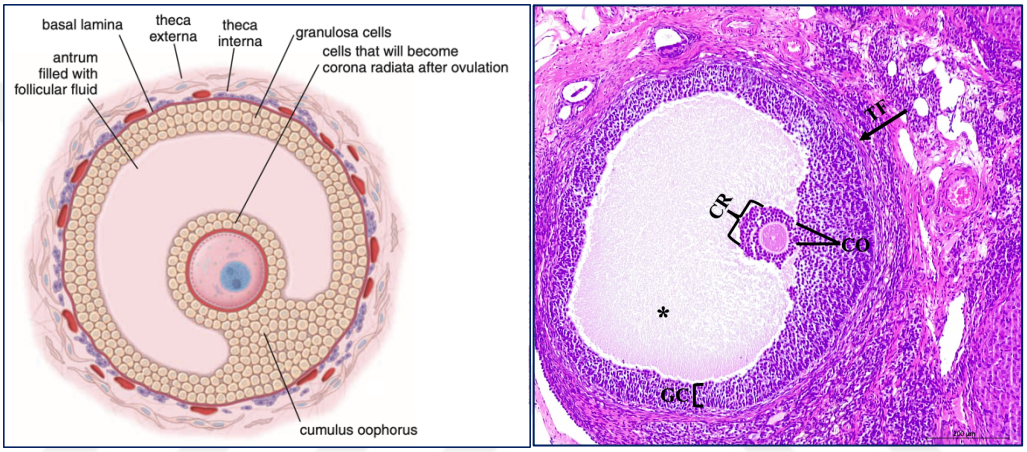

Figure 6. The Structure of the Graafian (Mature) Follicle [9]. *: antrum, CO: cumulus oophorus, CR: corona radiata, TF: theca folliculi. The scale bar represents 50 µm for x40 magnification.

2.1.5.5. Atretic Follicle

During each menstrual cycle, only one follicle matures, while the other follicles undergo atresia. During atresia, mitotic division stops. Granulosa cells separate from the basal lamina, and the oocyte degenerates. Granulosa cells generate hydrolytic enzymes. Neutrophils and macrophages migrate to the granulosa cells. The theca interna cells undergo hypertrophy, filling the resulting follicular space with connective tissue. The thickness of the basal membrane increases, forming a hyalinized band called the glassy membrane. The fragmented zona pellucida is phagocytized by macrophages [11].

2.1.6. Ovulation

The secondary oocyte, which has completed the first meiotic division, is thrown out of the follicle together with the cumulus cells around it, which defines ovulation. During the process of expulsion of the secondary oocyte, the follicular fluid pressure and volume enhance, the follicular wall is broken down by plasminogen, glycosaminoglycans accumulate amid the oocyte-cumulus complex and the stratum granulosum, and prostaglandins induce contraction of smooth muscle cells in the theca externa layer. Various hormonal and enzymatic factors play a role in all these events. In the moments leading up to ovulation a protrusion called the follicular stigma forms on the surface of the follicle and this protrusion ruptures. The oocyte expelled from the ruptured follicle, along with the surrounding cumulus cells, is captured through the fimbriae in the uterine tube. Cells formed as a result of the completion of the first meiotic division contain an equal amount of chromatin. One of the resulting sister cells becomes a secondary oocyte by receiving more cytoplasm. The other receives less cytoplasm and becomes the first polar body. Later, the secondary oocyte enters the 2nd meiotic division. The secondary oocyte undergoes the 2nd meiotic division before leaving the follicle. However, it pauses at the metaphase stage. Ovulation occurs at this stage. The secondary oocyte must be fertilized by a sperm to finalize the second meiotic division. Consequently, through fertilization, an ovum with a maternal pronucleus containing 23 chromosomes is formed [9].

2.1.7. Luteinization and Corpus Luteum

After the secondary oocyte is expelled from the follicle, the remaining follicular wall composed of granulosa and theca cells crumbles, forming the structure of the corpus luteum. Initially, bleeding occurs from the blood vessels in the theca interna layer into the follicular lumen. As a result of this event, a structure called corpus hemorrhagicum is formed. The former follicular cavity is invaded by connective tissue cells from the stroma. Granulosa and theca cells enter the process of luteinization. These cells increase in size and develop lipid droplets in their cytoplasm. They exhibit the characteristic of steroid-producing cells. Ultrastructurally, these cells have dense agranular endoplasmic reticulum (aER) and tubular cristae mitochondria. Cells are named granulosa lutein and theca lutein cells. The corpus luteum contains numerous vascular structures. It releases estrogen and progesterone. These hormones induce the growth of the endometrium, preparing it for pregnancy by stimulating glandular

activity. If pregnancy doesn't occur, a menstrual corpus luteum forms. If human chorionic gonadotropin (hCG) isn't secreted, the corpus luteum structure degenerates. Consequently, the secretion of estrogen and progesterone decreases. The cells, filled with lipid, gradually shrink and undergo autolysis. With the accumulation of hyaline material, it is replaced by the corpus albicans. Corpus albicans disappears after a few months [9].

2.1.8. The Female Reproductive Physiology

2.1.8.1. Hypothalamic-Pituitary-Gonadal Axis

Women with regular ovulatory cycles have a well-functioning hypothalamic-pituitary-ovary axis. Kisspeptin and its receptor (KiSS1R) stimulate gonadotropin-releasing hormone (GnRH) neurons through hypothalamic pathways, triggering the secretion of gonadotropins. When released pulsatively from GnRH terminals in the median eminence, GnRH passes into the hypophyseal portal system. GnRH triggers the anterior pituitary gland to release follicle-stimulating hormone (FSH) and luteinizing hormone (LH). Following that, these hormones go into the systemic circulation. FSH and LH not only promote the growth of follicles, ovulation, and the formation of the corpus luteum but are also responsible for steroidogenesis. Sex steroids such as estrogen and progesterone organize the endometrium for possible embryo implantation. They also regulate the release of FSH, LH, and GnRH through negative feedback (Figure 7) [12,13].

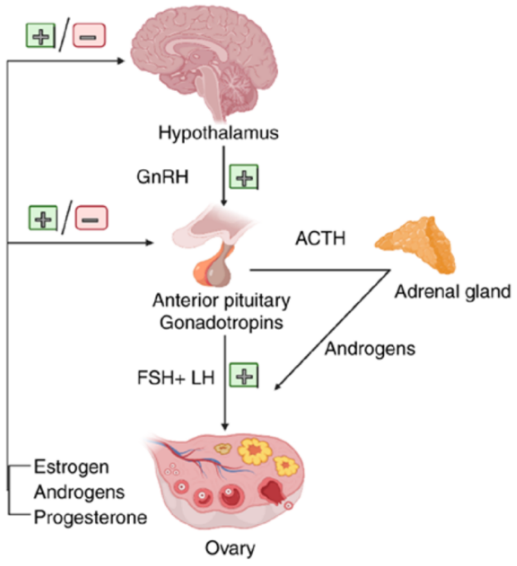

Figure 7. HPO Axis in Women [13].

The menstrual cycle is associated with cyclic changes in folliculogenesis, corpus luteum formation, and the release of steroids and proteins (inhibin) produced by the ovaries. The follicular phase is influenced by FSH and LH. FSH activates granulosa and theca cells. Androgens produced by the theca cells regulate FSH receptor expression. FSH influences follicular development by inducing the formation of aromatase and LH receptors in granulosa cells. One of the growing follicles becomes the dominant follicle, leading to enhance in estrogen. The effects of steroids on basal LH secretion occur through the arcuate nucleus via kisspeptin neurons. High levels of estradiol secreted from granulosa cells before ovulation inhibit FSH release from gonadotropins while causing raise in GnRH release in neurons at the preoptic area. This results in an increase in pulsatile release from the pituitary and the ovulatory fluctuation of LH. The sudden rise in LH induces ovulation. In the luteal phase, estrogen and predominantly progesterone are produced from the corpus luteum. Progesterone plays a role in preparing the endometrium for possible pregnancy. In the case of pregnancy, the corpus luteum continues to release estrogen and progesterone. If pregnancy doesn't occur, hormone levels decrease, and the corpus luteum degenerates. When menstrual bleeding occurs, the functional layer of the endometrium is removed from the environment (Figure 8) [14,15].

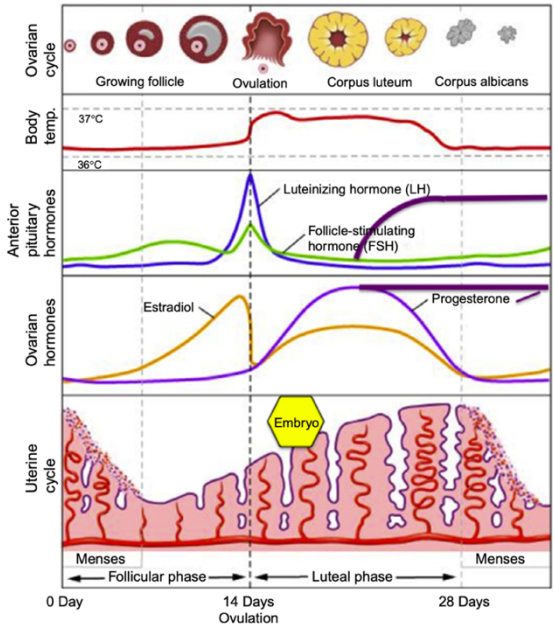

Figure 8. Menstrual Cycle in Women [15].

2.1.8.2. The Mechanism of Steroidogenesis Occurring in the Ovary

Steroidogenesis involves transforming cholesterol (low-density lipoprotein, LDL) into steroid hormones in the gonadal tissues, cortex of adrenal gland, and fatty tissue. Granulosa cells are the primary areas of estrogen synthesis [16]. In the initial step of steroidogenesis, cholesterol translocates to the inner mitochondrial membrane with the assistance of the steroidogenic acute regulatory protein (StAR). Luteinizing hormone (LH) binds to its G protein-coupled receptor located on the theca cells. Adenosine triphosphate (ATP) catalyzes the generation of cyclic adenosine monophosphate (cAMP). This process results in the expression of StAR. The generated cAMP stimulates protein kinase A (PKA) by catalyzing the phosphorylation of the cAMP reply element binding protein (CREB), which is responsive to cAMP. PKA activates the transcription of StAR and other factors linked to steroid hormone secreation. Cholesterol is converted to pregnenolone through the action of the P450scc enzyme located in the inner mitochondrial membrane or the cholesterol side-chain cleavage enzyme. Pregnenolone is converted to androstenedione via DHEA with the help of CYP17A1 (steroid 17-α-hydroxylase/17,20-lyase) and 3β-HSD (3β-hydroxysteroid dehydrogenase) enzymes. Androstenedione can undergo transformation into other androgens (testosterone and dihydrotestosterone) or spread to granulosa cells via the basal lamina. The CYP19A1 (aromatase) enzyme found in granulosa cells converts androstenedione into estrone. Estrone is converted into estradiol through the action of the 17β-HSD (17β-hydroxysteroid dehydrogenase) enzyme. FSH regulates the expression of CYP19A1 and 17β-HSD in granulosa cells (Figure 9) [17]. Estrogens are predominantly produced in the ovaries. However, lower amounts of production also occur in other tissues such as the liver, pancreas, adrenal glands, adipose tissue, breast, and placenta [18].

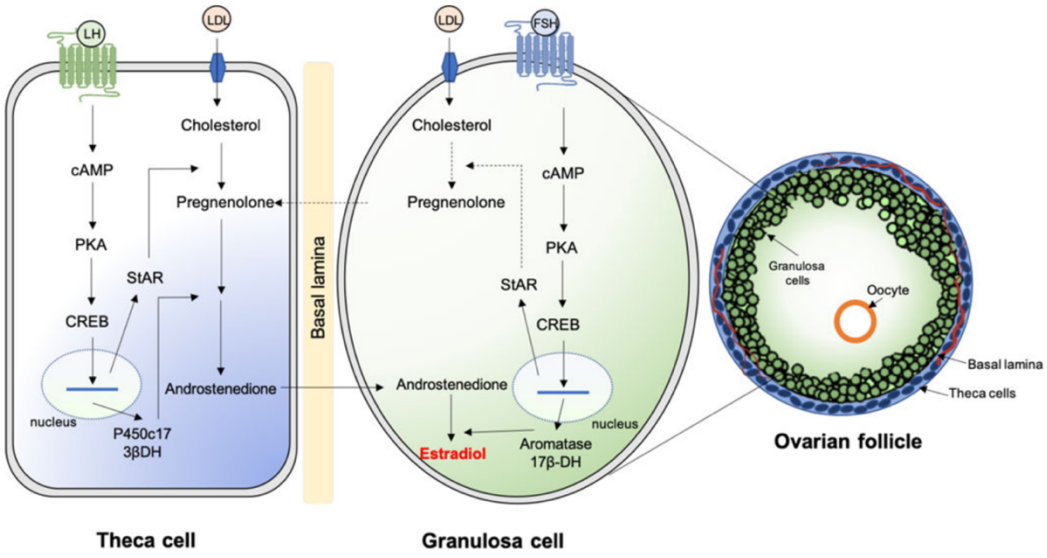

Figure 9. Ovarian Steroidogenesis Mechanism [17].

2.1.9. The Estrous Cycle in Female Rats

The estrous cycle in female rats typically lasts for an average of 4-5 days. The cycle length can be influenced by factors such as changes in light-dark cycles, age, temperature, nutrition, noise, and stress. The estrous cycle in rodent includes of the phases of proestrus, estrus, metestrus, and diestrus. The most commonly used method for determining the cycle is vaginal cytological examination. The ease and accuracy of this method make it a preferred choice for determining the estrous stage and assessing its effects on reproductive function. Through vaginal cytological examination, the cycle is determined by morphologically analyzing cells in the vaginal region. Three cell types are indicative of the estrous cycle: leukocytes, nucleated epithelial cells, and cornified epithelial cells (Figure 10) [19].

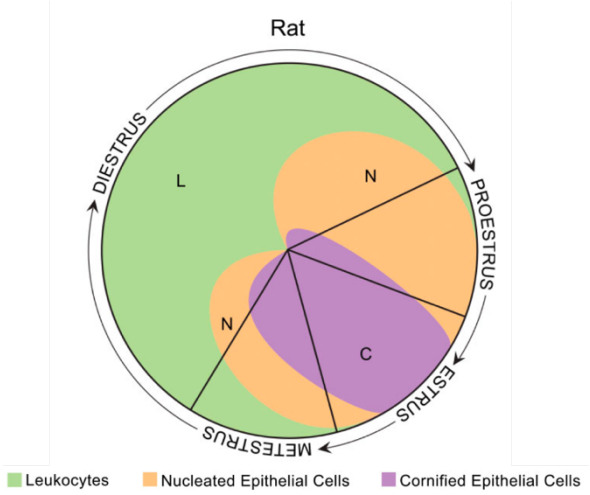

Figure 10. Phase of the Estrous Cycle and Cell Types. L: Leukocytes, N: Nucleated epithelial cells, C: Cornified epithelial cells [19].

2.1.9.1. Proestrus

This stage lasts approximately 12 hours. It corresponds to the proliferative stage of the menstrual cycle in humans. FSH and LH concentration increase throughout this stage, reaching their maximum levels towards the estrus phase. While estrogen levels are initially low at the beginning of proestrus, they reach their highest levels towards the end of this stage. Towards the end of proestrus, an increase in progesterone levels is observed. The high levels of LH trigger ovulation in the transition from proestrus to the estrus stage. During this stage, nucleus-containing epithelial cells (parabasal and intermediate) are the dominant cell types. A small amount of cornified cells may be observed, but neutrophils are not encountered (Figure 11-A) [19].

2.1.9.2. Estrus

This stage lasts for 24-48 hours. It corresponds to the late proliferative stage of the menstrual cycle in humans. Ovulation has just occurred before the estrus stage. A decrease in estrogen levels is observed. In vaginal smear samples taken during the estrus stage, partial cornified cells and fully cornified cells are visible. Towards the end of estrus, nucleus-containing epithelial cells may also be encountered. Neutrophils are not observed (Figure 11-B) [19].

2.1.9.3. Metestrus

This stage lasts for 6-8 hours. It corresponds to the beginning of the secretory stage of the menstrual cycle in humans. Estrogen and progesterone levels are low. The dominant cell types during this stage are intermediate cells, partial cornified cells, and numerous neutrophils (Figure 11-C) [19].

2.1.9.4. Diestrus

It is the longest phase of the estrous cycle. This phase lasts for 42-72 hours. It corresponds to the end of secretory stage of the menstrual cycle in humans. At the onset of diestrus, estrogen levels are low, but they begin to increase towards the end of this stage. The dominant cell type during this stage is neutrophils, often observed clustered around parabasal cells (Figure 11-D) [19].

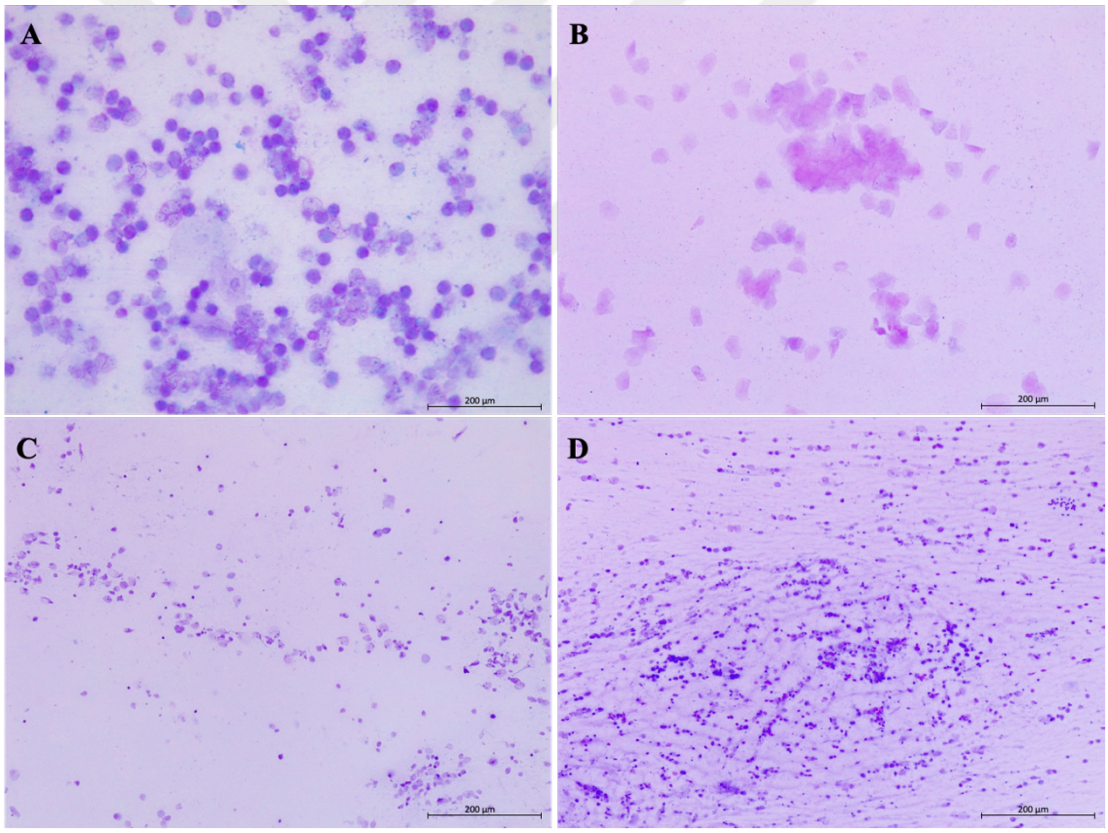

Figure 11. Vaginal smear images of the proestrus (A), estrus (B), metestrus (C) and diestrus (D) stage. Giemsa stain. The scale bar represents 200 µm for x10

The reproductive cycle in rats is similar to the menstrual cycle in humans, is influenced by the neuroendocrine system. In the proestrus phase, there is an raise in FSH, LH, and prolactin concentration. The rise in FSH induces the growth of ovarian follicles, leading to an increase in estrogen levels. Over time, estrogen reaches its maximum level. The increase in estrogen triggers an LH surge. The transition from proestrus to estrus is marked by a peak in LH release, triggering ovulation. Simultaneously, the corpus luteum forms. Towards the end of the estrus phase, estrogen levels decrease. Progesterone is the dominant hormone during the metestrus and diestrus stages. If pregnancy doesn't take place, the degeneration of the corpus luteum structure results in a decrease in progesterone levels (Figure 12). In summary, the proestrus stage involves follicular development, ovulation occurs during the estrus stage, the creation of the corpus luteum structure is observed in the metestrus stage, and diestrus is defined as a resting period [20].

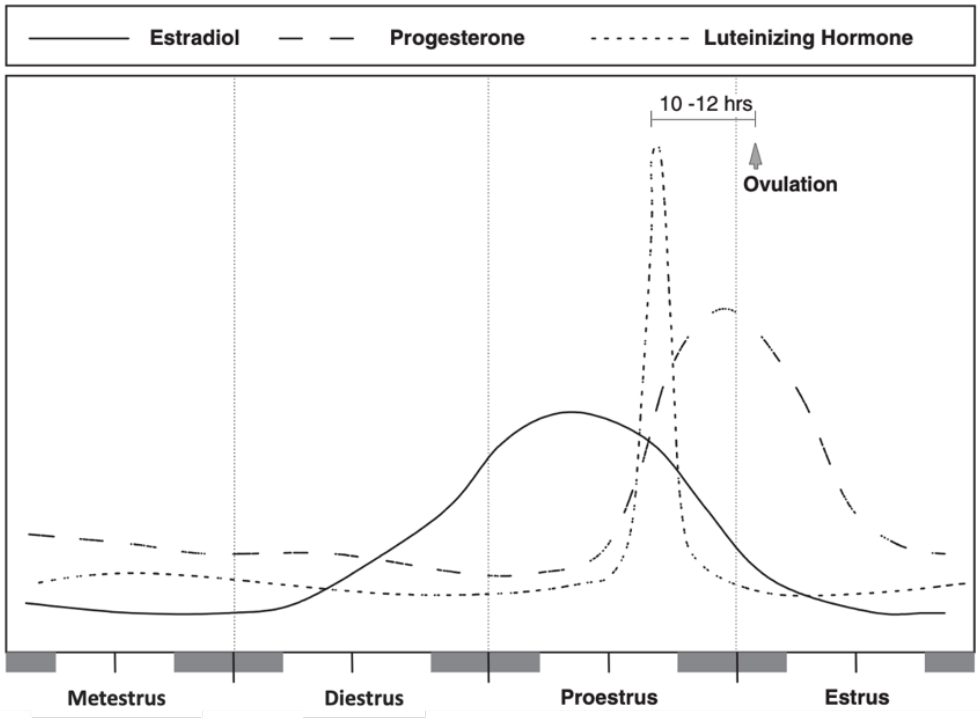

Figure 12. Hormonal Changes in the Estrous Cycle of Female Rats [20].

2.2. Polycystic Ovary Syndrome

PCOS; reproductive, endocrine, and metabolic dysfunction encompassing condition, is defined. It is the predominant reason for anovulatory infertility. PCOS-related infertility has a wide range of endocrine and metabolic abnormalities that result in hyperandrogenic [21], polycystic ovaries [22], ovulatory dysfunction [23] and chronic anovulation (manifested as oligomenorrhea or amenorrhea).

PCOS was first described by Chereau in 1884 as "changes in ovarian morphology" [24]. In 1935, it was recognized as a syndrome associated with anovulation in women by Irving F. Stein and Michael Leventhal [25]. By 2003, "Rotterdam Consensus Criteria" were established by The European Society of Human Reproduction and Embryology (ESHRE) and The American Society for Reproductive Medicine (ASRM) [26]. To diagnose PCOS according to the Rotterdam criteria, one must have a minimum of two of the criteria, including oligoovulation/anovulation, biochemical hyperandrogenism, polycystic ovary morphology on ultrasound.

Understanding the pathophysiology of PCOS is challenging. It requires understanding the nature of dysfunction within the ovaries and comprehending other factors, such as hypothalamic-pituitary and adrenal factors, that affect the ovaries. Anovulation in PCOS is accompanied with various metabolic disorders like hyperandrogenism, obesity, insulin resistance, hypertension, hyperhomocystinemia [27]. Insulin resistance plays a significant role within the pathogenesis of PCOS. Insulin synergistically behaves with LH to induce androgen synthesis in the ovaries. The increase in free testosterone levels suppresses sex hormone-binding globulin (SHBG) found in the liver [28]. Another characteristic increase pulsatility of GnRH, leading to elevated LH levels due to FSH deficiency [29]. The combination of high androgen levels and ovulatory dysfunction creates an ongoing cycle of endocrine dysfunction (Figure 13).

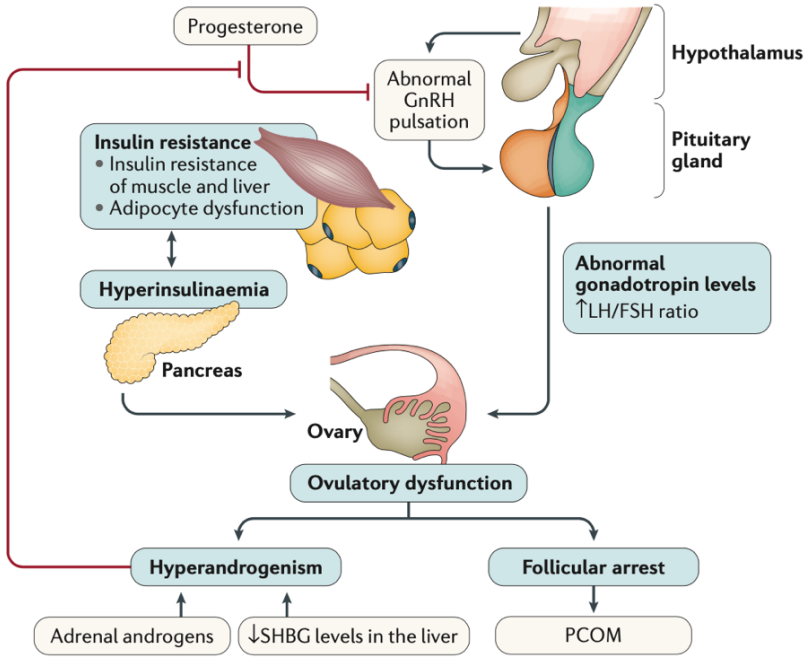

Figure 13. The pathophysiology of PCOS involves disruptions in the pulsatile release of GnRH. There is an excessive release of LH through the pituitary gland, causing ovarian dysfunction and hyperandrogenism. The dysregulated LH secretion is associated with impaired inhibition of GnRH release by progesterone. Follicles in PCOS exhibit increased resistance to FSH. This resistance may be linked to elevated intra-ovarian AMH levels. Insulin resistance disrupts gonadotropin secretion. SHBG secretion decreases, leading to the development of PCOM (polycystic ovarian morphology) [21].

2.2.1. Polycystic Ovary Morphology (PCOM)

PCOM, expanded ovaries characterized by augmented central stroma and abundant small (2-9 mm) antral follicles scattered throughout the periphery. It is observed that follicle growth stops, and degenerative changes occur. Antrum enlargement occurs due to the gathering of follicular fluid in the antrum. On the other hand, following apoptosis of the granulosa cells, the emergence of cystic follicles occurs [30]. Compared to normal ovaries, the numbers of growing pre-antral and antral follicles in PCOS are three times greater. Compared to normal ovaries, it has been observed that the number of primordial follicles is reduced in PCOS [31]. Delayed follicular development is observed in PCOS. In PCOS, the expression of GDF-9

(Growth differentiation factor-9) in follicles reduced during the transition from the primary follicle to the secondary follicle and from the secondary follicle to the Graafian follicle stage. GDF-9 is a member of the TGF-β family that is specific to oocytes. It is believed that there are defects in follicular development in the early stages of folliculogenesis [32]. Anti-Müllerian hormone (AMH) contributes to the elevation of antral follicle numbers in PCOS [33,34]. AMH is primarily secreted from the granulosa cells of developing follicles. It has adverse effects on the commencement and advancement of follicular growth [33]. When compared to normal ovaries, reduced expression of AMH is observed the primary follicles in PCOS [35]. This decrease in AMH leads to an increase in the number of follicles progressing to the pre-antral stage in PCOS. The concentrations of AMH in the serum and follicular fluid of women with PCOS are elevated [36]. In PCOS, low AMH levels in growing follicles allow for the advancement of follicular development. As it reaches the antral follicle stage, the increased number of follicles due to follicular growth results in higher AMH generation per granulosa cell. The elevated AMH in PCOS leads to defects in dominant follicle selection [37].

2.2.2. The Importance of Granulosa Cells in PCOS

Follicular degeneration is observed in PCOS. Despite this follicular degeneration, granulosa cells continue to function. The basic mechanism here is the increase in the sensitivity of granulosa cells to FSH due to the increase in insulin levels. When granulosa cells obtained from both normal ovaries and PCOS ovulatory, PCOS anovulatory ovaries are treated with insulin, an increase in estradiol and progesterone synthesis is observed in three types of granulosa cells. Additionally, the effect of insulin leads to early luteinization of granulosa cells, follicular disruption, and high androgen production [38]. Another noteworthy aspect is that androgens and estrogens also heighten the responsiveness of granulosa cells to FSH in PCOS. This results in a synergistic effect, including increased FSH receptor binding between estradiol and FSH, LH receptor stimulation, increased aromatase activity, and progestin production [39].

2.2.3. The Importance of Theca Cells in PCOS

Compared to the theca cells of a normal ovary, there are differences in the histological appearance of theca cells in PCOS. The theca cells are thicker and extend beyond the width of the granulosa layer. LH has an inductive effect on theca cells.

Elevated levels of LH play a role in hyperandrogenism in PCOS. Steroidogenic defects in the theca cells lead to ovarian hyperandrogenism [30].

In in vitro studies, it has been demonstrated that the theca cells of women with PCOS synthesize high levels of androgens both initially and after treatment with LH, compared to normal ovaries. Additionally, it is known that compared to ovulatory hyperandrogenic, anovulatory hyperandrogenic women with PCOS have higher concentration of 17-OH progesterone. The levels of androstenedione and 17-OH progesterone in women with PCOS are observed to be comparable to those in normal men [40]. After hCG administration to women with PCOS, the elevation in 17-OH progesterone levels is reported to be due to the excessive expression of 3β-HSD [41]. At this point, it can be said that dysfunction in ovarian steroidogenesis is effective in the pathogenesis of PCOS. Another important factor is insulin, which shows a synergistic effect alongside LH. When insulin secretion is suppressed in women with PCOS, a decrease occurs in serum LH and androgen levels [42]. It is believed that insulin, in conjunction with LH, exacerbates dysfunction in steroidogenesis in PCOS. Incubation of teka cells taken from normal women with insulin results in increased androgen synthesis. Similar results are observed when LH is added to insulin [42]. In animal studies, insulin and hCG treatment have been shown to increase androgen biosynthesis. Thinning of the granulosa layers, an increase in teka layers and stromal interstitial tissue, along with the development of numerous large cystic structures are observed. Additionally, there is high expression of P450scc and CYP17A1 in the theca cells and stromal cells. Therefore, a connection between hyperandrogenism and hyperinsulinemia can be suggested [43].

2.2.4. The Importance of Intra-ovarian Cytokines, Paracrine Modulators, Growth Factors in PCOS

Intraovarian factors derived from granulosa cells; It has various functions such as follicle choice, FSH response. Any dysfunction that may occur in the normal functioning process leads to abnormalities in the steroidogenic activity of the theca cells. It is known that inhibin from intraovarian factors induces androgen synthesis. Women with PCOS have elevated serum inhibin-B levels, and plasma inhibin and androstenedione levels show correlation. While inhibin triggers androgen synthesis, androgens, reciprocally, trigger inhibin synthesis, establishing a detrimental cycle leading to follicle arrest [44].

AMH plays a role in polycystic ovary morphology. Women with PCOS exhibit elevated expression of type II AMH receptors in granulosa cells. Additionally, these receptors are expressed in the theca cells as well. Consequently, AMH exerts a paracrine influence on androgen synthesis. The interconnection among FSH, AMH, and estradiol is closely associated with the heightened levels of androgens. FSH induces AMH expression in small follicles without aromatase expression. In normally developing follicles, the concentration of estradiol reaches a certain threshold. An increase in estradiol levels suppresses AMH expression and renders it ineffective against FSH stimulation. Polycystic follicles, despite having high AMH levels, lack estradiol production induced by FSH [45].

During the folliculogenesis process in the ovary, various bone morphogenetic proteins (BMP) are expressed. In PCOS, the presence of GDF-9 and BMP-15 is diminished, resulting in aberrant follicular development [46]. BMPs play a role in FSH response and steroidogenesis stimulated by FSH. Another significant factor is insulin-like growth factors. Insulin suppresses the synthesis of insulin-like growth factor-binding protein-1 (IGFBP-1) in the liver. When IGFBP-1 is suppressed, insulin-like growth factor-1 (IGF-1) and insulin-like growth factor-2 (IGF-2) increase.IGF-1 and IGF-2 affect androgen synthesis. IGF-2 is an active paracrine factor in the theca cells. IGF-2 enhances LH-induced androgen synthesis. Additionally, inhibin B influences teka cells to produce more androgens, along with IGF-1 and IGF-2 [47].

Some intrafollicular cytokines and growth factors play a role in the abnormal follicular development that occurs in PCOS (Figure 14). Fibroblast growth factor blocks antral follicle growth by inhibiting aromatase activity in granulosa cells. In PCOS, the concentration of epidermal growth factor is elevated, resulting in the suppression of estrogen synthesis [48]. Additionally, the expression of vascular endothelial growth factor (VEGF) is high. The increase in VEGF is thought to be insulin-related [49]. Additionally, there is an increase in VEGF expression in the dense hypertrophic stroma of polycystic ovaries. Therefore, stromal blood flow increases, and theca interna grows abnormally [50].

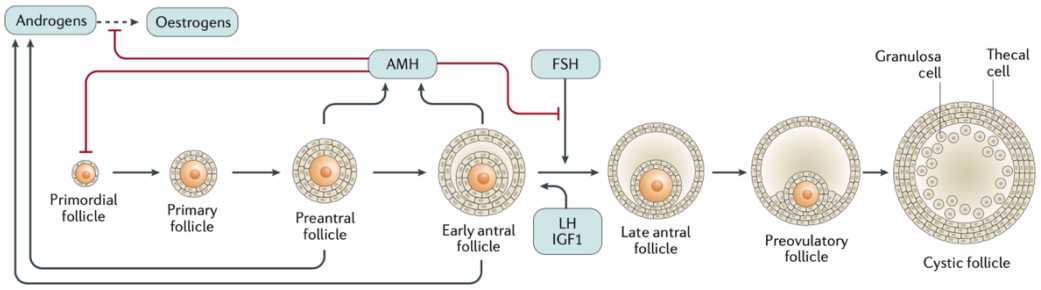

Figure 14. Ovarian follicular maturation arrest in PCOS [21].

2.2.5. HPO Axis in PCOS

In women with PCOS, 40-60% have elevated LH concentration [51]. While the precise mechanism driving this elevation in LH levels is not entirely comprehended, it is thought to be influenced by hyperinsulinemia. Several hypotheses have been proposed at this point. It is thought that insulin affects the activity of GnRH neurons and influences the anterior pituitary to respond more to GnRH [52]. Another hypothesis suggests that progesterone regulates GnRH pulse frequency. In cases where ovulation doesn't occur, the decrease in progesterone levels is thought to interrupt the negative feedback on GnRH release [53]. However, it is observed that the high levels of LH seen in prepubertal girls with uninitiated cyclic ovarian function and elevated androgen levels aren't a direct result of the signaling eliminated by progesterone [54]. A third hypothesis suggests that in women with PCOS and hypogonadotropic hypogonadism, serum LH concentration are high after GnRH-induced ovulation. This increase in LH levels occurred before the increase in estradiol (Figure 15). Therefore, the excessive secretion of LH isn't due to a disorder in hypothalamic pulse regulation. The fundamental problem here is the disruption in the ovarian-pituitary feedback mechanism [55].

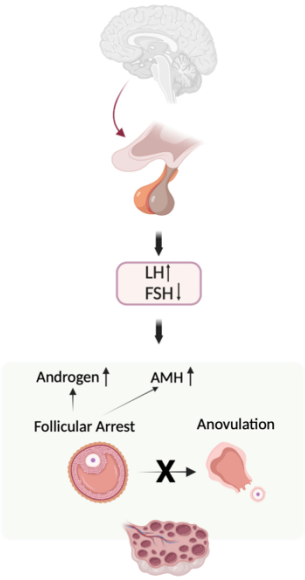

Figure 15. HPO Axis in PCOS. Abnormal secretion of GnRH from the hypothalamus cause to excessive LH secretion from adenohypophysis. As LH increases, FSH secretion decreases. Androgen levels rise. AMH levels increase. Numerous cystic follicles and anovulation develop.

2.2.6. PCOS Animal Models

One of the most serious problems of PCOS is hyperandrogenism. Therefore, high levels of androgens are applied in PCOS animal models to induce PCOS characteristics observed in humans. The most commonly used ones are Testosterone, Dihydrotestosterone and DHEA[56,57].

2.2.6.1. Testosterone

Frequently utilized in rats, but its application in neonatal mice is also considered. Administering dose of 100 µg testosterone propionate or testosterone to female mice for the first 3 days of the neonatal period is reported to result in anovulation, the formation of cystic-like structures and the development of polycystic ovaries [58].

2.2.6.2. Dihydrotestosterone

Dihydrotestosterone is an androgen that can't be aromatized, meaning it can't convert to estradiol like testosterone. Dihydrotestosterone exhibits a higher affinity for the androgen receptor compared to testosterone. Exposure to prenatal dihydrotestosterone in mice and rats leads to disruptions in the estrous cycle,

diminishment of corpus luteum, a raise in secondary follicle count and results in a thinner granulosa layer accompanied by a thicker theca layer. Furthermore, it induces an elevation in insulin resistance, coupled with increased levels of LH, testosterone and GnRH. Conversely, administration of dihydrotestosterone during the prepubertal period results in anestrus, absence of corpus luteum, an increase in cystic follicles and the development of atretic follicles. Additionally, it provokes an elevation in leptin levels and a reduction in adiponectin levels [56].

2.2.6.3. DHEA

DHEA, an androgen derived from the adrenal glands, exhibits elevated levels in women suffering from PCOS [59]. In this regard, dehydroepiandrosterone (DHEA) is the first choice for inducing PCOS in different rodent models. When administered to prepubertal rats at a dose of 6 mg/100 g body weight dissolved in 0.2 ml sesame oil, these rats manifest acyclicity and anovulation [60,61]. In rats treated with DHEA, numerous cystic follicles are developing. Degeneration occurs in the granulosa cell layer, and increases in ovarian weight take place [60,62]. Application of DHEA at a dosage of 6 mg/100 g body weight for 20 days in 25-day-old mice resulted in infertility, along with the emergence of abundant atretic and cystic follicles in the rodent ovaries [63,64].

2.3. Hydrogen Sulfide

Since the 1980s, H2S has been active in mammalian tissues. However, during those years, it was considered a metabolic waste without physiological activity. H_2S was initially identified as a neuromodulator in brain tissue. The researchers who first described this are Abe and Kimura. These researchers have demonstrated that H2S plays crucial roles in brain functions, regulating synaptic activities modulated by steroid hormones and neurotransmitters [65]. This finding has become the focus of many research groups, and the biological activity of H_2S has been investigated in various tissues. Therefore, looking at the studies of the last two decades, the active involvement of H_2S in regulating various physiological functions has made it highly significant.

2.3.1. Biosynthesis of Hydrogen Sulfide

Gasotransmitters are endogenously produced signaling molecules. In mammalian tissues, H_2S is produced through enzymatic (trans-sulfuration pathway) or non-enzymatic pathways (Figure 16). In the non-enzymatic pathway, elemental sulfur, formed as a result of glucose oxidation is reduced to H_2S along with metabolites such as

NADH, NADPH, and GSH. Three enzymes produce H_2S through enzymatic pathways in various cells and tissues: 3-mercaptopyruvate sulfurtransferase (3-MST), cystathionine gamma-lyase (CSE, also known as CTH and CGL), cystathionine beta-synthase (CBS). CBS and CSE reside in the cytosol, whereas 3-MST is present in both the mitochondria and cytosol. There are two main substrates in the endogenous generetion of H_2S: homocysteine and L-cysteine. The enzymes responsible for H_2S production, CSE, and CBS, primarily synthesize it from L-cysteine, with small amounts from homocysteine. Additionally, the catabolism of cysteine through cysteine aminotransferase (CAT) and the 3-MST pathway results in H_2S production. H_2S is released from persulfide-modified 3-MST under the influence of thioredoxin (Trx) or reductive factors. Additionally, the enzyme methanethiol oxidase (MTO) produces H_2S from methanethiol. Finally, it has been demonstrated that cysteinyl-tRNA synthetase 2 (CARS2), which participates in a new pathway, produces H_2S by integrating into proteins and forming cysteine persulfide (cysteine-SSH). H_2S is generated from persulfides through Trx or other mechanisms. Intestinal microbiota plays a role in endogenously producing H_2S by utilizing non-enzymatic H2S-releasing molecules present in food [66,67].

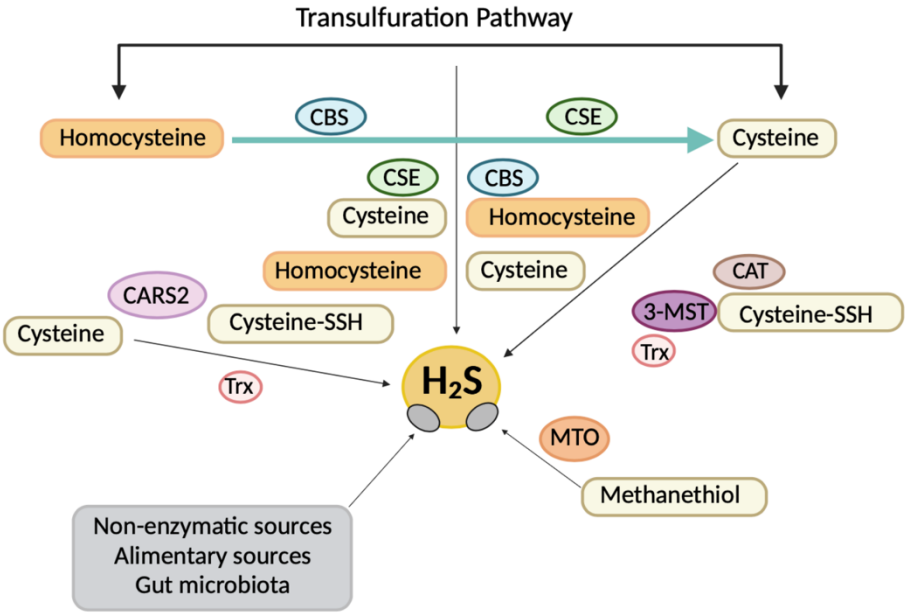

Figure 16. Pathways involved in hydrogen sulfide synthesis.

2.3.2. Catabolism of Hydrogen Sulfide

The liver is primarily where H_2S undergoes degradation. After synthesis, it undergoes metabolism through various pathways such as oxidation in the mitochondria, cytoplasmic methylation and binding with hemoglobin. In the oxidative breakdown, thiosulfate ($S_2O_3^{-2}$) is initially formed. Subsequently, thiosulfate is enzymatically converted by thiosulfate sulfurtransferase (TST) to sulfite (SO_3^{-2}) and sulfite is further oxidized to sulfate (SO_4^{-2}) through the action of sulfite oxidase enzyme. H2S activates a non-enzymatic pathway associated with mitochondrial respiratory electron transport during its oxidation to thiosulfate. The final product of H2S metabolism is sulfate. The end products of cysteine catabolism are sulfate (comprising 77-92% of eliminated sulfur in urine), ester sulfate (7-9%), and taurine (2-6%). In a second pathway of H_2S catabolism, it undergoes methylation via thiol S-methyl transferase enzyme, resulting in methanethiol and demethylsulfide. Finally, H_2S binds to methemoglobin, forming sulfhemoglobin [5,68].

2.3.3. H_2S Donors

In physiological conditions, one-third of H_2S is found in its unmetabolized form. Two-thirds of it, however, dissociates into H^+ (hydrogen ion) and HS^- (hydrogen sulfide ion) forms. Solid H_2S donors have been produced to facilitate the experimental usability of gaseous H_2S. In this respect, the use of synthetic donors and sulfide salts takes precedence. NaHS and sodium sulfide (Na_2S) are the most frequently used sulfide salts in biological studies and are also referred to as donors. These donors used to assess the effect of exogenous H_2S are in solid form. Under physiological conditions, NaHS breaks down into Na^+ and HS^- forms. The dissociated HS^- reacts with ambient H^+, resulting in the formation of H_2S. Therefore, NaHS is considered a good H_2S donor. Synthetic donors are divided into two groups: diallyl trisulfide (DATS), which releases rapidly, and GYY4137, which releases slowly. Slow-releasing donors are water-soluble. Due to their therapeutic potential, synthetic donors are more preferred in phase studies. GYY4137 from synthetic donors is liberated with H_2S by hydrolysis. Compared to sulfide salts, the release of synthetic donors takes longer. For example, GYY4137 is released in phosphate buffer at physiological pH in 10 minutes, while NaHS releases in 10 seconds. In terms of concentration, NaHS has a 40-fold higher concentration than the synthetic donor GYY4137 [67].

2.3.4. Physiological Action of H_2S

In recent years, many aspects of H_2S have been revealed in studies. For instance, some of its functions include intracellular signal transduction, angiogenesis, vasodilation, anti-inflammatory, antioxidant, and anti-apoptotic activities. CSE is predominantly expressed in the heart and peripheral vascular tissues. On the other hand, CBS is present at higher levels in the central and peripheral nervous systems [65,3]. In many tissues, CBS and CSE enzymes work in coordination to produce H_2S, while in some tissues, only one of the two enzymes is necessary [2]. CBS mRNA expression has been detected in various regions of the rat brain. These regions include the cerebellum, brainstem, cerebral cortex, and hippocampus [65,69]. H_2S stimulates long-term potentiation in the hippocampus, facilitates pain perception, influences neuronal hyperpolarization (especially in the CA1 region of the hippocampus and the dorsal raphe nucleus), activates enteric neurons, and induces relaxation of smooth muscles. All these effects have been clearly demonstrated in scientific studies conducted in both humans and animals [2,69,70]. There are many interactions between H_2S and intracellular signaling pathways. H_2S is a direct activator of adenylate cyclase, ATP-sensitive potassium channels, the mitogen-activated protein kinase system, and nuclear erythroid-related factor-2 (NF-E2). H_2S controls neuronal activity, induces relaxation of smooth muscles in blood vessels, promotes cell proliferation, and regulates the balance of oxidant/antioxidant through these pathways [71,72,73,74].

The quantity of CSE and CBS in the tissue is variable. Studies have shown that H_2S induces relaxation in arterial blood vessels [65,75,76] small bronchial walls [77,78], human corpus cavernosum [79], rat vas deferens [5] and the smooth muscles of the gastrointestinal and urogenital tracts [80]. H_2S stimulates the proliferation of spermatogonial germ cells. It relaxes the smooth muscles in the vas deferens and contributes to erectile function [81,79,82]. CSE has been detected in the testicular tissues of rats, particularly in immature spermatogonia and Sertoli cells. CBS, on the other hand, has been identified in Leydig cells, Sertoli cells, and germ cells [4]. H_2S regulates testosterone secretion by affecting LH release [83]. H_2S donor NaHS showed protective effects against oxidative stress and inflammation in cisplatin-induced testicular damage [84]. Additionally, CBS expression has been found to be low in sperm samples obtained from human asthenozoospermic patients. While H_2S inhibitors inhibit sperm motility, H_2S donors support spermatozoa production and activity [85].

2.3.5. H_2S in the Female Reproductive System

The presence of CBS and CSE has been reported in the female reproductive organs of humans, rats, and mice [86,81.] The presence of CBS and CSE enzymes has been demonstrated in the uterine tissues, placenta, and fetal membrane structures of pregnant rats, while in non-pregnant rats, they were shown only in uterine tissues. In human tissues, CSE and CBS expression have been shown in the myometrium, amnion, chorion, and placenta [86]. CBS mRNA expression was detected in the uterus of pregnant and non-pregnant mice [87]. There is CBS enzyme activity in the decidual and placental tissues of rats [88]. In this context, the existence of CBS and CSE enzymes in female reproductive organs implies that H_2S might have significant functions in the reproductive system. H_2S ensures uterine quiescence during pregnancy. CBS and CSE raise during pregnancy, increasing local H_2S production in the myometrium and placenta. The elavated synthesis of H_2S during pregnancy prevents uterine contractions [86]. However, when H_2S is administered to rats, the birthing process is extended. [89]. In vitro studies have shown that H_2S donors block spontaneous uterine contractions [90]. Additionally, studies in mice and rats have shown that H_2S functions as a vasodilator and is involved in regulating blood pressure [91,76]. However, besides its vasodilatory impact, H_2S can also cause vasoconstriction depending on concentration. In this context, low levels of H_2S cause vasoconstriction, while higher levels of H_2S contribute to vasodilation [77].

Studies have demonstrated the necessity of the CBS enzyme for female reproductive function, showing that $CBS^{-/-}$ mice exhibit infertility characteristics [87, 92]. These mouse exhibit changes in the estrous cycle, and it is reported that the fetuses don't develop normally, and the born pups can't survive [87]. In another study, it was shown that $CBS^{-/-}$ mice have decreasing numbers of growing follicles and irregular, shorter estrous cycles, while $CSE^{-/-}$ mice exhibit fertile characteristics. It is also known that fertility is diminished in CBS+/- mice in comparison to wild-type mice [93].

Even though H_2S has been acknowledged as a signaling mediator, research on its role in oocyte physiology is limited. In a conducted study, it was shown that enzymes releasing H_2S, including 3-MST, CSE, and CBS exhibit mRNA and expression of protein in pig oocytes. The study revealed that CSE mRNA expression remains constant in germinal vesicle (GV) intact oocytes and Metaphase-I (MI) oocytes, while CBS mRNA expression is limited in MI-phase oocytes and increases in Metaphase-II (MII)-

phase oocytes. Additionally, 3-MST mRNA expression occurs shortly before the resumption of meiotic division. The study also demonstrated that the addition of inhibitors of these three enzymes to the culture medium suppresses meiotic maturation, while the use of the exogenous H_2S donor NaHS accelerates meiotic maturation [94]. In another study, it was documented that there is CBS mRNA expression in mouse cumulus cells and oocytes, highlighting the involvement of H_2S in oocyte maturation [95,96]. When CBS expression is reduced in mouse granulosa cells, the meiotic maturation of oocytes is suppressed [97].

The Fallopian tube is of vital importance for the transport of gametes and embryos. Because it provides a suitable microenvironment for the oocyte and embryo in the early stages of fertilization and embryonic development. The CBS and CSE enzymes are dispersed throughout the human fallopian tube epithelium. The H_2S signal assists in the spontaneous contraction of the human oviduct and the transport of oviductal embryos. Moreover, abnormal H_2S signaling is reported to disrupt the oviductal transport of embryos and impair preimplantation embryo development. The application of the H_2S donor NaHS is reported to restore these effects [98].

In in vitro and in vivo studies conducted in mouse and humans, the H_2S-producing system is observed to play a role in ovulation. It is reported that the increase in LH before ovulation enhances the expression of enzymes catalyzing H_2S production, and the H_2S donor NaHS induces an elavation in the mRNA expression of AREG, EREG, and plasminogen activators, which play a significant role in ovulation. Additionally, it is observed that CSE inhibitors block ovulation, and ovulation suppressed by a CSE inhibitor is reversed by the H_2S donor NaHS (Figure 17) [99]. Therefore, it can be said that H_2S also plays an essential part in the follicle rupture process in the ovary after the LH peak. While the precise mechanism of H_2S action hasn't been fully elucidated, it is believed that its primary impact occurs at the level of MMP and plasminogen activators. It is thought that LH-induced H_2S may increase EREG and AREG expression strengthen the preovulatory cascade, but primarily affect the activities of PLAT, MMP9, MMP2, and to ensure follicle wall breakdown.

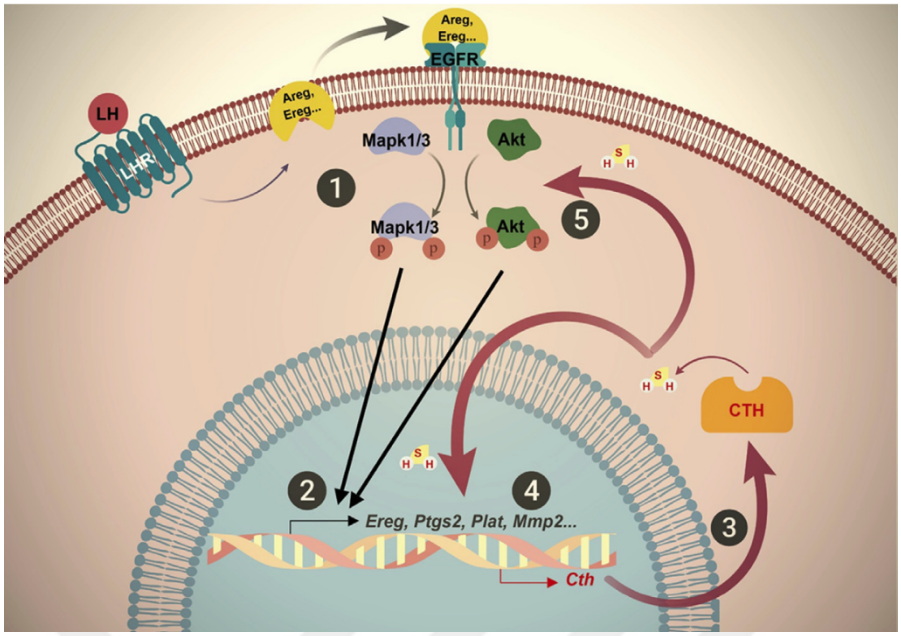

Figure 17. The mechanism of action of H_2S during the ovulation process [99].

Studies conducted to date indicate that PCOS adversely affects women's reproductive potential [100,101,102,103,104]. Understanding the mechanisms beneath the adverse effects of PCOS on the ovaries is particularly important. However, there is no study in the literature examining the role of the H_2S-producing system against possible infertility associated with PCOS. Therefore, considering the positive effects of H_2S-generation system on the female reproductive system, the question arises, "Can NaHS alleviate impaired steroidogenesis, follicular arrest, and anovulation occurring in PCOS?"

Based on the information obtained from the literature, the hypothesis of this study is; in the rat PCOS model triggered through DHEA, changes leading to infertility in female rats (anovulation/oligoovulation, follicular arrest, impaired steroidogenesis) may occur, and the exogenous H_2S donor NaHS may have a fertility-enhancing effect by alleviating anovulatory infertility, impaired follicular development, and impaired steroidogenesis associated with PCOS.

In line with our hypothesis, we aimed to explore the efficacy of the H_2S donor NaHS against possible damage mechanisms by examining the effects of DHEA on the ovaries of female Wistar Albino rats in terms of histological, immunohistochemical, molecular and biochemical aspects.

3. MATERIAL and METHODS

3.1. Animals Procurement

In order to carry out the thesis study, ethical approval was obtained from the Yeditepe University Animal Experiments Local Ethics Committee (Decision No: 2022/04-2 dated 28.04.2022). We adhered to ethical principles in our study. 30 adult female Wistar Albino rats were asured from the Animal Experiments Center. The rats were kept in an environment with a temperature of 21-23°C and a 12-hour light-dark cycle. The animals were fed ad libitum.

3.2. Readiness of Solutions

In our study, DHEA (Santa Cruz, catalog number: sc-202573) was used. DHEA was administered to rats in the PCOS and PCOS+NaHS groups for 20 days. 0.01 ml of 95% ethanol, dissolved in accordance with a dose of 6 mg/100 g body weight per rat, mixed with 0.09 ml of sesame oil based on the body weight of each rat.

In our study, NaHS (Sigma-Aldrich, USA, catalog number: 161527-5G) was used. NaHS and PCOS+NaHS groups were administered for 20 days. NaHS, dissolved in physiological saline at a dose of 200 μg/kg/day according to the body weight of each rat

3.3. Creating Experimental Groups and Establishing the PCOS Model

In our study, experimental groups were formed with 5 groups, each consisting of 6 animals. All rats were subjected to injections during the estrus phase. Rats in the control group received no injections. To create the PCOS model, rats in the PCOS group were subcutaneously injected with DHEA at a dose of 6 mg/100 g body weight for 20 days [105]. Rats in the Vehicle group were subcutaneously injected with a mixture of 0.01 ml 95% ethanol and 0.09 ml sesame oil. Rats in the NaHS group were intraperitoneally injected with a dose of 200 μg/kg/day NaHS [84]. Rats in the PCOS+NaHS group were initially subcutaneously injected with DHEA at a dose of 6 mg/100 g body weight, followed by an intraperitoneal injection of 200 μg/kg/day NaHS 2 hours later. The experimental groups are summarized in Figure 18.

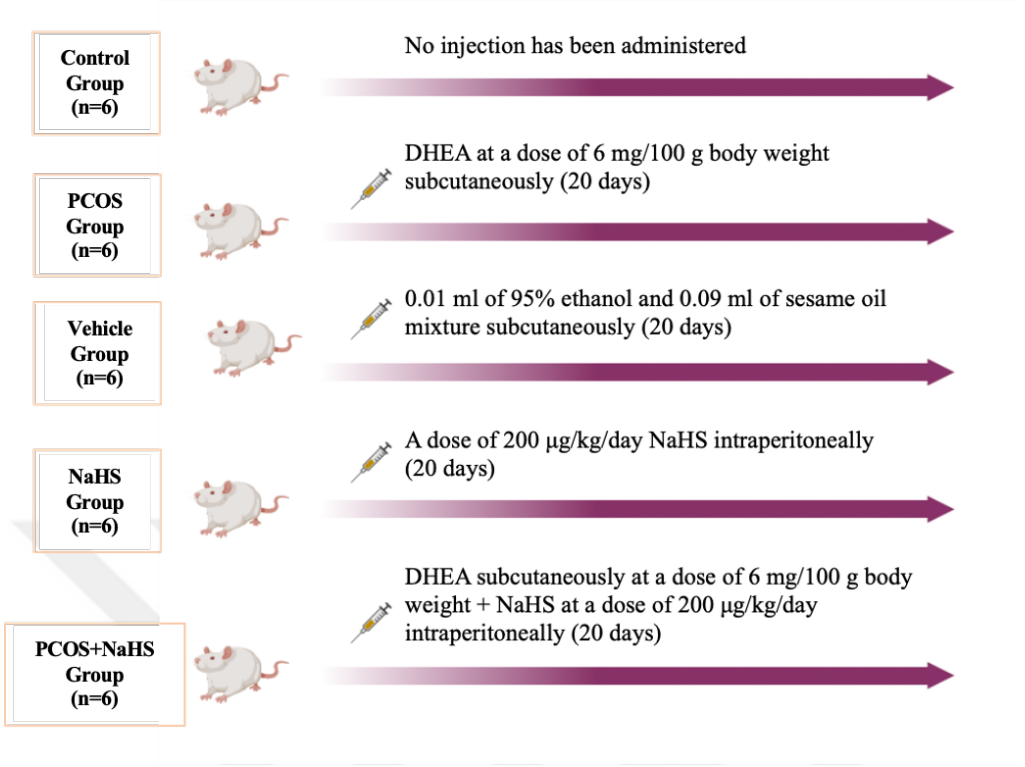

Figure 18. Experimental groups.

Before the experiment started, blood samples were taken from all rats. Additionally, vaginal smears were obtained daily from all rats throughout the experiment. At the end of 20 days, the evaluation of the vaginal smear findings was planned to ensure a certain standardization for experiment termination during the estrus phase. However, due to disruptions in the estrous cycle observed in the PCOS group, the sacrifice of all rats couldn't be performed on the same day. The experiment was completed in 22 days. Upon completion of the experiment, all rats were subjected to carbon dioxide inhalation, and intracardiac blood samples were collected before decapitation. The abdominal regions of the rats were opened, and bilateral oophorectomy was performed. The right ovaries were placed in 10% neutral buffered formalin for histopathological analysis. Three of the left ovaries were stored at -80°C for Reverse Transcription Polymerase Chain Reaction (RT-PCR) analysis. Additionally, three pieces of left ovarian tissue were placed in 10% neutral buffered formalin for immunohistochemical staining (Figure 19).

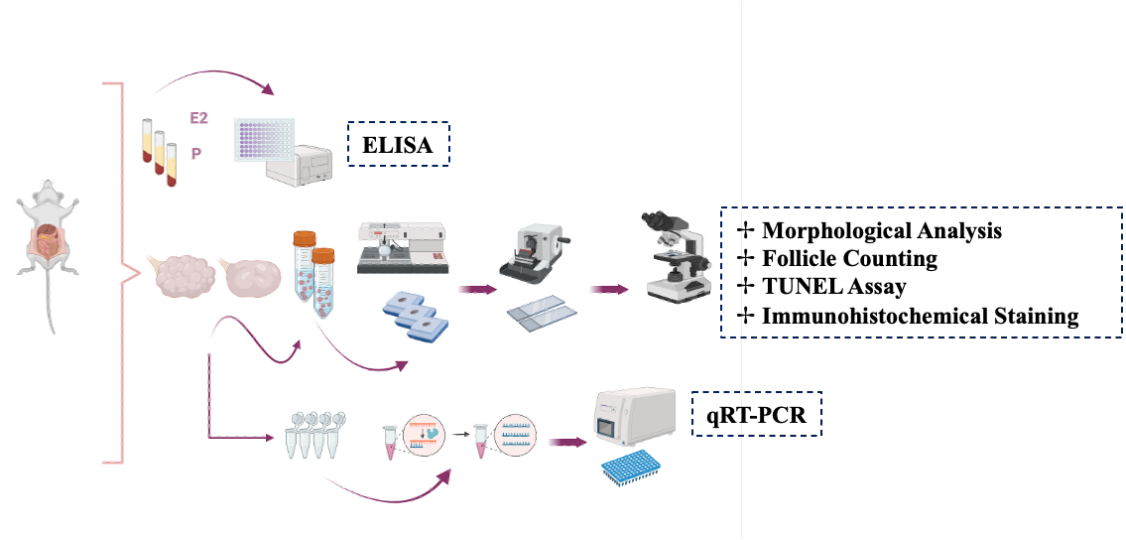

Figure 19. Flowchart of the experiment.

3.4. Biochemical Analyses

3.4.1. Assessment of Estrogen and Progesterone Levels in Serum

Blood samples taken before and after the experiment were centrifuged at 3000 rpm for 10 minutes to obtain serum samples. The obtained serum specimens were then moved to eppendorf tubes and stored at -80°C until analyses were conducted.

ELISA kits were employed for the analysis of E_2 (China, BT Lab, catalog no: EA0011Ra) and Progesterone (China, BT Lab, catalog no: EA0063Ra) levels in serum samples. Once the ELISA kit reached room temperature, standards, samples, diluent and wash solution were prepared. Specific standards and samples were pre-determined for each well and recorded. In standard wells, 50 µL of the standard was added while in sample wells, 50 µL of the serum sample was added. Each well received 50 µL of biotinylated antigen and was incubated at 37°C for 60 minutes. The wells were washed five times with 300 µL wash buffer. Subsequently, 50 µL of avidin-HRP was added to each well, and the plate was incubated at 37°C for another 60 minutes. After washing the wells 50 µL of substrate solution was added and the plate was incubated in the dark at 37°C for 10 minutes. Following this, 50 µL of stop solution was added to each well. The absorbance of the wells was read at 450 nm using a spectrophotometer. Blank wells received only substrate and stop solutions.

3.5. Histological Preparation

3.5.1. Preparation and Evaluation of Vaginal Smear Samples

A cotton swab moistened with saline was used to collect a smear sample from the vagina, which was then spread on a glass slide. The obtained smear samples were air-dried, fixed and stained with Giemsa stain for 20 minutes. Vaginal epithelial cells were identified according to criteria specified in the literature [19]. Each finding was recorded daily. At the end of the experiment, in order to compare the durations of estrus phases, the percentage of days in each phase was calculated [20]. The calculated indices are as follows:

- Proestrus index= Number of proestrus days/Total duration of the experiment*100
- Estrus index= Number of estrus days/Total duration of the experiment*100
- Metestrus index= Number of metestrus days/Total duration of the experiment*100
- Diestrus index= Number of diestrus days/Total duration of the experiment*100

3.5.2. Preparation of Ovarian Tissue Samples

The right and left ovarian tissues were fixed in 10% neutral buffered formalin for 48 hours. After fixation, the tissues were washed and dehydrated in a series of 70%, 90%, 96% and 100% ethanol, followed by clearing with xylene. After being held in hot paraffin, the tissues were embedded into paraffin blocks using a paraffin embedding device (Leica EG, 1160). Serial sections of 5 μm thickness were obtained from paraffin-embedded right ovarian tissue blocks using a microtome (Leica, RM 2245). Sections of the left ovarian tissues, also 5 μm thick, were mounted on poly-L-lysine-coated slides (Poly-Lysine, Thermo Fisher Scientific, 165014).

3.5.3. Hematoxylin&Eosin Staining Protocol

Sections obtained for morphological analysis and follicle counting were stained with hematoxylin and eosin (H&E). All sections were deparaffinized by incubating in a 60°C oven for 40 minutes. Subsequently, they were immersed in xylene for 2x20 minutes to completely remove paraffin. After deparaffinization, the sections were passed through alcohol series (100%, 96%, 90%, 80% and 70%). Following a wash with distilled water, the sections were stained for 2 minutes with hematoxylin (Gill's hematoxylin No.3, Bio-Optica, 05-06015/L). After staining with hematoxylin, the

sections were rinsed in running tap water and then stained for 1 minute with eosin (Eosin Y Alcoholic Solution, Bio-Optica, 05-10003/L). After a 2-minute wash with distilled water, the sections were dehydrated in increasing alcohol series. Following a 40-minute incubation in xylene, the sections were coverslipped using a xylene-based mounting medium (Bio Mount HM, Bio-Optica, 05-BMHM500). All stained sections were examined using a light microscope (Leica, CTR 6000).

3.5.4. Periodic Acid-Schiff (PAS) Staining Protocol

Following deparaffinization and hydration of tissue sections, ovarian tissue sections were stained with the Periodic Acid-Schiff Kit (Periodic Acid-Schiff, Bio Optica, 04-130802). The sections were soaked in periodic acid solution for 10 minutes and then washed with distilled water. Subsequently, they were soaked in Schiff Reagent solution for 20 minutes and washed with distilled water. Sections, after being soaked in potassium metabisulfite solution for 2 minutes, were then kept in fixative solution for an additional 2 minutes without washing. After washing with distilled water, they were soaked in Mayer's hematoxylin for 3 minutes and rinsed in running tap water. Following dehydration in increasing alcohol series, the sections were coverslipped using a xylene-based mounting medium. Preparations were examined under a light microscope to evaluate the integrity of the zona pellucida.

3.5.5. Histopathological Assessment

Histopathological evaluation using light microscopy was performed on sections stained with H&E to determine tissue damage and its severity (follicular cell degeneration, vascular congestion/hemorrhage, and inflammation). Scoring was done on a scale of 0-3 based on the severity of the damage. The scoring system was defined as follows: 0; no pathological findings, 1: mild, 2: moderate, 3: severe.

3.5.6. Follicle Counting in Hematoxylin&Eosin Stained Tissue Sections

Follicles in the entire right ovarian tissue were classified and counted in H&E stained preparations. To prevent the counting of the same follicle multiple times, only follicles where the oocyte nucleus was clearly visible were counted. The structure of primordial, primary, secondary, Graafian, cystic follicles, atretic follicles, and corpus luteum was counted. A primordial follicle was characterized by a single layer of flat granulosa cells surrounding the primary oocyte. A primary follicle was defined as having one or more layers of cuboidal granulosa cells surrounding the primary oocyte

(without the formation of an antrum). A secondary follicle showed the amass of follicular fluid among the cells of the granulosa layer and distinct layers of the theca interna and theca externa could be distinguished. A Graafian follicle was identified as having a single antral cavity containing follicular fluid, with the primary oocyte eccentrically located within the antrum. It exhibited a well-defined corona radiata and cumulus oophorus cells surrounding the primary oocyte. Atretic follicles were identified as follicles containing degenerate oocytes with a pycnotic nucleus and granulosa cells. A cystic follicle was identified as an enlarged follicle with a thin granulosa layer containing spaces filled with follicular fluid [106].

3.5.7. TUNEL Assay

The determination of apoptotic cells was carried out using the MyBiosource TUNEL Assay kit (MyBiosource, catalog no: MBS2557027). Sections affixed to poly-L-lysine-coated slides underwent deparaffinization by incubating at 60°C in an oven for 1 hour, followed by two 5-minute treatments in xylene for deparaffinization. They were then subjected to 2-minute incubations in alcohol series of 100%, 96%, 90%, 80% and 70% and washed three times for 5 minutes each with PBS. Subsequently, the sections were treated with Proteinase K for 30 minutes at room temperature. After three 5-minute washes with PBS, they were incubated in a blocking solution (3% hydrogen peroxide) for 10 minutes at room temperature. Another wash with PBS was performed. The sections were then incubated with Tdt enzyme at 37°C for 1 hour in an oven. Following a wash with PBS, the sections were treated with DAB for 1 minute and washed again with PBS. Counterstaining was carried out with Gill's hematoxylin. After washing with tap water, the sections were passed through alcohol series of 70%, 80%, 90%, and 100% and finally kept in xylene. The sections were sealed with coverslips using a xylene-based mounting medium. The apoptotic index was determined as the ratio of TUNEL-positive (+) cells to the total cell count in all follicle types [107].

3.5.8. Immunohistochemical Staining Protocol

A process of immunohistochemical staining was conducted on sections taken from slices affixed to slides coated with poly-L-lysine, with a thickness of 5 μm. This process aimed to identify the localization of StAR, 3β-HSD, CYP19A1, CTH and CBS proteins.

After incubating the sections in an oven at 60°C for 1 hour, they were deparaffinized by soaking them twice for 15 minutes each in xylene. Following this, the sections were subjected to a series of alcohol (100%, 96%, 90%, 80%, and 70%) for 3 minutes each and then washed with Phosphate Buffer Saline (PBS, pH=7.4). A citrate buffer was prepared by dissolving Sodium Citrate Tribasic Dihydrate (Sigma Aldrich, 6132-04-3) in distilled water. For antigen retrieval, the sections were microwaved at 300 watts for 1 minute in the prepared Citrate buffer (10 mM, pH 6.0). After cooling at room temperature and washing with PBS, the sections were treated with a 3% hydrogen peroxide solution in methanol for 10 minutes to block endogenous enzymes. Following the PBS wash, the sections were subjected to a blocking step (2.5% Normal Horse Serum, Vector Laboratories, 30022) for 30 minutes. Subsequently, the sections were immersed overnight at +4°C in a refrigerator with a mixture of primary antibodies prepared in PBS: StAR Polyclonal Antibody (Invitrogen, catalog no. PA5-106859) at a 1:100 dilution, 3β-HSD Polyclonal Antibody (Invitrogen, catalog no. PA5-27791) at a 1:500 dilution, CYP19A1 Polyclonal Antibody (Invitrogen, catalog no. PA5-86466) at a 1:200 dilution, CTH Polyclonal Antibody (Invitrogen, catalog no. PA5-29725) at a 1:100 dilution, and CBS Polyclonal Antibody (Invitrogen, catalog no. PA5-94923) at a 1:200 dilution. The next day, after two 5-minute washes with PBS, the sections were treated with biotinylated pan-specific secondary antibody (Vector Laboratories, 30144) for 30 minutes. Following another PBS wash, the sections were incubated for 30 minutes in streptavidin/peroxidase complex (Vector Laboratories, 30143), then treated for 1 minute with a mixture of 1:20 DAB and DAB substrate after a PBS wash. After rinsing with distilled water, a 2-minute counterstain was applied using hematoxylin (Gill's hematoxylin No.3, Bio-Optica, 05-06015/L), followed by washing under running tap water. The sections were dehydrated through alcohol series of 70%, 80%, 90% and 100%, followed by xylene and eventually sealed with a xylene-based mounting medium using a coverslip.

The intensity and distribution of StAR, 3β-HSD, CYP19A1, CTH, and CBS expression were assessed using the semi-quantitative H-Score (Histo Score/H-Score) method. This method involves calculating the H-Score by multiplying the percentages of positively stained cells with their respective weighted staining intensities. The formula for the H-Score is expressed as: $HSCORE= \sum_i P_i (i + 1)$. In this equation Pi represents the percentage of cells stained at each intensity level (%0-100) and i

corresponds to the staining intensity, with i= 1 denoting weak, i= 2 indicating moderate and i=3 representing strong staining [108,109].

3.6. Molecular Analyses

3.6.1. Quantitative Real Time Polymerase Chain Reaction (qRT-PCR)

3.6.2. RNA Extraction, cDNA Creation and Analysis of Gene Expression

The qRT-PCR method was employed to detect the mRNA expression levels of StAR, 3β-HSD, CYP19A1, CTH and CBS in the ovarian tissues of the experimental groups. Ovarian tissues were preserved at -80°C until RNA isolation was conducted.

Ovarian samples were initially on ice and homogenized using a Bullet Blender X24 (NextAdvance) in 500 µL TRIzol at Speed 10 for 5 minutes. RNA was extracted following the protocols provided by the DirectZol™ RNA MiniPrep Plus kit (Zymo Research, R2072). The homogenates obtained were centrifuged at 10,000 G for 2 minutes. Post-centrifugation, the upper phase containing RNA was transferred to clean 1.5 mL tubes. Subsequently, 500 µL of 100% ethanol was added, thoroughly mixed and the solution was transferred to tubes containing RNA isolation columns. After centrifugation at 10,000 G for 30 seconds, the solution remaining in the Eppendorf tubes was discarded and the RNA-containing columns were washed with 400 µL RNA Wash buffer and centrifuged at 10,000 G for 30 seconds. The columns were then transferred to newly autoclaved tubes.

A solution of 5 µL DNase + 75 µL DNA digestion buffer was prepared and a total of 80 µL of the solution was transferred to the columns, followed by a 15-minute incubation at room temperature. After incubation, the columns were washed with 400 µL RNA Prep buffer. Following centrifugation at 10,000 G for 30 seconds, the columns were washed with 700 µL RNA Wash buffer and centrifuged at 10,000 G for 30 seconds. After an additional wash with 400 µL RNA Wash buffer, the columns were centrifuged at 10,000 G for 1 minute. The purity and concentration of the obtained RNA samples were determined using the NanoDrop® ND-100 spectrophotometer. The samples were stored at -20°C until analysis.

The obtained RNA was quantified and cDNA was synthesized according to the instructions of the iScript™ cDNA Synthesis Kit (Bio-Rad, 1708891) using an equal amount of RNA (200 ng). Primer sequences for the genes Cth, Cbs, CYP19A1, 3β-HSD, StAR and β-Actin were formulated using the online tool Primer3web version

4.1.0 (https://primer3.ut.ee/) and specific primer sequences for each gene are detailed in Table 2. Subsequently, gene sequences were amplified by qRT-PCR using Insta Q96® Plus (HiMedia) and SsoAdvanced™ Universal SYBR® Green Supermix (Bio-Rad, 1725270). Comparative gene expression analysis relative to the control group was performed using the $2^{-\Delta\Delta CT}$ method. Thermal cycling conditions are provided in Table 3. The specificity of each primer and the presence of primer dimers were investigated through the melt curve step performed at the end of PCR cycles.

Table 1. Primers for *Cth, Cbs, CYP19A1, 3β-HSD, StAR* and *β-Actin* used in qRT-PCR.

Primer ID	Sequence (5′-3′)
Cth_F	AAAGCACTGTTTGACCTTCG
Cth_R	GCCTCCATACACTTCATCCA
Cbs_F	CTCACATCTCCCTCCTTTCC
Cbs_R	AGGCACTCATTCCAGGAAAA
CYP19A1_F	GTGTTGAGGGTAAGTGGGAA
CYP19A1_R	GGAGCACGAACTGAGAGTAA
3β-HSD_F	TTGGTGCAGGAGAAAGAACT
3β-HSD_R	TAACATTGTCACCTTGGCCT
StAR_F	AACATGAAAGGACTGAGGCA
StAR_R	AGTGTTGCTTCCAGTTGAGA
β-Actin_F	TCTTCCAGCCTTCCTTCCTG
β-Actin_R	CACACAGAGTACTTGCGCTC

F: Forward, R: Reverse

Table 2. qRT-PCR Protocol for *Cth, Cbs, CYP19A1, 3β-HSD* and *StAR.*

Step	Temperature	Duration	Number of Cycles
Initial Denaturation	95 ºC	30 sec	1
Denaturation	95 ºC	15 sec	
Annealing	52 ºC	20 sec	45
Extension	60 ºC	20 sec	

3.7. Statistical Analysis

The statistical analyses were conducted using GraphPad Prism version 10.0.2 software. The data are expressed as mean ± standard deviation. The normal distribution of the data was assessed using the Shapiro-Wilk normality test. For data conforming to normal distribution, a one-way analysis of variance (ANOVA) followed by Tukey's multiple comparison test was performed. For data not conforming to normal distribution, the Kruskal-Wallis test followed by Dunn's multiple comparison test was used for evaluation. $p < 0.05$ values were considered statistically significant.

4. RESULTS

4.1. Biochemical Findings

To confirm the establishment of the PCOS experimental model in rats, serum specimens were obtained both pre and post experiment and ELISA analysis was performed to determine the serum E_2 and P values.

4.1.1. Serum E_2 Level

Standard concentration measurements were made in serum samples before and after the experiment to obtain a standard curve graph (Figure 20). When comparing serum E_2 levels in all groups before and after the experiment, a notable increase in serum E_2 levels experienced of the PCOS group after DHEA treatment (Figure 21).

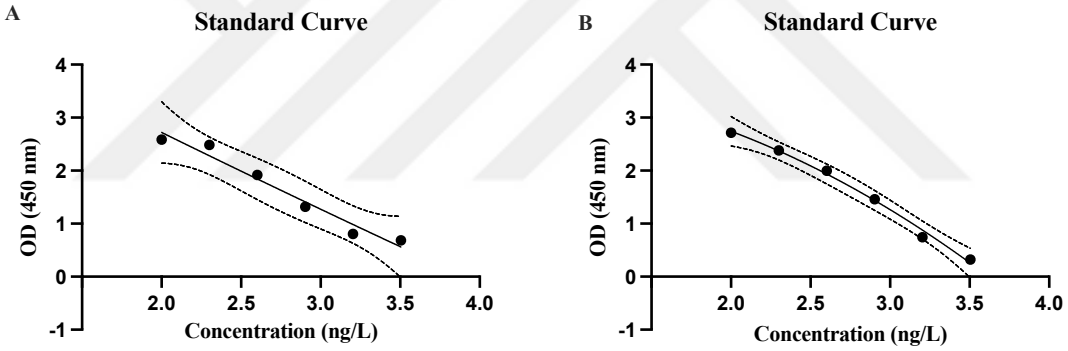

Figure 20. E_2 Standard Concentration Curve. A) Before the experiment. B) After the experiment.

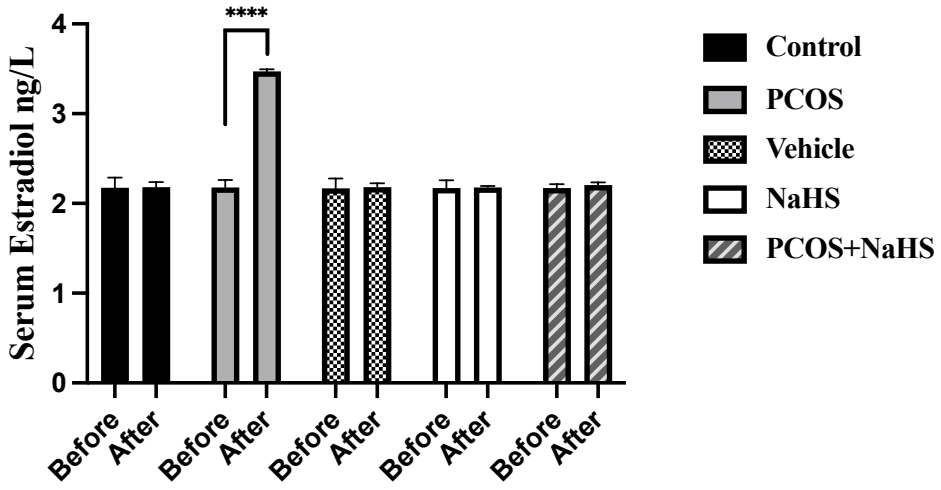

Figure 21. Comparison of serum E2 levels between groups before and after the experiment. ****: p<0.0001.

4.1.2. Serum P Level

Standard concentration measurements were performed on pre-experiment and post-experiment serum samples to obtain a standard curve (Figure 22). When comparing serum P levels before and after the experiment in all groups, a notable increase in serum P levels experienced of the PCOS group after DHEA treatment (Figure 23).

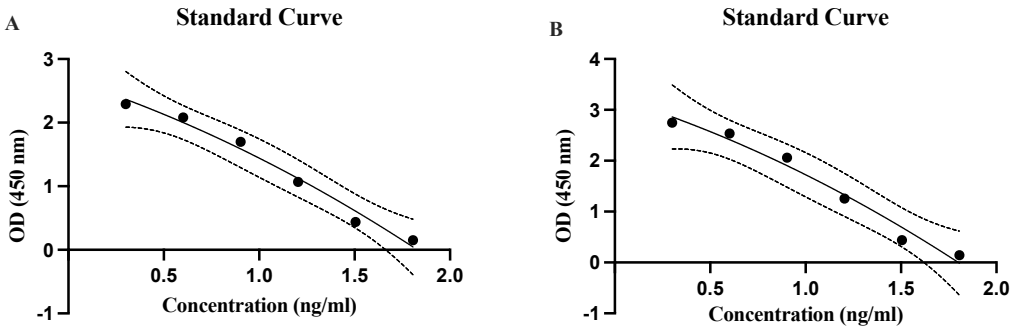

Figure 22. Progesterone Standard Concentration Curve. A) Before the experiment. B) After the experiment.

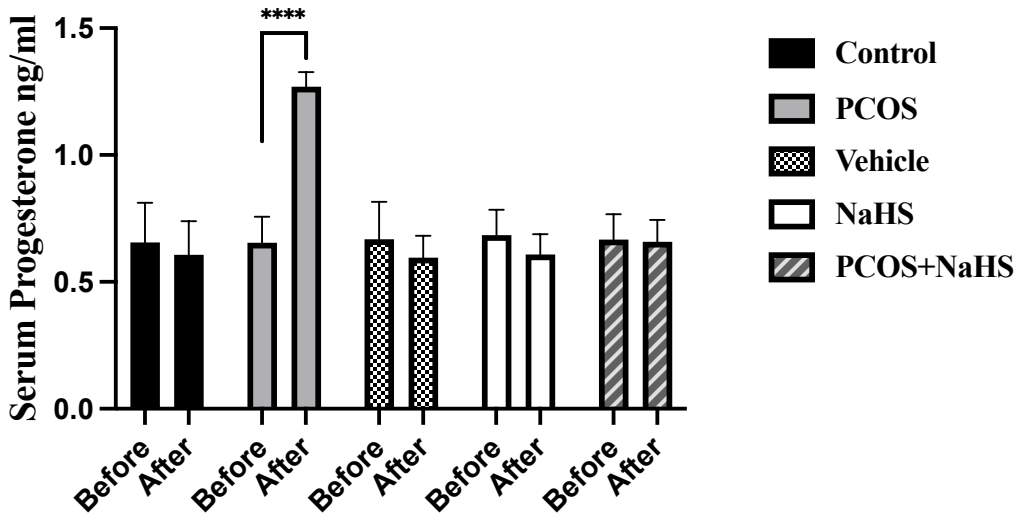

Figure 23. Comparison of serum P levels between groups before and after the experiment. ****: $p<0.0001$.

4.2. Histological Findings

4.2.1. Vaginal Smear Observations

As oligoovulation/anovulation is a prominent feature of PCOS, vaginal smear samples from all groups of rats were analyzed for monitoring the estrous cycle. Through daily analysis of vaginal smears over a period of 20 days, it was saw that rats in the control, solvent and NaHS groups exhibited all stages of the estrous cycle. Furthermore, they displayed a more consistent estrous cycle along with normal cycle lengths. In contrast, rats in the PCOS group exhibited noteworthy irregularities in their estrous cycles upon examination of vaginal smear samples. Following consecutive cycle monitoring, it was noted that rats in this group were consistently blocked in the diestrus stage, failing to display proestrus, estrus, and metestrus stages. When examining vaginal smear samples from the PCOS+NaHS group, it was observed that, unlike the PCOS group, they exhibited a more consistent estrous cycle. Additionally, animals in this group were found to display all phases of the estrous cycle similar to the control, vehicle, NaHS groups (Figure 24).

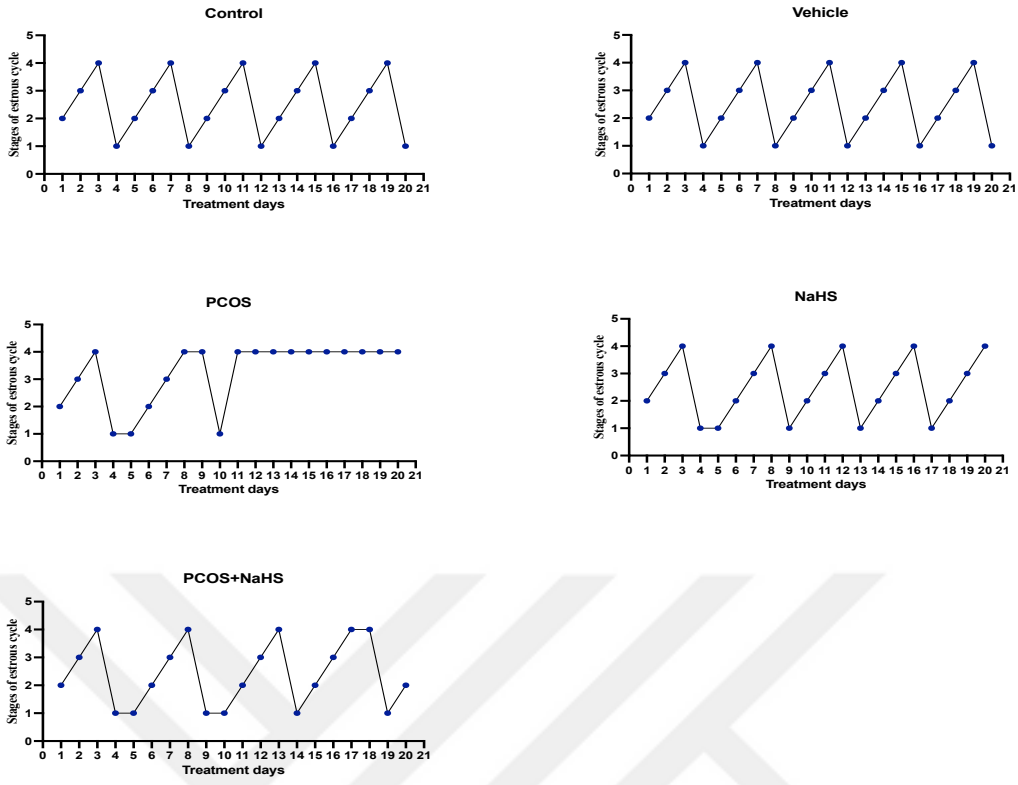

Figure 24. Estrous cycle changes in representative rats from 5 groups. 1=proestrus-nucleated epithelial cells, 2=estrous stage-cornified cells, 3=metestrus stage-nucleated, cornified and leucocytes, 4=diestrous stage-leucocytes.

At the conclusion of the experiment, the percentage of days in each estrous cycle stage was calculated for all groups and estrous cycle durations were compared. Regarding the proestrus index, no significant differences were found among the control, vehicle, NaHS and PCOS+NaHS groups. However, a remarkable distinction was identified among the PCOS group with the other four groups, indicating a lower proestrus index in the PCOS group ($p < 0.0001$).

When comparing the estrus index among groups, no statistical differences were observed among the control, vehicle, NaHS and PCOS+NaHS groups. In contrast, a significant decrease in the estrus index was noted in the PCOS group as compared with the other groups ($p < 0.0001$).

For the metestrus index, no differences were found when evaluating the control, vehicle, NaHS, PCOS+NaHS groups. However, in the PCOS group, the metestrus index was found to be lower than in the other groups ($p < 0.0001$).

Comparing the diestrus index among groups, a significant increase was observed in the PCOS group ($p < 0.0001$), while no differences were determined among the control, vehicle, NaHS and PCOS+NaHS groups.

In summary, considering all results, the PCOS group exhibited a decrease in the proestrus, estrus, and metestrus indices and a notable enhance in the diestrus index as compared with the control, vehicle, NaHS, PCOS+NaHS groups (Figure 25).

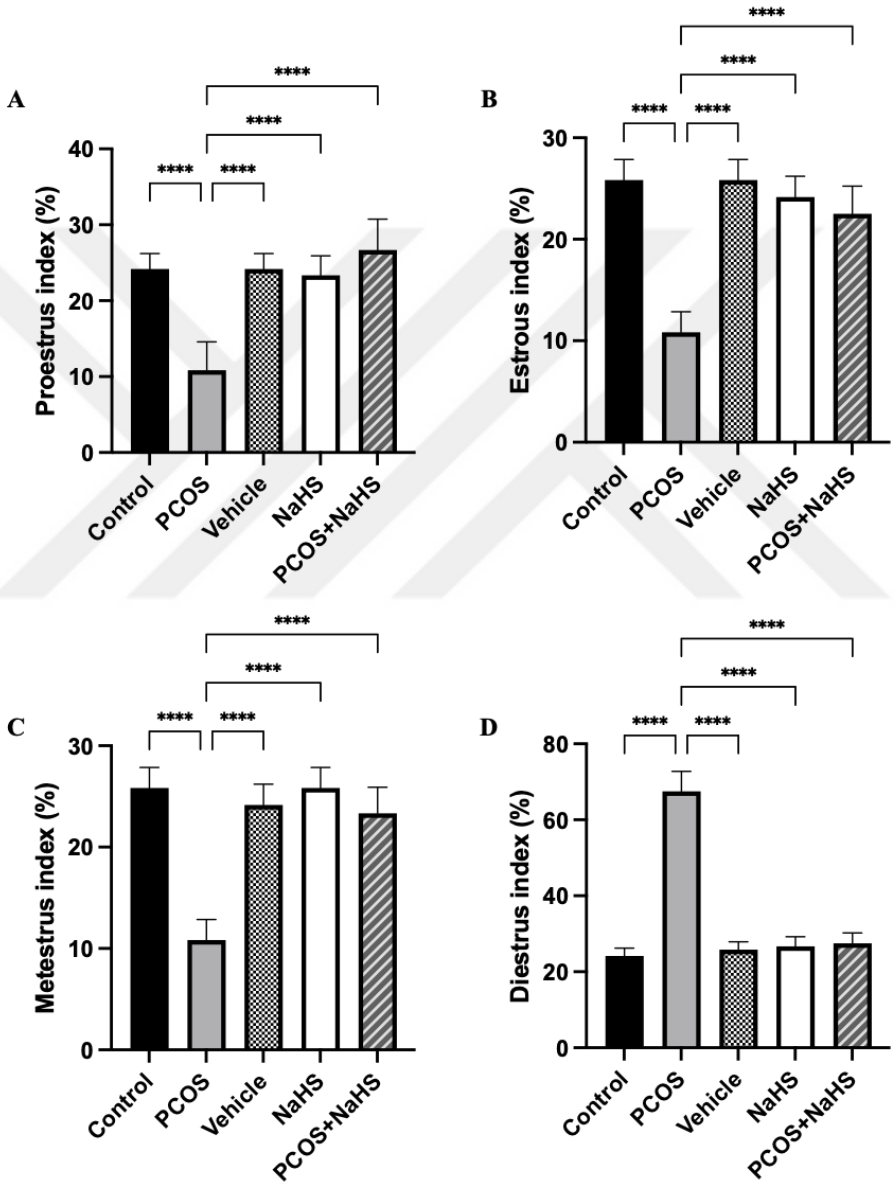

Figure 25. Proestrus, estrus, metestrus and diestrus indices of the experimental groups ****: $p<0.0001$.

4.2.2. Histopathological Findings

Ovarian tissue sections stained with H&E were examined under a light microscope for each group. In the ovarian tissue sections of the control group and vehicle group, the ovary surface was surrounded by a single layer of flat or single-layered cubic epithelium (germinal epithelium). Beneath the germinal epithelium, the tunica albuginea was observed. Numerous ovarian follicles at different stages of development were observed in the cortex layer and these follicles appeared normal. There was no degeneration observed in granulosa cells, and the theca cells were seen as uniformly arranged cells around the follicles. Many corpus luteum structures were present. The theca layer, blood vessels in the medulla and the ovarian stroma appeared normal (Figure 26, Figure 27).

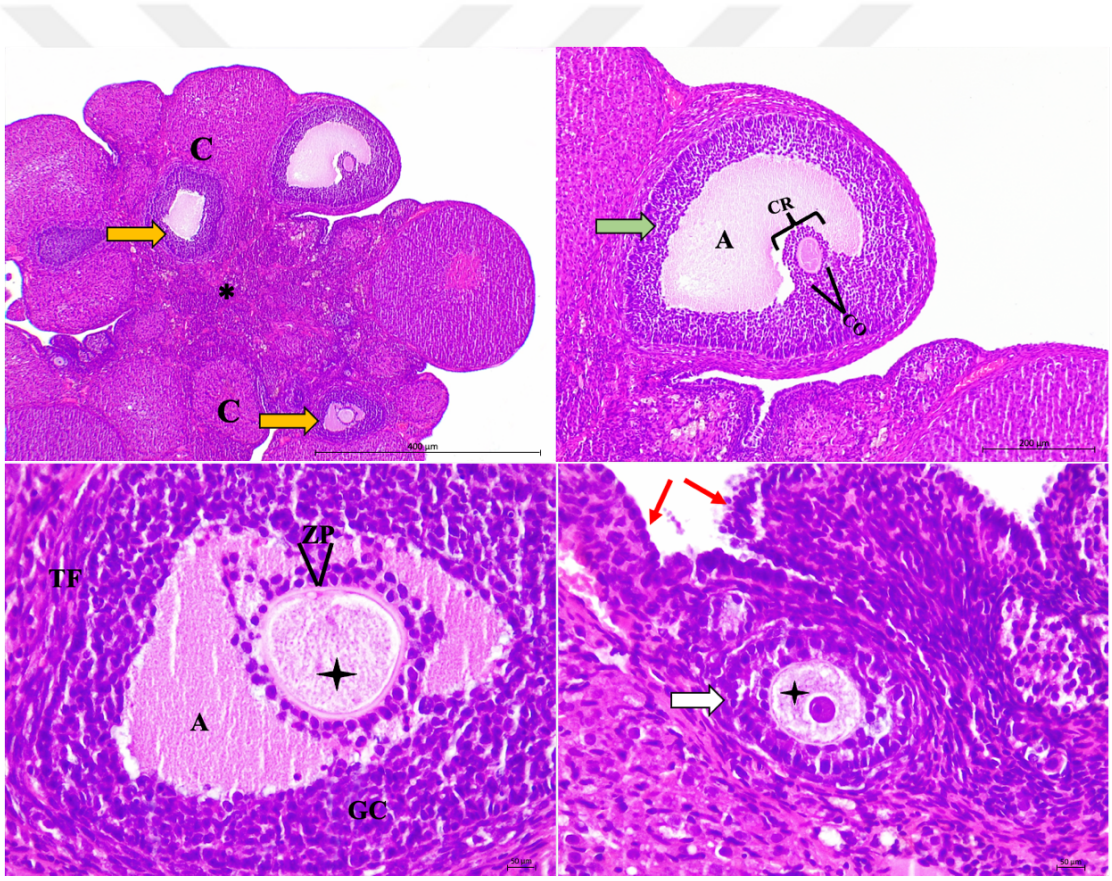

Figure 26. Ovarian sections from the control group stained with H&E. Yellow arrow: secondary follicle, *: medullary region, C: cortex region, CO: cumulus oophorus, CR: corona radiata, green arrow: Graafian follicle, A: antrum, four-pointed star: oocyte, GC: granulosa cells, TF: theca folliculi, ZP: zona pellucida, red arrow: germinal epithelium, white arrow: primary follicle. The scale bar represents 400 µm, x4, 200 µm, x10, and 50 µm, x40.

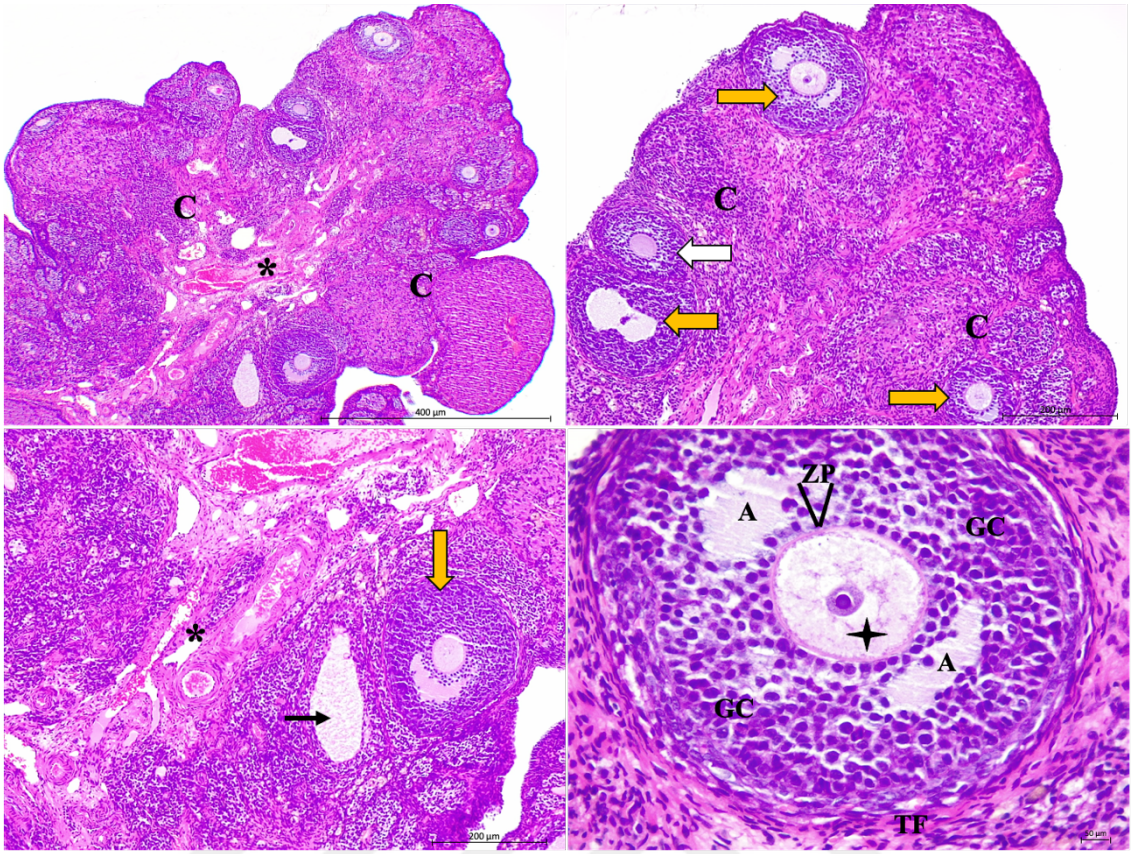

Figure 27. Ovarian sections from the vehicle group stained with H&E. C: cortex region, *: medullary region, yellow arrow: secondary follicle, white arrow: primary follicle, black arrow: atretic follicle, A: antrum, GC: granulosa cell, ZP: zona pellucida, four-pointed star: oocyte, TF: theca folliculi. The scale bar represents 400 µm, x4, 200 µm, x10, and 50 µm, x40.

In the ovarian tissue sections from the PCOS group, numerous cystic follicular structures filled with fluid were observed at different stages of development, along with ovarian follicles. The zona pellucida structures exhibited a loose and occasionally dilated appearance, losing their normal features. Many granulosa cells were observed to have apoptotic nuclei, suggesting the apoptotic condition of these cells. Some follicles that failed to complete development became atretic follicles, while others turned into cystic follicles filled with fluid, mostly losing their oocytes. Some cystic follicles showed the presence of degenerative oocytes. Additionally, granulosa cells were observed in the lumen of some cystic follicles. The ovarian stroma exhibited a hyperplastic and edematous structure. However, dilation and hypervascularization in the theca layer and medullary vessels have been identified. The occasional presence or

absence of corpus luteum structures in this group indicates disrupted ovulation. Animals in this group were observed to have anovulatory/oligoovulatory cycles (Figure 28).

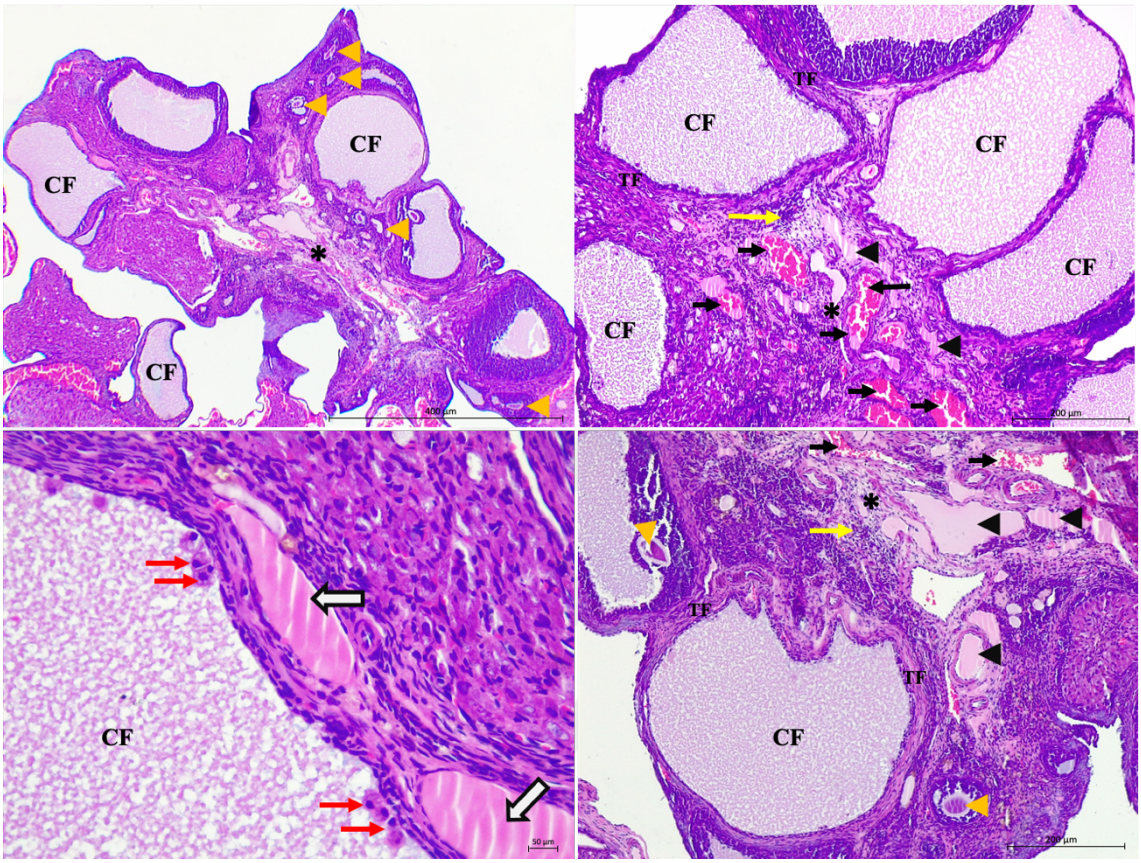

Figure 28. Ovarian sections from the PCOS group stained with H&E. *: medullary region, CF: cystic follicle, yellow arrowhead: follicles leading to degenerated atresia, black arrow: vascular congestion, black arrowhead: hyalinization in vessels, yellow arrow: inflammatory cells, red arrow: granulosa cells spilling into the antrum of cystic follicles, white arrow: dilation in vessels of the theca layer, TF: thickened theca layer. The scale bar represents 400 µm, x4, 200 µm, x10, and 50 µm, x40.

When ovarian tissue sections from the NaHS group were histologically examined, morphologically similar findings to the control and vehicle groups were observed. Numerous follicular structures with normal morphology at different stages of development were observed in the ovarian tissue. A significant presence of corpus luteum structures was noted. This indicates that there were no irregularities in ovulation in the NaHS group. The medulla was characterized by vascularized connective tissue (Figure 29).

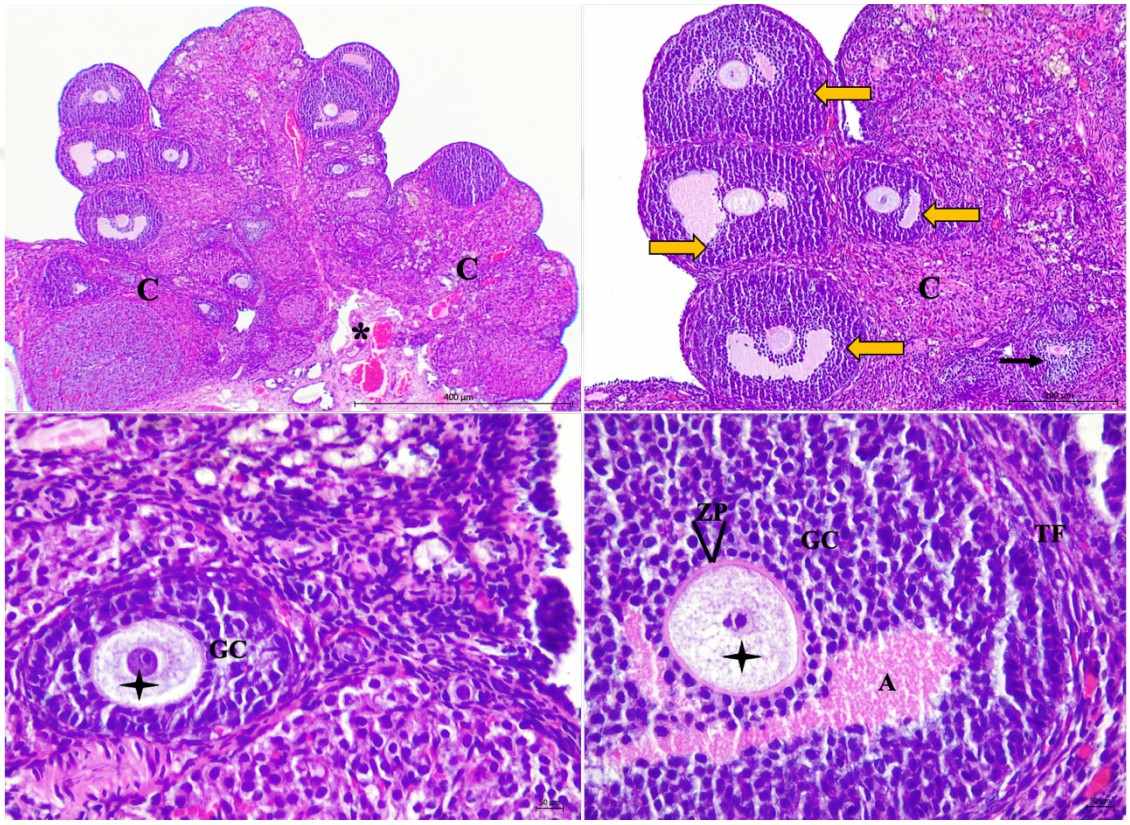

Figure 29. Ovarian sections from the NaHS group stained with H&E. C: cortex region, *: medullary region, yellow arrow: secondary follicle, black arrow: atretic follicle, four-pointed star: oocyte, GC: granulosa cells, ZP: zona pellucida, A: antrum, TF: theca folliculi. The scale bar represents 400 µm, x4, 200 µm, x10, and 50 µm, x40.

When the ovarian tissue sections of the PCOS+NaHS group were histologically examined, cystic follicle structures were observed sporadically in the cortex. However, compared to the PCOS group, it was determined that there were fewer cystic follicle structures in this group. The granulosa cell layer in the follicle structures exhibited morphological features close to those in the control, vehicle, and NaHS groups. In the ovarian tissue of this group, the follicles were observed to begin forming antrum, the corona radiata took shape and the zona pellucida structure assumed its normal appearance. The theca layer appeared normal. Additionally, it was observed that there were fewer atretic follicle structures in this group compared to the PCOS group. Furthermore, in this group, there were more corpus luteum structures as compared with the PCOS group. It is evident that there is no irregularity in ovulation in the PCOS+NaHS group (Figure 30).

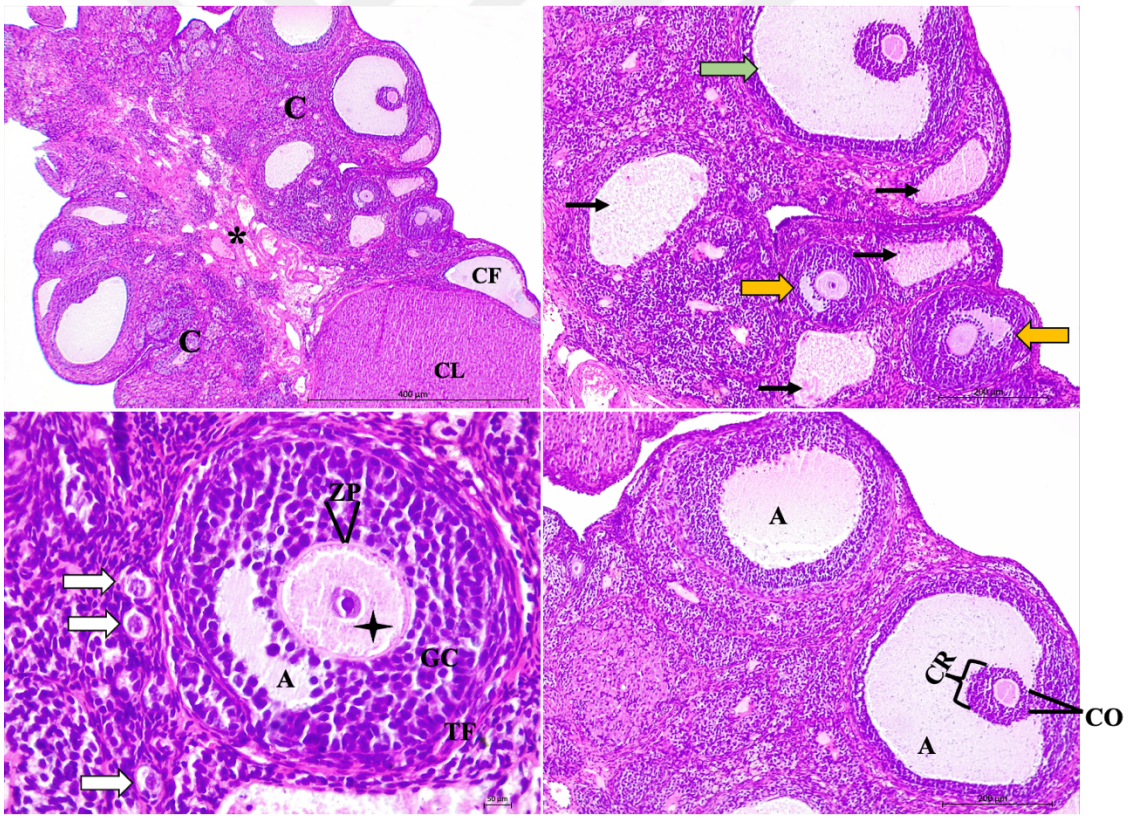

Figure 30. Ovarian sections from the PCOS+NaHS group stained with H&E. C: cortex region, *: medullary region, CL: corpus luteum, black arrow: atretic follicle, CF: cystic follicle, yellow arrow: secondary follicle, green arrow: Graafian follicle, white arrow: primordial follicle, A: antrum, four-pointed star: oocyte, ZP: zona pellucida, TF: theca folliculi, CR: corona radiata, CO: cumulus oophorus. The scale bar represents 400 µm, x4, 200 µm, x10, and 50 µm, x40.

The comparison of histopathological scorings for the ovarian tissue in different groups is presented in Figure 31.

In the control, vehicle and NaHS groups, follicular degeneration was observed in very small areas, with no statistically remarkable distinction among the groups. In the PCOS group, remarkable enhance in follicular cell degeneration as compared with other groups was determined ($p<0.0001$). In the PCOS+NaHS group, it was identified that follicular cell degeneration was less than that in the PCOS group. There was no statistical significance in terms of follicular degeneration among the PCOS+NaHS group with the Control, Vehicle, NaHS groups.

When tissue sections were evaluated for vascular congestion, it was observed that there were very few hemorrhagic areas in the control, vehicle and NaHS groups. In the PCOS group, an enhance in vascular congestion was determined ($p<0.0001$). Statistically remarkable distinction were identified in terms of having fewer hemorrhagic areas in the PCOS+NaHS group as compared with the PCOS group ($p<0.0005$). There was no statistically remarkable distinction among the PCOS+NaHS group with the Control, Vehicle, NaHS groups.

In the ovarian tissue sections of the control, vehicle and NaHS groups, no signs of inflammation were observed. However, in the PCOS group, the inflammation rate was determined to be significantly higher than in the other groups ($p<0.0001$). Although signs of inflammation were found in the PCOS+NaHS group, no statistically remarkable distinction was detected when compared to the control, vehicle and NaHS groups. Compared to the PCOS group, remarkable diminish in inflammation determined in the PCOS+NaHS group ($p<0.0001$).

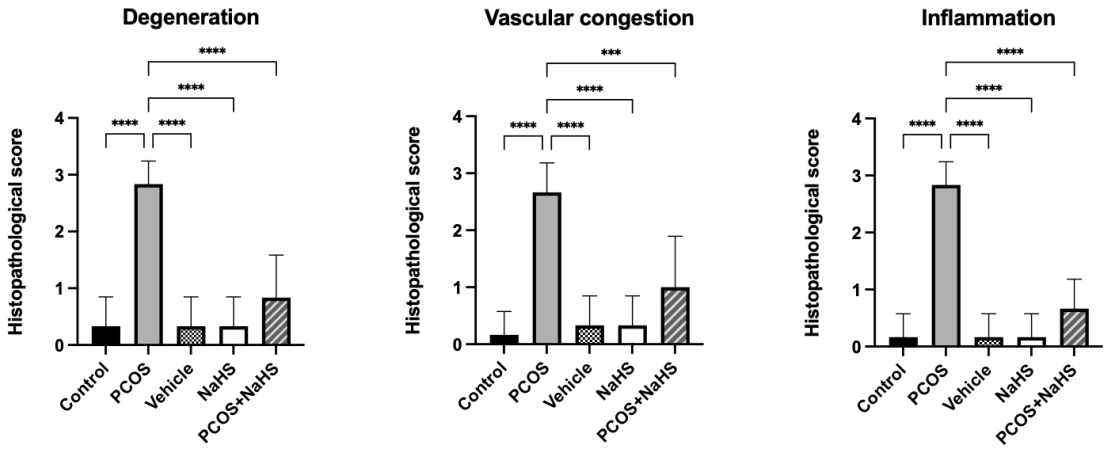

Figure 31. Histopathological score graph for the groups. ****: p<0.0001, ***: p<0.0005.

4.2.3. Periodic Acid-Schiff Staining Results

PAS staining was performed on ovarian tissue from all experimental groups to assess the integrity of the zona pellucida. In the control group, developing follicles showed positive PAS reaction in the zona pellucida surrounding the oocytes. In the vehicle and NaHS groups, a PAS-positive reaction similar to the control group was observed. In ovarian tissue sections from the PCOS group subjected to PAS staining, weak staining with PAS indicating zona pellucida degeneration was present. In the PCOS+NaHS group, PAS-positive reactions similar to the control group were observed. The PAS staining results for the PCOS+NaHS group indicated less zona pellucida degeneration compared to the PCOS group (Figure 32).

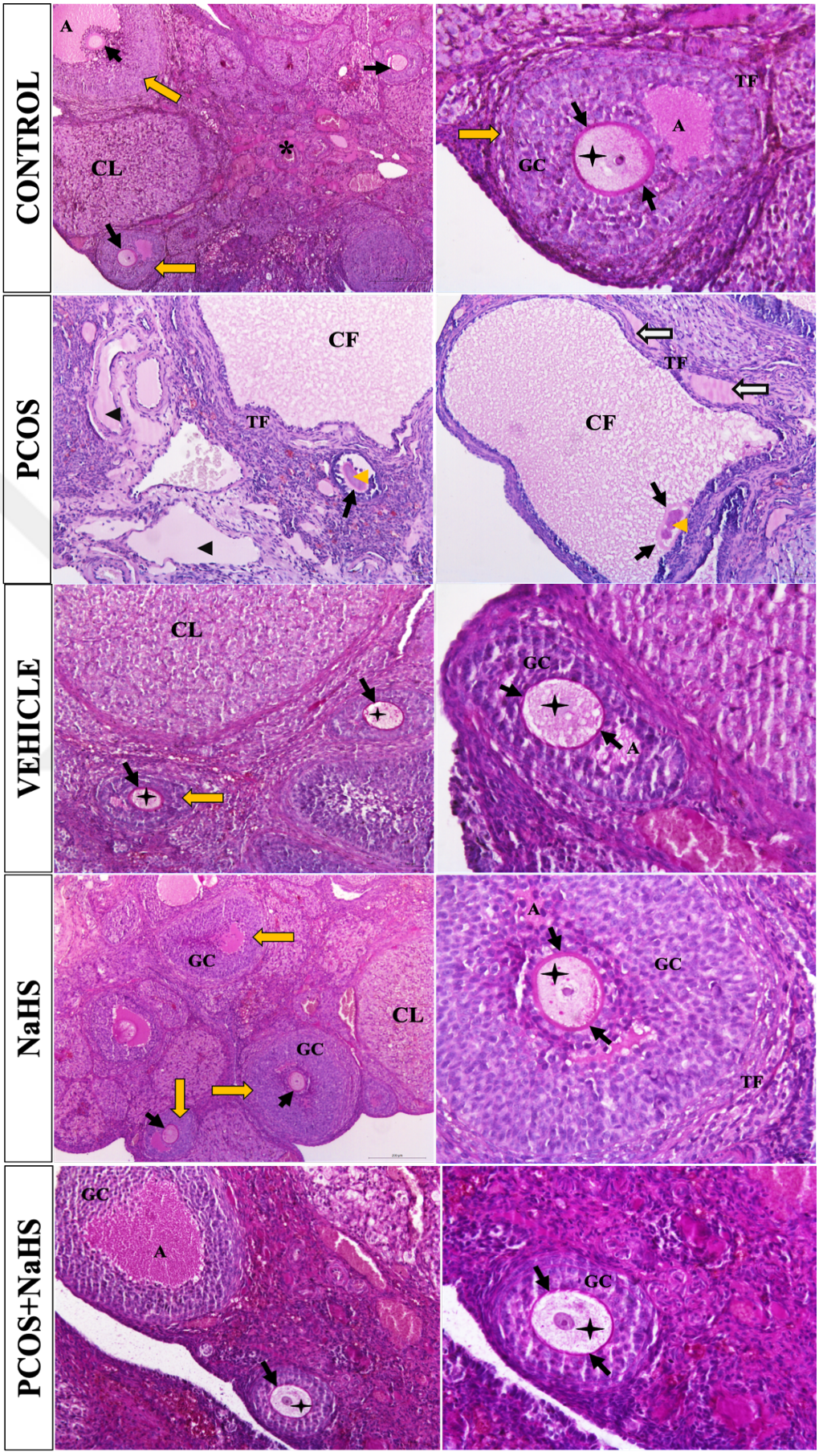
CONTROL
A
CL
*
TF
A
GC
PCOS
CF
TF
TF
CF
VEHICLE
CL
GC
A
NaHS
GC
CL
GC
A
GC
TF
PCOS+NaHS
GC
A
GC

Figure 32. PAS staining for each group. Black arrows: zona pellucida, CF: Cystic Follicle. *: medullary region, TF: theca layer, black arrowhead: hyalinization in vessels, white arrow: dilation in vessels of the theca layer, A: antrum, GC: granulosa cell, four-pointed star: oocyte, yellow arrow: secondary follicle, CL: corpus luteum, yellow arrowhead: degenerated oocyte. The scale bar represents 200 μm for x10 and 50 μm for x40 magnification. Black arrow: zona pellucida.

4.2.4. Follicle Counting Results

Upon statistical evaluation of follicle numbers across all groups, significant differences among the groups were identified through one-way ANOVA analysis for primordial, primary, secondary, Graafian, cystic, atretic follicle counts and corpus luteum numbers. The variations in counts of primordial, primary, secondary and Graafian follicles for each group are illustrated in Figure 33.

No statistically remarkable distinction was identified in the number of primordial follicles when comparing within the control, vehicle, NaHS and PCOS+NaHS groups. However, a notable decrease in the quantity of primordial follicles was noted in the PCOS group. This reduction was statistically remarkable in the PCOS group as compared with the control, vehicle, NaHS and PCOS+NaHS groups ($p < 0.0001$).

When comparing the number of primary follicles between groups, no remarkable distinction was found within the control, vehicle, NaHS and PCOS+NaHS groups. Conversely, the PCOS group displayed a statistically remarkable diminish in the number of primary follicles compared to all other groups ($p < 0.0003$).

Statistical significance wasn't identified in the number of secondary follicles among the control, vehicle, NaHS and PCOS+NaHS groups. However, a significant enhance in the number of secondary follicles was identified in the PCOS group compared to the control, vehicle, NaHS and PCOS+NaHS groups ($p < 0.0001$).

When evaluating the counts of Graaf follicles, a significant diminish in the number of Graaf follicles in the PCOS group was determined as compared with the counts in the control, vehicle, NaHS and PCOS+NaHS groups ($p < 0.0001$). There was no remarkable distinction difference in the counts of Graaf follicles when comparing within the control, vehicle, NaHS and PCOS+NaHS groups.

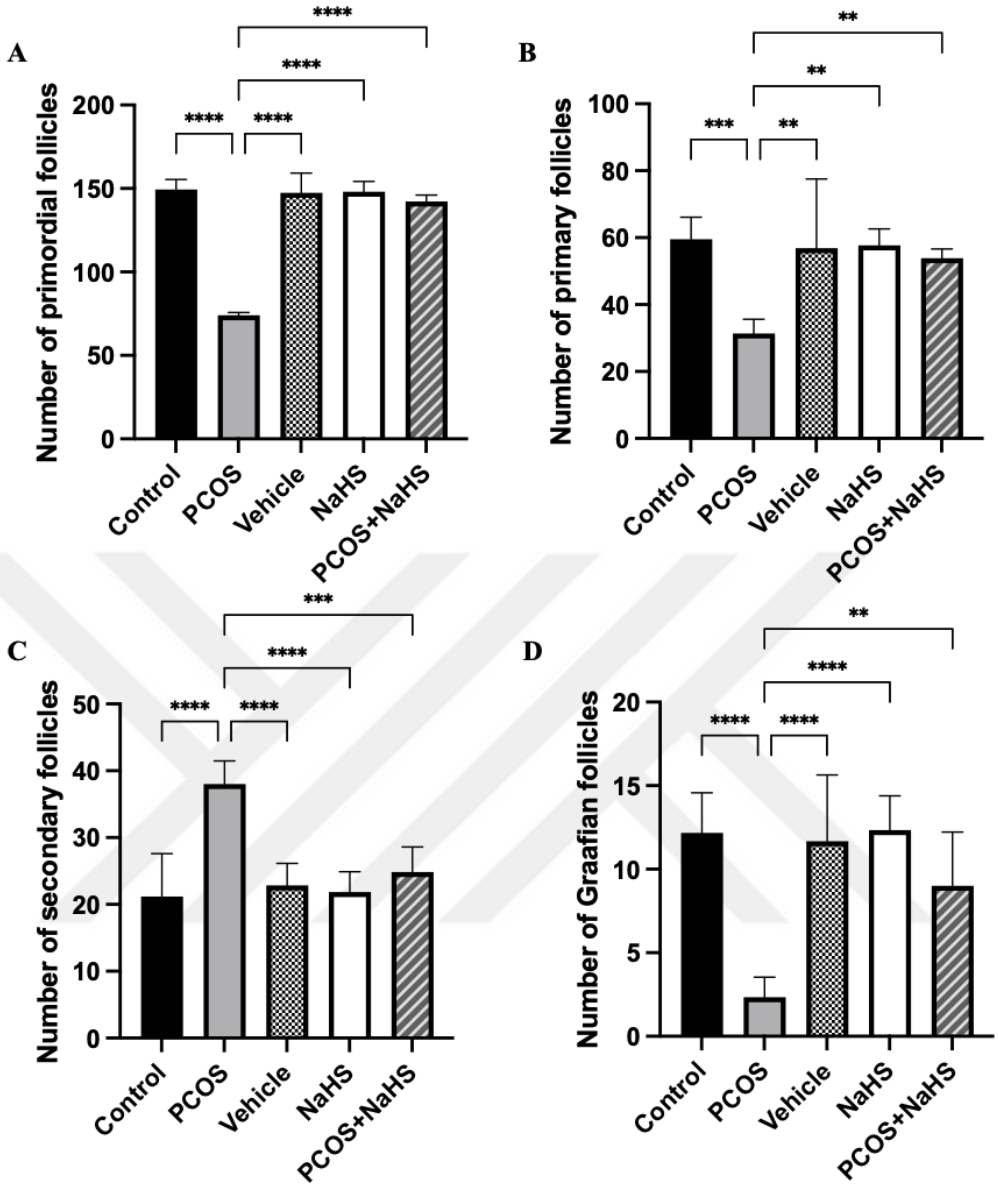

Figure 33. Comparison of follicle numbers among groups. A Primordial follicle count. ****: p<0.0001; compared to the PCOS group. B Primary follicle count. ***: p≤0.006; when compared between the Control and PCOS groups, **: p=0.0019; when compared between the PCOS and PCOS+NaHS groups. C Secondary follicle count. ****: p<0.0001; compared to PCOS; when compared to the Control, Vehicle and NaHS groups, ***: p≤0.0001; when compared between the PCOS and PCOS+NaHS groups. D Graafian follicle count. ****: p<0.0001; when compared to PCOS with the Control, Vehicle and NaHS groups, **: p≤ 0.0025; when compared between the PCOS and PCOS+NaHS groups.

The changes in the numbers of cystic, atretic follicles and corpus luteum in each group are presented in Figure 34.

When comparing the cystic follicle numbers between groups; there is no statistical significance in the control, vehicle and NaHS groups ($p<0.0001$). In contrast, the PCOS group showed a significant increase in cystic follicle numbers compared to other groups ($p<0.0001$). The PCOS+NaHS group exhibited a significantly lower number of cystic follicles compared to the PCOS group ($p<0.0001$). There was a significant difference in the cystic follicle numbers of the PCOS+NaHS group compared to the control, vehicle and NaHS groups ($p\leq0.0001$).

In the PCOS group, there was a significant increase in the number of atretic follicles ($p<0.0001$). Conversely, in the PCOS+NaHS group, the count of atretic follicles was found to be lower compared to the PCOS group ($p<0.0001$). No significant difference was observed in the atretic follicle numbers of the PCOS+NaHS group when compared to the control, vehicle and NaHS groups.

When comparing the numbers of corpus luteum across groups, a statistically significant decrease was identified in the PCOS group ($p<0.0001$). However, no significant difference was found in the numbers of corpus luteum between the control, vehicle and PCOS+NaHS groups.

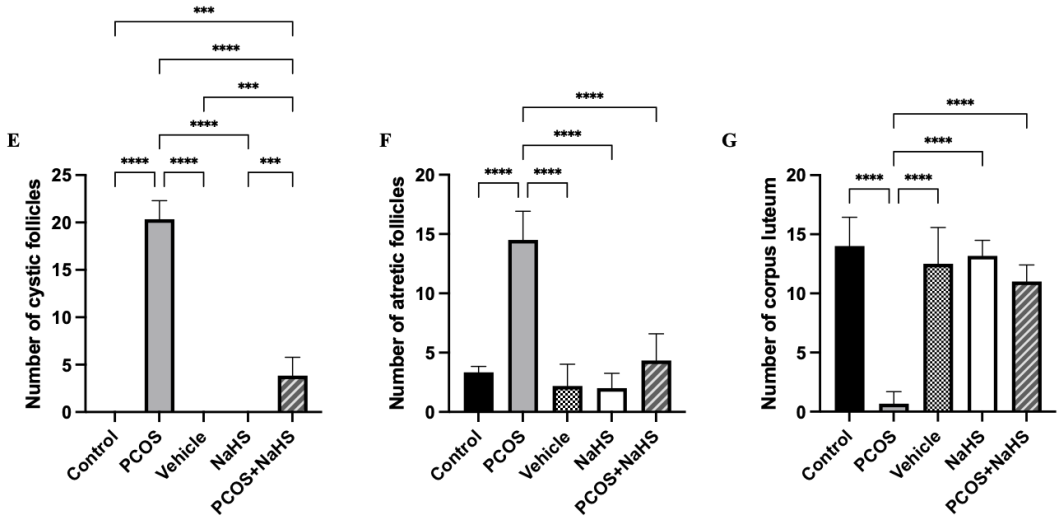

Figure 34. Comparison of the numbers of cystic, atretic follicles, and corpus luteum across groups. E Cystic follicle ****: $p<0.0001$; when compared to the PCOS group with the Control, Vehicle, NaHS and PCOS+NaHS groups, ***: $p\leq0.0001$; when compared to the Control, Vehicle and NaHS groups with the PCOS+NaHS group.

4.3. TUNEL Findings

Apoptotic cells in ovarian follicles of control and experimental groups were marked using TUNEL assay, and the apoptotic index was calculated. In this context, it was determined that the apoptotic index in follicles of the PCOS group significantly increased compared to the control, vehicle, NaHS and PCOS+NaHS groups ($p<0.0001$). However, no statistical significance was observed in the apoptotic index between the control, vehicle and NaHS groups. In the PCOS+NaHS group, the apoptotic index significantly decreased compared to the PCOS group ($p<0.0001$). Nevertheless, despite the decrease in the apoptotic index in the PCOS+NaHS group compared to the PCOS group, it was found to be higher than the apoptotic index values in the control, vehicle and NaHS groups. This difference was statistically significant between the PCOS+NaHS group and the control, vehicle and NaHS groups in terms of apoptotic index values ($p<0.0001$) (Figure 35, Figure 36).

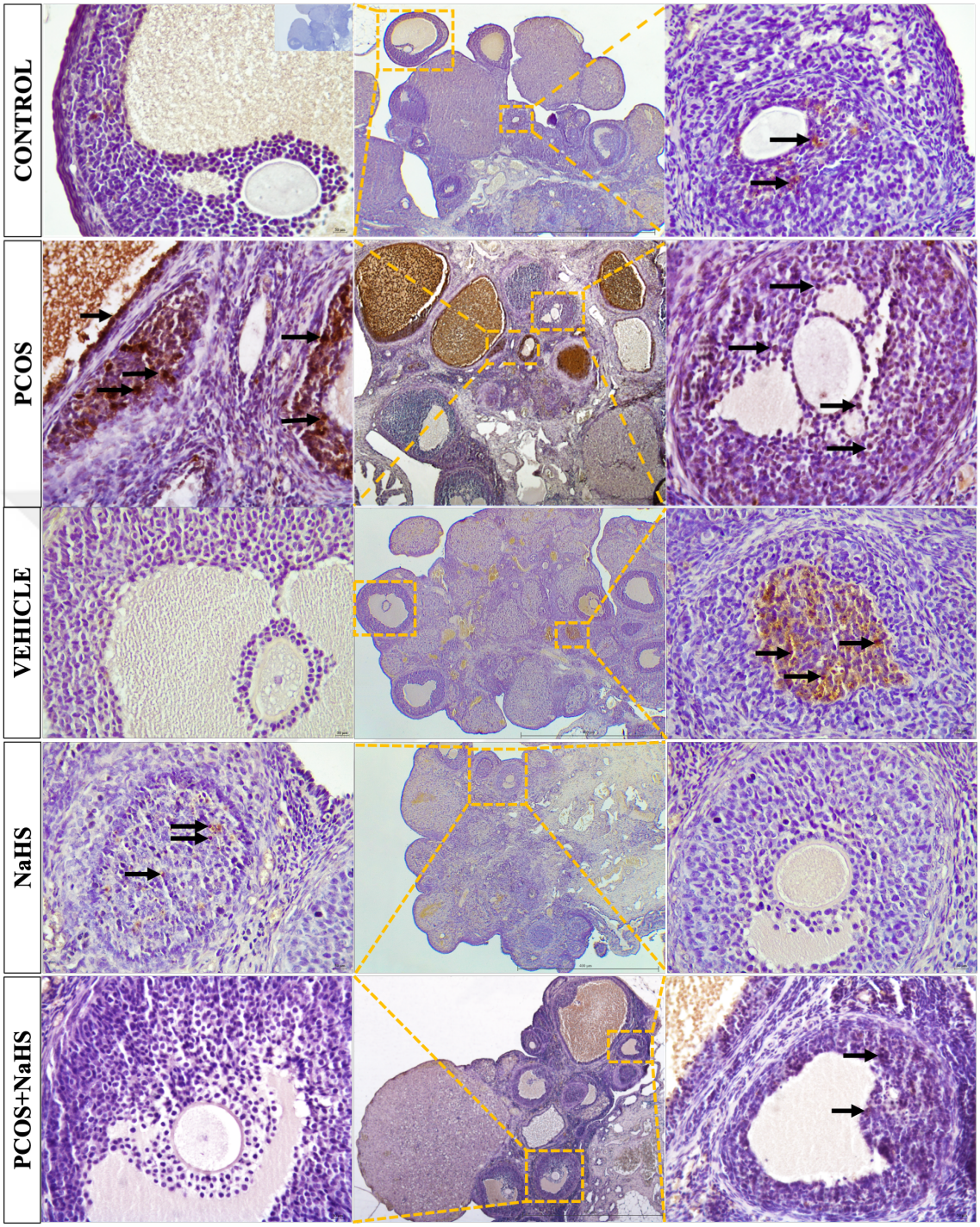

Figure 35. Apoptotic follicles in ovarian tissues of the groups shown by TUNEL assay. Black arrows indicates TUNEL (+) cells. The scale bar represents 400 µm, x4, 200 µm, x10, and 50 µm, x40.

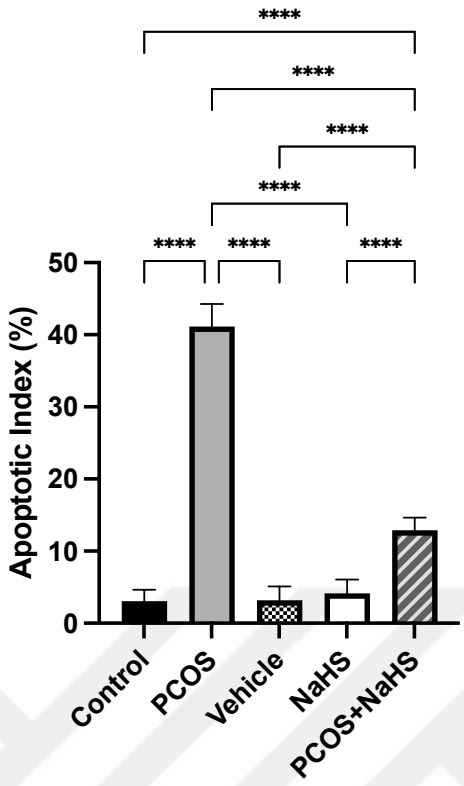

Figure 36. Apoptotic index graph of the groups. ****: p<0.0001.

4.4. Immunohistochemical Results

4.4.1. Immunohistochemical Localization of Steroidogenic Proteins

In the regulation of reproductive functions in the ovaries, steroidogenesis pathways play a crucial role in the generation of estrogen and progesterone hormones. This process occurs through the collaboration of the theca and granulosa cells. In our study, we applied immunohistochemical staining procedures to determine the localization of StAR, 3β-HSD and CYP19A1 proteins involved in the steroidogenesis pathway. Immunoreactivity of StAR, 3β-HSD and CYP19A1 in granulosa and theca cells of all follicles was semiquantitatively evaluated using the H-Score method, considering staining intensity and extent. Results obtained from each group were statistically compared. No immunoreaction was observed in negative control samples.

StAR is a protein that facilitates the transport of cholesterol from the outer mitochondrial membrane to the inner mitochondrial membrane [110]. To assess StAR localization, we observed ovarian follicles at different maturation stages and corpora lutea in sections stained with StAR antibody through immunohistochemical staining in

the ovaries. When evaluating StAR immunoreactivity in ovarian tissue samples from all groups, positive immunoreactivity was observed in the cytoplasm of the theca interna cells, interstitial cells, and granulosa lutein cells in the corpora lutea of the control, vehicle, NaHS and PCOS+NaHS groups. Additionally, occasional weak immunoreactivity was observed in the cytoplasm of granulosa cells of some preovulatory follicles. In tissue samples from the PCOS group, it was determined that the immunoreactivity in the cytoplasm of the theca interna cells, granulosa cells and stromal cells, as well as in the granulosa lutein cells in the corpora lutea, was stronger compared to other groups (Figure 37). However, the expression in the theca interna layer of cystic follicles was found to be weaker.

We evaluated the intensity and prevalence of immunohistochemical StAR staining in the ovarian tissues of all groups using the H-Score method. In this context, it was determined that StAR immunoreactivity significantly increased in the PCOS group ($p<0.0001$). No remarkable distinction were found in StAR expression among the control and treatment groups (Figure 38).

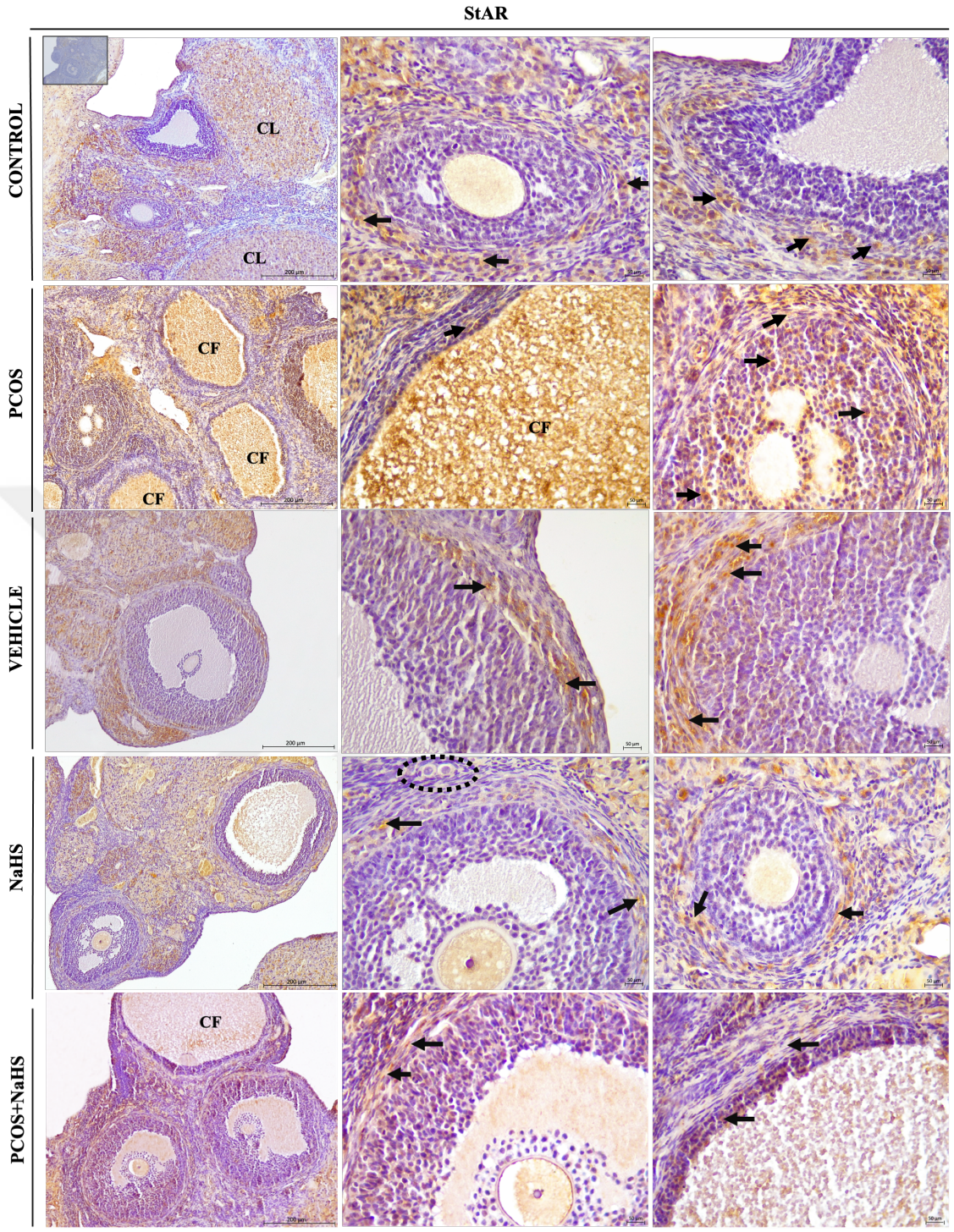

Figure 37. StAR localization in ovarian tissues of the groups demonstrated by immunohistochemical staining. Black dashed circle: primordial follicles, CF: cystic follicle, CL: corpus luteum, black arrow: indicates StAR immunoreactivity. There is no staining pattern in the negative control in the additional image. The scale bar represents 200 µm at x10 and 50 µm at x40 magnifications.

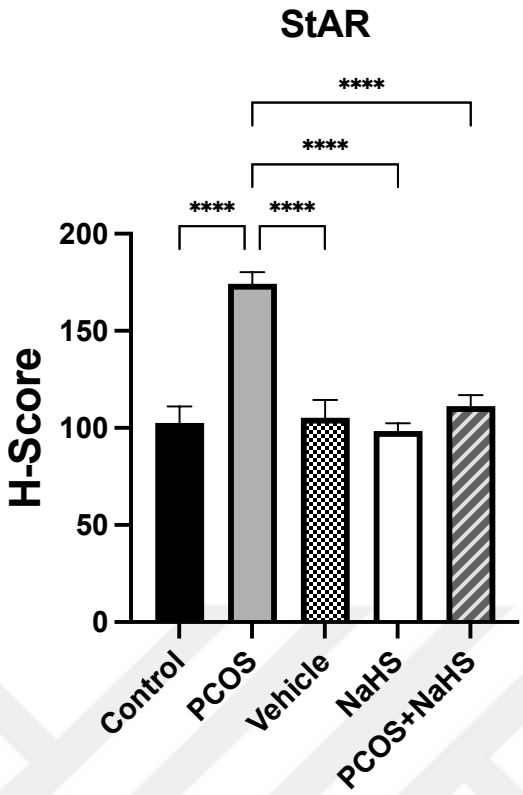

Figure 38. H-Score Graph of StAR in Ovarian Tissues of the Groups. ****: p<0.0001.

Another protein involved in the steroidogenesis pathway is 3β-HSD, which facilitates the conversion of pregnenolone to androstenedione via DHEA [18]. To evaluate the localization of 3β-HSD, we observed ovarian follicles at different maturation stages and the corpus luteum in sections stained with 3β-HSD antibody through immunohistochemical staining. Teka interna cells, interstitial cells, and granulosa lutein cell cytoplasm of tissue samples from the control, vehicle, NaHS and PCOS+NaHS groups exhibited a positive staining pattern for the 3β-HSD protein. In the PCOS group, stronger 3β-HSD expression was detected in the cytoplasm of teka interna cells and interstitial cells. Additionally, cytoplasmic 3β-HSD expression was identified in granulosa cells in this group. While more intense immunoreactivity was observed in the granulosa cells of cystic follicles, weaker immunoreactivity was detected in teka interna cells. Strong expression was detected in the cytoplasm of granulosa lutein cells in the corpus luteum occasionally encountered. In the control, vehicle, NaHS and PCOS+NaHS groups, immunoreactivity for 3β-HSD wasn't observed in the granulosa cells of follicles at all stages (Figure 39).

We assessed the staining intensity and prevalence of 3β-HSD in ovarian tissues of all groups using the H-Score method. In this context, it was determined that 3β-HSD immunoreactivity significantly increased in the PCOS group ($p<0.0001$). No significance was detected in 3β-HSD expression between the control and treatment groups (Figure 40).

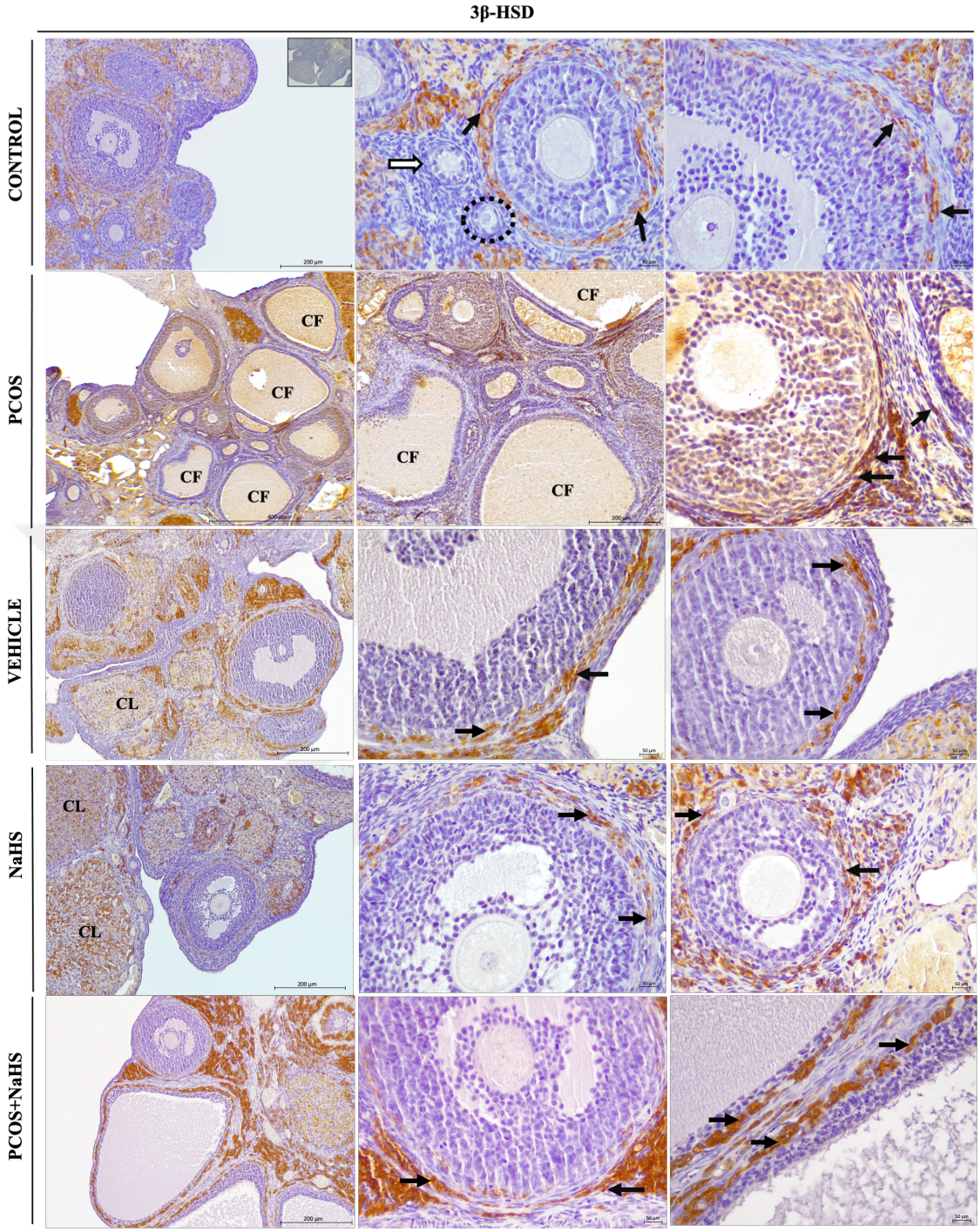

Figure 39. Localization of 3β-HSD in ovarian tissues of the groups is shown by immunohistochemical staining. Black dashed circle: primordial follicle, white arrow: primary follicle, CF: cystic follicle, CL: corpus luteum, black arrow: indicates 3β-HSD immunoreactivity. There is no staining pattern in the negative control shown in the additional image. The scale bar represents 400 µm for x4, 200 µm for x10, and 50 µm for x40 magnifications.

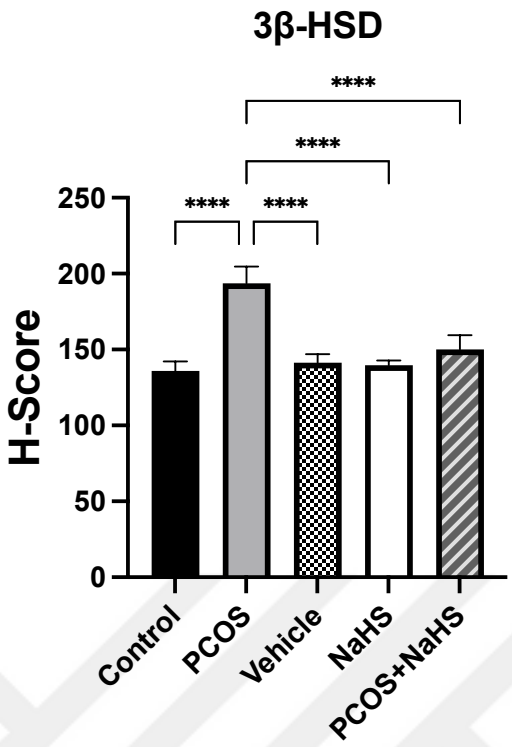

Figure 40. H-Score Graph of 3β-HSD in Ovarian Tissues of the Groups. ****: $p<0.0001$.

CYP19A1, also known as aromatase, is an essential protein involved in estrogen biosynthesis. This protein facilitates the conversion of testosterone and androstenedione to estradiol and estrone in granulosa cells [18]. To assess the localization of CYP19A1, we observed ovarian follicles at different maturation stages and corpus luteum sections stained with CYP19A1 antibody through immunohistochemical staining in the ovaries. Positive immunoreactivity was detected in the cytoplasm of granulosa cells of primary, secondary and Graaf follicles in tissue samples from the control, vehicle, NaHS and PCOS+NaHS groups. Additionally, expression for CYP19A1 was observed in granulosa lutein cells in the corpus luteum. In the PCOS group, strong expression was detected in the cytoplasm of granulosa cells of primary, secondary, Graafian and cystic follicles. There was no immunoreactivity for CYP19A1 in the follicular cells of primordial follicles (Figure 41).

We evaluated the intensity and prevalence of immunohistochemical staining for CYP19A1 in ovarian tissues of all groups using the H-Score method. In this context, it was determined that CYP19A1 immunoreactivity significantly increased in the PCOS

group ($p<0.0001$). No remarkable distinction was detected in CYP19A1 expression between the control and treatment groups (Figure 42).

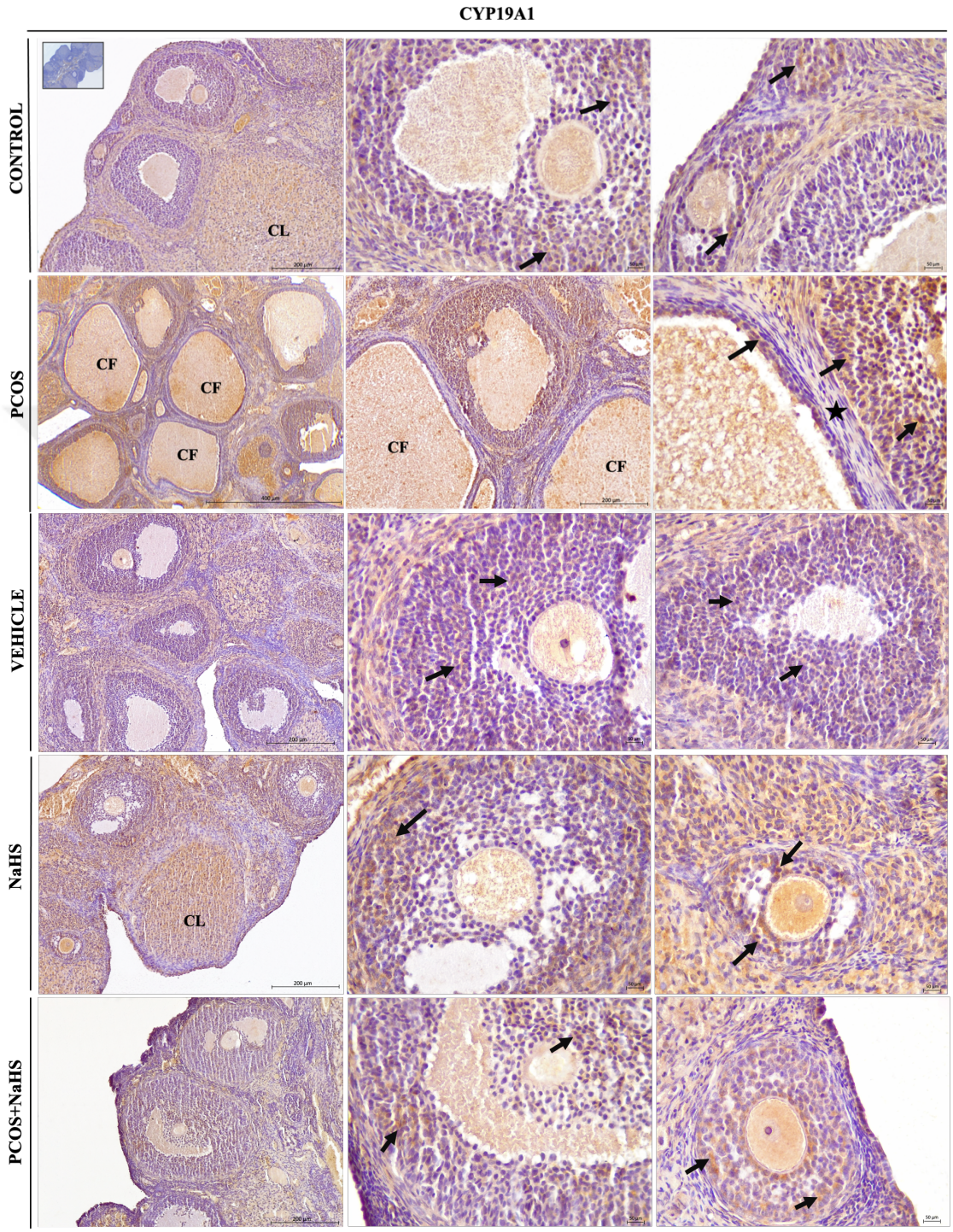

Figure 41. Localization of CYP19A1 in ovarian tissues of the groups is shown by immunohistochemical staining. CF: cystic follicle, star: theca layer, CL: corpus luteum, black arrow: indicates CYP19A1 immunoreactivity. There is no staining pattern in the negative control image. The scale bar represents 400 µm x4, 200 µm x10 and 50 µm x40.

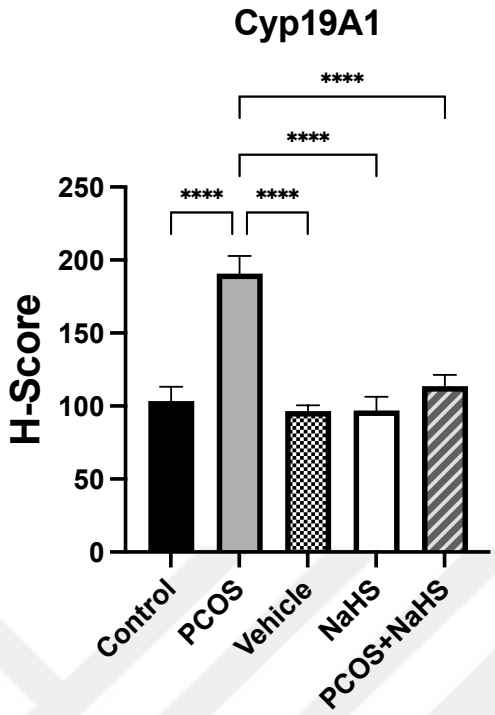

Figure 42. H-Score Graph of CYP19A1 in ovarian tissue of the groups. ****: $p<0.0001$.

4.4.2. Immunohistochemical Localization of H_2S-Producing Proteins

CBS and CTH are important enzymes involved in H_2S synthesis in various tissues. To assess CBS localization, we observed sections stained with CBS antibody by immunohistochemistry in ovarian follicles at different maturation stages and corpus luteum. Tissue samples from the control, vehicle, NaHS and PCOS+NaHS groups exhibited positive staining for CBS protein in the cytoplasm of granulosa cells of primordial, primary, secondary and Graafian follicles. Additionally, we observed strong immunoreactivity for CBS protein in primary and secondary oocytes. We determined CBS expression in the cytoplasm of theca cells, interstitial cells, luteal cells in the corpus luteum and smooth muscle cells. In the PCOS group, we found weaker immunoreactivity in the cytoplasm of follicular cells, theca cells and interstitial cells. In this group, we couldn't detect immunoreactivity for CBS protein in oocytes (Figure 43).

We evaluated the immunohistochemical CBS staining intensity and prevalence in ovarian tissues of all groups using the H-Score method. In this context, a remarkable diminish in CBS immunoreactivity was determined in the PCOS group ($p<0.0001$). No

significance in CBS expression was detected among the control and treatment groups (Figure 44).

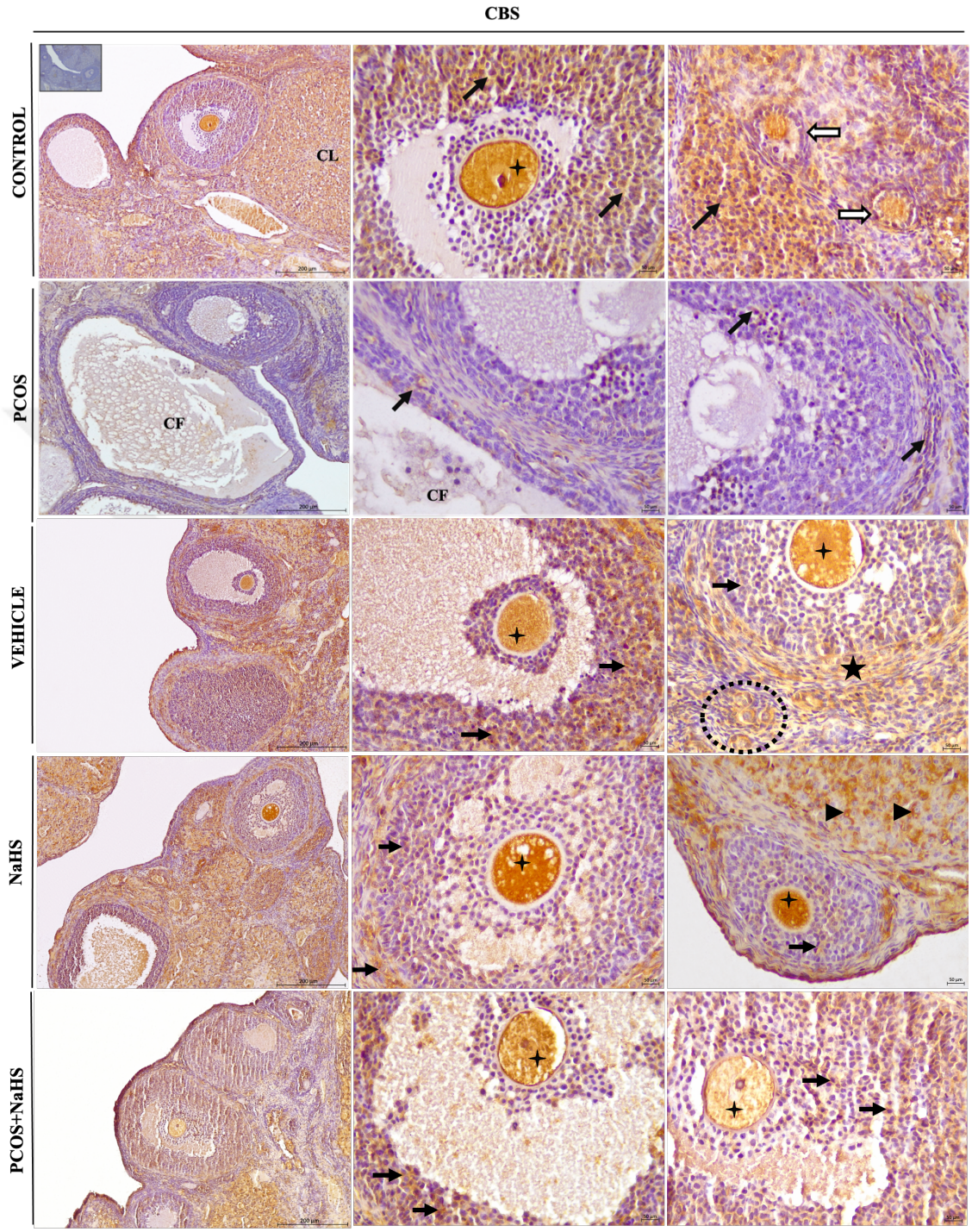

Figure 43. Immunohistochemical localization of CBS in ovarian tissues of the groups is shown by staining. CF: cystic follicle, four-pointed star: oocyte, black dashed circle: primordial follicle, white arrow: primary follicle, star: theca layer, CL: corpus luteum, black arrow and black arrowhead: indicate CBS immunoreactivity. There is no staining pattern in the negative control image. The scale bar represents 200 µm, x10, and 50 µm, x40.

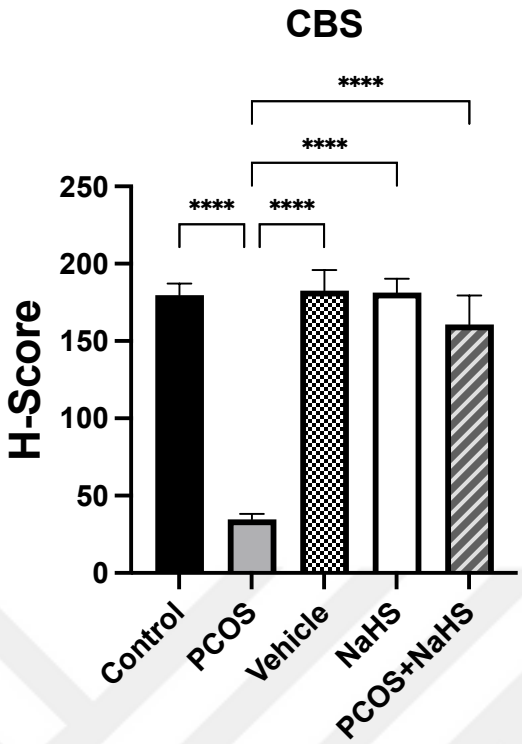

Figure 44. H-Score Graph of CBS in Ovarian Tissue of the Groups. ****: p<0.0001.

To evaluate CTH localization, we observed ovarian follicles at different maturation stages and corpus luteum sections stained with CTH antibody through immunohistochemical staining in ovaries. Tissue samples from control, vehicle, NaHS and PCOS+NaHS groups exhibited positive staining patterns for CTH protein in the cytoplasm of primordial, primary, secondary and Graafian follicles' granulosa cells. The CTH expression in granulosa cells was stronger than that of CBS. Additionally, we identified CTH expression in the cytoplasm of primary and secondary oocytes. However, the expression in oocytes wasn't as strong as CBS. We also observed CTH expression in the cytoplasm of theca cells, interstitial cells, luteal cells in the corpus luteum and smooth muscle cells. In the PCOS group, we found weaker immunoreactivity in the cytoplasm of follicular cells, theca cells and interstitial cells. We couldn't detect immunoreactivity for CTH protein in oocytes in this group (Figure 45).

We evaluated the intensity and prevalence of immunohistochemical CTH staining in ovarian tissues of all groups using the H-Score method. In this context, a significant decrease in CTH immunoreactivity was determined in the PCOS group

($p<0.0001$). No remarkable distinction in CTH expression were detected among the control and treatment groups (Figure 46).

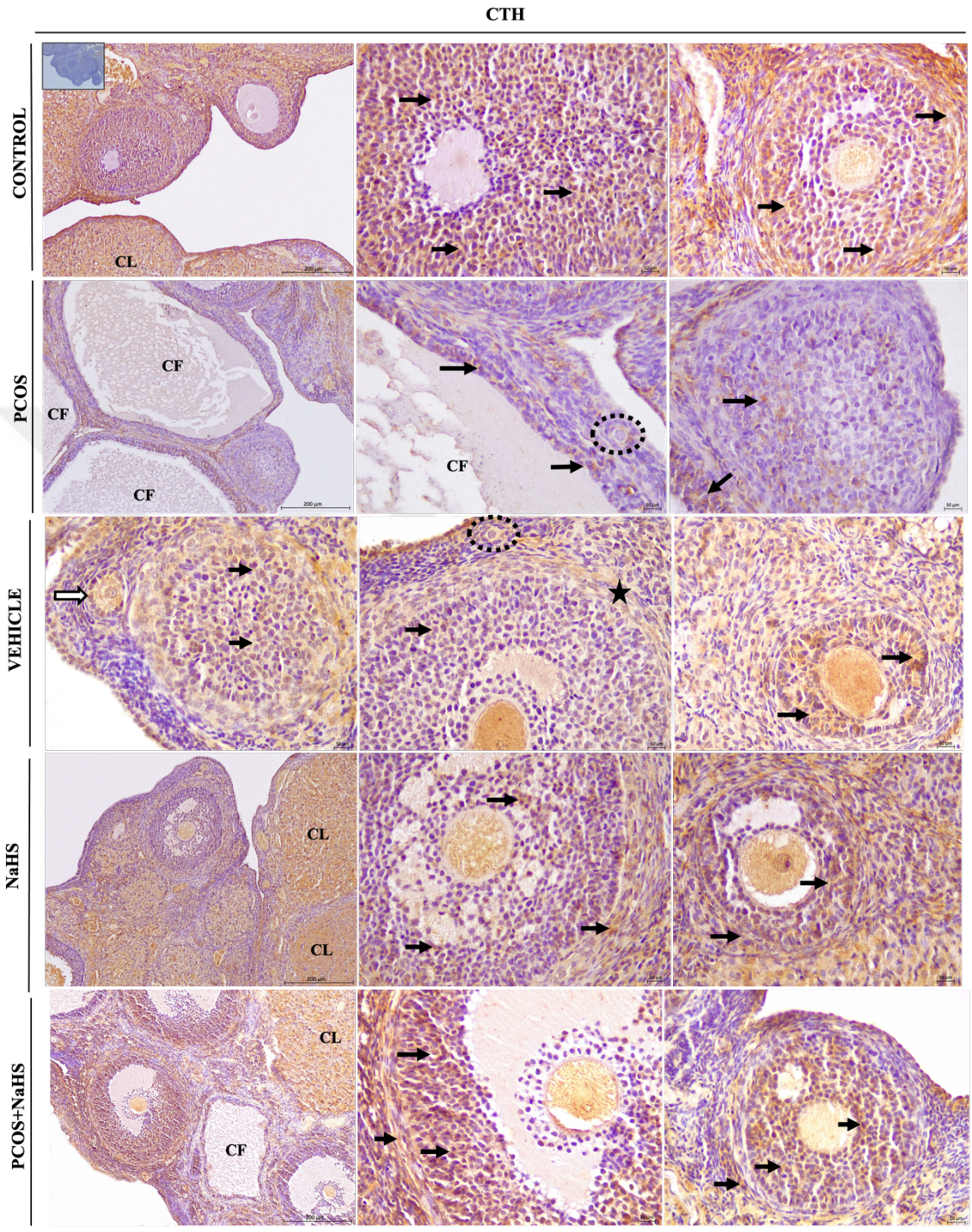

Figure 45. Immunohistochemical localization of CTH in ovarian tissues of the groups is shown. CF: cystic follicle, dashed black circle: primordial follicle, white arrow: primary follicle, star: theca layer, CL: corpus luteum, black arrow: indicates CBS immunoreactivity. The staining pattern is absent in the negative control image. The scale bar represents 200 µm, x10, and 50 µm, x40.

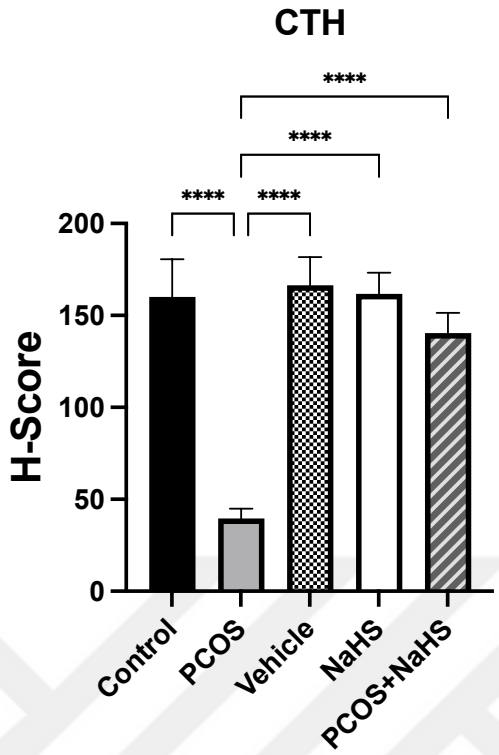

Figure 46. H-Score Graph of CTH in ovarian tissue of the groups. ****: p<0.0001.

4.5. Molecular Findings

4.5.1. qRT-PCR Results of Steroidogenic Genes

mRNA obtained from ovarian tissues was converted to cDNA and amplified using the RT-PCR method. The expression of steroidogenic genes (StAR, 3β-HSD, CYP19A1) was determined in control and experimental groups. The mRNA expressions of StAR, 3β-HSD and CYP19A1 for each group are presented in Figure 47.

When comparing StAR mRNA expression between the control, vehicle, NaHS, and PCOS+NaHS groups, no remarkable distinction was found. However, in the PCOS group, a remarkable enhance in StAR mRNA expression was observed and this increase was statistically significant compared to the control, vehicle, NaHS and PCOS+NaHS groups (p<0.0006).

In the comparison of 3β-HSD mRNA expression among groups, no statistical significance was found in the control, vehicle, NaHS, and PCOS+NaHS groups. However, in the PCOS group, a significant increase in 3β-HSD mRNA expression was

determined as compared with the control, vehicle, NaHS, and PCOS+NaHS groups ($p<0.0005$).

When the CYP19A1 mRNA expression of the groups was compared in the control, vehicle, NaHS and PCOS+NaHS groups, no remarkable distinction was detected among the groups. However, an increase in CYP19A1 mRNA expression in the PCOS group was statistically significant as compared with the other four groups ($p<0.0001$).

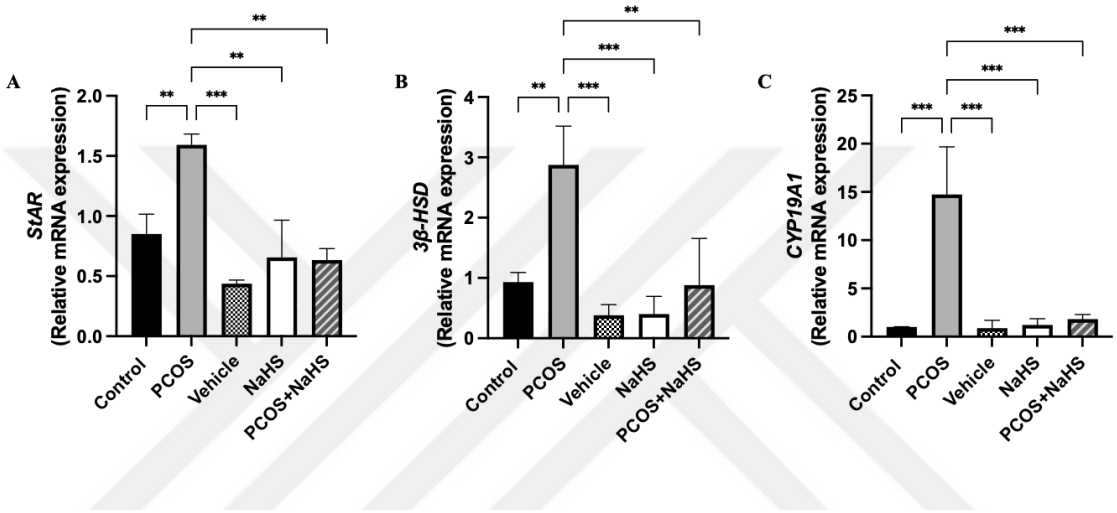

Figure 47. Relative mRNA expressions of StAR, 3β-HSD, and CYP19A1 for the groups. A StAR, **: $p<0.0091$, when compared between the control group and the PCOS group, ***: $p<0.0004$, when compared between the PCOS group and the vehicle group, **: $p<0.0024$, when compared between the PCOS group and the NaHS group, **: $p<0.0012$, when compared between the PCOS group and the PCOS+NaHS group. B 3β-HSD, **: $p<0.0041$, when compared between the control group and the PCOS group, ***: $p<0.0006$, when compared between the PCOS group and the vehicle group, ***: $p<0.0007$, when compared between the PCOS group and the NaHS group, **: $p<0.0034$, when compared between the PCOS group and the PCOS+NaHS group. C CYP19A1, ***: $p<0.002$, when compared between the PCOS group and the control, vehicle, and NaHS groups, ***: $p<0.0003$, when compared between the PCOS group and the PCOS+NaHS group.

4.5.2. qRT-PCR Results of H_2S-Producing Genes

CBS and CTH are enzymes involved in H_2S synthesis. The mRNA expressions of these enzymes in ovarian tissue were determined using the qRT-PCR method. The CBS and CTH mRNA expressions for each group are presented in Figure 48.

When comparing CBS mRNA expressions between the control, vehicle, NaHS and PCOS+NaHS groups, no statistically remarkable distinction were observed. In the PCOS group, CBS mRNA expression was significantly decreased as compared with the control, vehicle, NaHS, and PCOS+NaHS groups ($p<0.0083$).

It was determined that CTH mRNA expression was lower in the PCOS group. This decrease was found to be statistically significant compared to the control, vehicle, NaHS and PCOS+NaHS groups ($p<0.0024$). No remarkable differences were found in mRNA expressions as compared with the control, vehicle, NaHS and PCOS+NaHS groups.

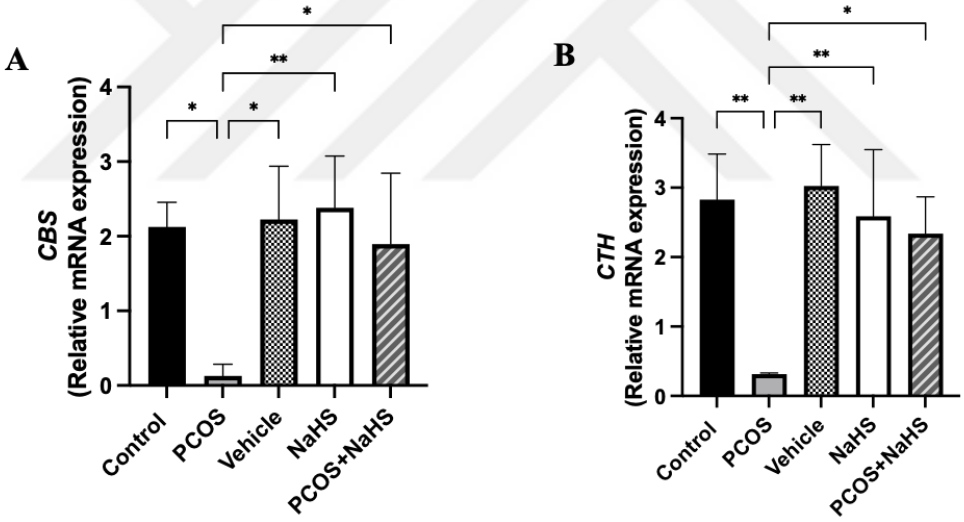

Figure 48. Relative mRNA expressions of CBS and CTH for each group. A. CBS, *: $p<0.0212$, when compared between the control and PCOS groups, *: $p<0.0158$, when compared between the PCOS group and the vehicle group, **: $p<0.0100$, when compared between the PCOS group and the NaHS group, *: $p<0.0420$, when compared between the PCOS group and the PCOS+NaHS group. B. CTH, **: $p<0.0046$, when compared between the control and PCOS groups, **: $p<0.0026$, when compared between the PCOS group and the vehicle group, **: $p<0.0090$, when compared between the PCOS group and the NaHS group, *: $p<0.0188$ when compared between the PCOS group and the PCOS+NaHS group.

5. DISCUSSION and CONCLUSION

While there is no perfect animal model that closely resembles PCOS in humans, researchers have utilized rodent PCOS models induced by androgens in studies to explore the cellular and molecular foundations of PCOS, aiming to replicate numerous phenotypic characteristics of human PCOS [111 ,112 ,113]. DHEA is an androgen produced in the adrenal glands, and its levels are elevated in women suffering from PCOS. Many studies in the literature indicate that rodent PCOS models induced by DHEA effectively mimic various phenotypic features of human PCOS [114,64,115,116,117]. Therefore, the use of DHEA is preferred in rodent models to induce PCOS. DHEA possesses a mild androgenic effect, and its conversion to testosterone is necessary for executing indirect biological effects in the peripheral tissues of rats. Consequently, in our study, we opted to use DHEA to establish a PCOS model, to avoid the direct effects of androgens.

Previous studies have revealed numerous adverse effects of PCOS on reproductive potential [100,118,102,103,104]. However, there has been no investigation into the impact of the endogenous gas H_2S production system on the negative effects of PCOS on ovaries. In our study, we examined the impacts of NaHS, on anovulatory infertility, impaired follicular development and disrupted steroidogenesis mechanisms in a rat PCOS model induced by DHEA. Our investigation encompassed histological, immunohistochemical, biochemical and molecular aspects.

It is thought that one of the underlying mechanisms for the cessation of folliculogenesis in PCOS is due to hormonal imbalance. As a result of disruptions in the HPO axis in PCOS, an increase in GnRH pulsatility occurs in the hypothalamus [29]. This increase in GnRH leads to increased LH secretion from the adenohypophysis. The early acquisition of LH receptors by growing follicles results in increased ovarian androgen production [29]. Studies suggest that dysfunction in the theca cells is among the mechanisms contributing to hyperandrogenism in PCOS [119,120]. Abnormal elevation of LH in PCOS leads to theca hyperplasia, causing an increase in ovarian androgen production [121,122]. Furthermore, various studies indicate a rise in cytochrome P450 17-alpha-hydroxylase and StAR activities in the theca cells of women with PCOS [123,124,125.] These findings reflect steroidogenesis dysfunction in PCOS, suggesting an excessive response to gonadotropin stimulation. Additionally, it is reported that isolated theca

cells obtained women with PCOS produce more testosterone, 17-alpha-hydroxyprogesterone and progesterone compared to normal theca cells [126]. Moreover, it is suggested that elevated E_2 and progesterone levels in women with PCOS involve impaired negative feedback on LH secretion [127]. Evaluation of steroid production in granulosa cells after LH stimulation in PCOS reveals that progesterone production in 4 mm follicles is higher than that in 9-10 mm follicles in normal ovaries [127]. Additionally, many studies report that hyperinsulinemia is another cause of hyperandrogenism observed in PCOS. Insulin, exhibiting a synergistic effect with LH, induces the steroidogenic response in the ovary [128,129,130]. When granulosa cells of ovulatory and anovulatory PCOS ovaries are incubated with insulin, an increase in E_2 and progesterone production is observed [131]. The mRNA expression of LH receptors in granulosa cells of women suffering from PCOS is elevated than in granulosa cells of normal follicles [132]. This finding supports the idea that granulosa cells in PCOS ovaries acquire LH receptors early in folliculogenesis, leading to early luteinization [133]. Kyei et al. reported significantly elevated serum E_2 and progesterone levels in pre-pubertal mice following subcutaneous DHEA injection [134]. Consistent with this finding, many studies on DHEA-induced PCOS animal models have also reported higher levels of serum E_2, progesterone, testosterone, LH and prolactin compared to the control group[135,136,137,117,138,139,140]. In our study, we evaluated serum concentration of E_2, progesterone in pre-experimental and post-experimental samples to demonstrate ovulatory dysfunction. Our assessment revealed no significant difference in pre-experimental and post-experimental serum E_2 and progesterone levels in the control, vehicle, NaHS and PCOS+NaHS groups, while we found that the post-experimental serum E_2 and progesterone levels of the PCOS group rats were higher. This finding is evidence that the PCOS experimental model in rats was successfully established, parallel to the characteristics of PCOS in humans. However, there is no study in the literature evaluating the effect of H_2S on the HPO axis. For the first time in this study, the corrective effect of NaHS treatment on the impaired HPO axis due to DHEA has been demonstrated. NaHS may exert this effect by mitigating damage at the level of hyperinsulinemia, impaired steroidogenesis mechanism, or hormonal synthesis pathway or receptor. Further studies can provide a complete understanding of its mechanism.

Oligo/anovulation holds a significant place in PCOS. Therefore, the primary reason for women with PCOS to seek assistance from assisted reproductive technology (ART) centers is this irregularity. Experimental studies involving the injection of

DHEA to trigger PCOS in rats have reported the manifestation of disrupted estrous cycles [136,115,116,141,142]. In our study, we monitored the estrous cycle by taking vaginal smear samples from rats to detect oligo/anovulation, one of the symptoms of PCOS. When we analyzed vaginal smears daily for 20 days, we observed that animals in the control, vehicle, NaHS and PCOS+NaHS groups exhibited all stages of the estrous cycle and had more regular estrous cycles. However, examination of vaginal smears from the PCOS group revealed that rats in this group were blocked in the diestrus stage and exhibited prolonged estrous cycles. This led us to consider that this condition might be related to disturbances in LH and FSH secretion from the adenohypophysis and E_2 release in the ovaries. Additionally, the absence of corpus luteum in ovarian sections of animals in the PCOS group or the occasional presence of few corpus luteum structures indicates a lack of ovulation in these animals. Our findings support our vaginal smear results and once again confirm the successful establishment of the experimental PCOS model.

In in vivo and in vitro investigations carried out in mice and humans, the H_2S producing system is reported to play a role in ovulation. The pre-ovulatory increase in LH stimulates the expression of enzymes catalyzing H_2S production and the H_2S donor NaHS induces a raise in the mRNA expression of AREG, EREG, PLAT. Additionally, it is observed that inhibitors of CSE (also known as CTH) block ovulation and the ovulation suppressed by a CSE inhibitor is reversed by NaHS. Furthermore, H_2S induced by LH fluctuations acts on MMP-2, MMP-9 and PLAT activities, ensuring follicle rupture [99].

Parallel to the regulatory effect of H_2S on ovulation, our study revealed that the cycles of animals in the PCOS+NaHS group were more regular and they exhibited all phases of the estrous cycle. Additionally, the existence of numerous corpus luteum structures in ovarian sections of animals in this group indicates that ovulation occurred. Our results demonstrate that NaHS improves the functional disorder of the estrous cycle and the pattern of oligo/anovulation in PCOS rats.

The ovaries of women with PCOS harbor numerous small (2-9 mm) antral follicles and due to the increase in central stroma, these follicles exhibit a peripheral distribution [30]. Histologically, growing pre-antral follicles in PCOS resemble follicles in a normal ovary. The initiation of early antral follicle formation may seem normal. However, when the follicle reaches the mid-antral stage, it fails to develop normally. Follicular growth halts and begins to show degenerative changes. There is a continuous

build-up of follicular fluid and expansion of the antrum. The granulosa layer undergoes apoptosis and gradually becomes atretic. Ultimately, thin-walled cystic follicular structures emerge. The mechanism responsible for the inability of follicle development in PCOS to progress beyond the mid-antral stage during this process isn't fully understood. However, it is thought that one of the mechanisms at this point involves premature granulosa cell differentiation and insufficient FSH release [30]. Similar to PCOS in humans, an abnormal follicular development is also observed in the mouse PCOS model induced by DHEA [102]. Studies conducted in mice and rats have reported an increase in fat and stroma in the ovaries, along with an increase in numerous fluid-filled cystic follicles [104,143,144]. However, severe morphological degenerations in the zona pellucida and granulosa cells are reported, along with oligo/anovulation in animals, the presence of degenerate oocytes, increased follicle atresia and inflammation [107]. It is observed that high levels of androgens can lead to oocyte degeneration due to the presence of androgen receptors on oocytes [145].

In our study, when evaluating the effect of DHEA on the ovary histopathologically, we observed significant signs of degeneration in the zona pellucida and oocytes and an increase in follicular degeneration, inflammation, vascular congestion and hyalinization in the vascular structures. These parameters were supported by semi-quantitative scoring and are consistent with previous studies. As a result of NaHS treatment, it was determined that the findings induced by DHEA significantly regressed and approached the histological features of the control groups. This study is important as the first to demonstrate the therapeutic effect of NaHS against DHEA-induced histopathological findings in the ovary.

Studies reporting that chronic inflammation contributes to PCOS and a pro-inflammatory genotype is associated with PCOS [146,147,148,149]. An increase in NF-κB (Nuclear Factor kappa B) activation triggers inflammation in PCOS by leading to a significant elevation in the serum level of the pro-inflammatory cytokine IL-1β (Interleukin-1-β) [148]. However, various studies suggest the anti-inflammatory effects of H_2S. It is reported that H_2S reduces serum concentrations of pro-inflammatory cytokines such as IL-1β and TNF-α (tumor necrosis factor-alpha) and increases the concentration of the anti-inflammatory cytokine IL-10 [150,151]. NaHS has been observed to prevent the formation of inflammatory cytokines in testicular damage induced by cisplatin [84]. Additionally, NaHS is known to exhibit protective effects against cardiotoxicity by reducing the formation of IL-1β and other pro-inflammatory cytokines

[152]. Considering the anti-inflammatory effects of H_2S, we believe that NaHS may have demonstrated anti-inflammatory effects in PCOS ovaries.

In our study, when evaluating all groups in terms of follicle numbers, we discovered that the PCOS group was lower numbers of primordial and primary follicles as compared with the control and treatment groups. The decrease the number of primary follicles may be attributed to some of these follicles transitioning into secondary follicles, while others may undergo atresia. Our observation of a rise the numbers of secondary and atretic follicles supports this hypothesis. We identified a decrease in the number of Graafian follicles and corpus luteum in the PCOS group, attributed to the rise the number of secondary follicles. The halt in folliculogenesis at the secondary follicle stage in PCOS, where secondary follicles fail to transform into Graafian follicles and consequently ovulation doesn't occur, leads to a decrease in corpus luteum numbers. The decrease in the count of Graafian follicles, coupled with the majority of these follicles progressing to atresia and forming cystic follicles, also supports our findings. Furthermore, our vaginal smear results align with the decrease in corpus luteum numbers. In addition to these follicles, an increase in the count of atretic and cystic follicles is observed in the PCOS group as compared with the control and treatment groups. Our results align with studies that have reported a decrease in primordial, primary, and Graafian follicle numbers, along with an increase in secondary, atretic, and cystic follicle numbers in the mouse and rat PCOS model [104,153,144]. The atretic follicles observed in sections stained with H&E are further supported by our TUNEL assay findings.

It has been reported in the literature that $CBS^{-/-}$ mice, which are deficient in H_2S-producing enzymes, are infertile [87,92]. In $CBS^{-/-}$ females, a decrease in follicle numbers, shortened and irregular estrous cycles, as well as shorter estrus and menopausal periods have been documented [87]. Another study indicates that $CBS^{-/-}$ mice have reduced numbers of growing follicles and irregular, shorter estrous cycles, while $CSE^{-/-}$ mice exhibit fertile characteristics. Fertility is revealed to be decreased in $CBS^{+/-}$ mice as compared with wild-type mice [93].

Consistent with the literature, we didn't observe a statistically important difference among the PCOS+NaHS group and the control groups or the NaHS group in terms of follicle numbers and corpus luteum numbers. From this perspective, NaHS appears to regulate folliculogenesis and facilitate ovulation. Therefore, it can be concluded that NaHS treatment is effective in the follicular growth process. NaHS may

achieve this effect by inhibiting the transition from primordial follicles to primary follicles. However, the uncertainty remains regarding which signaling pathways mediate this effect in the ovary. Therefore, further studies evaluating the impact of H_2S on various signaling pathways involved in follicular development are needed.

The PI3K-Akt-mTOR signaling pathway has regulatory influences on the dormancy and activation of primordial follicles. Excessive activation of the PI3K-Akt signaling pathway leads to the formation of immature follicles and numerous small antral follicles [154]. The inability of ovarian follicles to transform into dominant follicles and the generation of numerous cystic follicles are significant features of PCOS. Several studies have reported the effectiveness of the PI3K-Akt-mTOR signaling pathway in the generation of cystic follicles [155,156,157,158,159]. Restuccia and colleagues demonstrated the formation of cystic follicles as a result of the inhibition of Akt2 [159]. On the other hand, the effective role of the mTOR signaling pathway in granulosa and theca cell proliferation and hormonal dysfunction in the mouse ovaries has also been reported [160].

There are various studies in the literature regarding H_2S and the PI3K/AKT/mTOR signaling pathway. It has been documented that H_2S concentration decrease in liver cells treated with oleic acid, and exogenous NaHS treatment provides protection against oxidative stress by diminishing the phosphorylation of AKT, PI3K, and mTOR [161]. Additionally, exogenous H_2S (NaHS) suppresses cell proliferation and migration in a melanoma cell line by inhibiting the PI3K/AKT/mTOR pathways [162]. NaHS has also markedly suppressed the expression of p-PI3K, p-Akt and mTOR proteins in the hepatocellular carcinoma cell line, similar to Rapamycin. Furthermore, the biological function of H_2S in hepatocellular carcinoma cells increases with the addition of Rapamycin [163]. In a traumatic brain injury mouse model, NaHS has been shown to activate the PI3K/AKT/mTOR signaling pathway, inhibit autophagy, protect blood-brain barrier integrity and neurons from apoptosis, induce remyelination and axonal repair and preserve mitochondrial function [164]. However, the H_2S donor GYY4137 reverses the suppression of PI3K/Akt/mTOR signaling pathways caused by lipopolysaccharide-induced acute lung injury [165]. In another study, it was stated that NaHS could inhibit excessive autophagy, improve doxorubicin-induced myocardial fibrosis by suppressing excessive endoplasmic reticulum stress and activate the PI3K/AKT/mTOR pathway [166]. Therefore, it is observed that H_2S plays a dual role in the PI3K/AKT/mTOR pathway. H_2S can regulate a series of signaling pathways within the cell. However, this regulation may vary depending on the cell type, environmental

conditions, H_2S concentration and many other factors. In PCOS, the PI3K/AKT/mTOR pathway is an active signaling pathway in the formation of cystic follicles. In this context, our study suggests that the regulatory effect of H_2S on folliculogenesis may occur through the PI3K/AKT/mTOR pathway. However, our study didn't investigate the signaling pathways that contribute to regulating folliculogenesis.

Apoptosis is crucial for maintaining tissue homeostasis in multicellular organisms. Several pathophysiological changes observed in PCOS are closely linked to apoptosis occurring in ovarian granulosa cells [167,168]. Androgens exhibit a dual effect on follicular development, not only influencing it positively but also promoting follicular atresia when present at abnormally high levels [169]. However, the underlying pathophysiological mechanisms at play remain largely unknown. Shen et al. reported an elevated incidence of follicular atresia and a high apoptotic index in the rat PCOS model triggered through DHEA, indicating a potential correlation with PCOS [170]. Additionally, in PCOS, it is suggested that granulosa cells undergo apoptosis due to the stalling of follicular growth and ensuing degenerative changes, progressively becoming more atretic. These atretic follicles display an increased TUNEL-positive staining [171,172].

There is no study in the literature that demonstrates the relationship between follicular atresia and H_2S. However, there are studies indicating the anti-apoptotic effects of H_2S in various tissues. In embryonic fibroblasts and endothelial cells lacking CSE, accelerated cellular aging has been observed as compared with wild-type mice. It has been reported upon that supplementation with H_2S reverses the aging induced by CSE deficiency [173,174]. Inhibition of H_2S biosynthesis in various cell types leads to the initiation of apoptotic responses [175,176]. Numerous researches have shown that H_2S demonstrates a conservation effect against various apoptotic stimuli [177,178,179,180]. In doxorubicin-induced myocardial fibrosis, H_2S significantly reduces the expression levels of caspase-2, caspase-3, caspase-9, Bax and Keap1, while significantly increasing the expression levels of Bcl-2 and Nrf-2 [181].

In our study, upon evaluating apoptosis in ovarian tissues using the TUNEL assay, we observed a higher apoptotic index in the PCOS group as compared with the other groups. This observation aligns with the rised number of atretic follicles detected in PCOS. However, when comparing the PCOS+NaHS group with the other groups regarding the number of atretic follicles, we didn't find a significant difference. Nevertheless, a significant distinction in terms of the apoptotic index emerged when comparing the PCOS+NaHS group with the control, vehicle, NaHS and PCOS groups.

We attribute the inconsistency between these findings to the fact that, in PCOS, the histological features of pre-antral and early antral follicle formation resemble those of normal follicles. However, as it progresses to the mid-antral stage, degenerative changes become evident. Despite this, the lower apoptotic index ratio in the PCOS+NaHS group as compared with the PCOS group suggests that NaHS exerts anti-apoptotic effects in ovarian tissue. Our findings harmonize with studies demonstrating the anti-apoptotic influences of H_2S.

In women suffering from PCOS, elevated androgen levels and insulin resistance cause disturbances in the steroidogenesis pathway. This condition leads to ovarian dysfunction and abnormal follicular development [182,183]. CYP19A1, 3β-HSD and StAR are crucial steroidogenic enzymes involved in the arrangement of the steroidogenesis pathway [184]. StAR transports cholesterol from the outer membrane to the inner membrane of mitochondria, converting it into pregnenolone [185,186]. Pregnenolone serves as a substrate for progesterone synthesis through the mediation of 3β-HSD [187,188]. CYP19A1 is the key enzyme in granulosa cells that converts androgens to estradiol [189]. Any disruption in the regulation of steroidogenic enzymes and steroid hormone secretion in granulosa cells can lead to endocrine disorders and consequently, impaired follicular development [190]. Various researches have explored the effects of androgen administration on the activity of steroidogenic enzymes. Continuous intake of exogenous DHEA leads to increased expression of 3β-HSD and StAR, enhanced conversion of DHEA to androstenedione and subsequently elevated levels of dihydrotestosterone and testosterone, resulting in the appearance of hyperandrogenism [191]. DHEA exposure induces high levels of estradiol and progesterone in mouse serum, leading to increased steroidogenic activity [192,193]. The elevated steroidogenic activity in PCOS results in the formation of follicular cysts, hindering the development of dominant follicles [194]. Mice exposed to DHEA show increased expression of CYP11A1, CYP19A1, 3β-HSD and StAR enzymes in granulosa cells of polycystic ovaries [195]. The addition of testosterone and androstenedione to the culture medium induces increased gene expression of 3β-HSD and CYP19A1 in human granulosa cells [196]. Abnormal steroid secretion is observed in the cystic ovary of cows [197]. The key enzyme involved in progesterone production, 3β-HSD, is found at high levels in estrogen-active cysts [198]. Wu et al. reported an increase in the gene and protein expression of CYP19A1, 3β-HSD and StAR in PCOS ovaries after subcutaneous DHEA treatment for 21 days [199]. In another study, a significantly high increase in mRNA and protein expression of 3β-

HSD, CYP19A1, CYP11A1, and StAR was observed in a DHEA-induced PCOS mouse model [134].

In this study, we examined steroidogenic enzymes (StAR, 3β-HSD and CYP19A1) both immunohistochemically and at the gene level. Following DHEA administration, we observed higher immunoreactivity of StAR, 3β-HSD and CYP19A1 in the PCOS group as compared with other groups. Consistent with our findings, we also identified an increase in mRNA expression of CYP19A1, 3β-HSD and StAR in the PCOS group. Our outcomes support the elevation of serum E_2 and progesterone observed in the PCOS group. In light of these data, we can say that DHEA alters the expression of steroidogenic enzymes involved in steroid hormone synthesis, leading to follicular atresia and the formation of cystic follicles.

There is no study in the literature that investigates the effect of H_2S on steroidogenesis and estrogen synthesis pathways in the ovary. In contrast to the data in the PCOS group in our investigation, we observed a decrease in both StAR, 3β-HSD and CYP19A1 immunoreactivity and CYP19A1, 3β-HSD and StAR mRNA expression in the PCOS+NaHS group; there was no notable distinction compared to the control, vehicle and NaHS groups. In this research, it is first reported occurrence that the impaired steroidogenesis pathway, induced by DHEA is restored by the exogenous application of the H_2S donor NaHS.

In PCOS, hyperinsulinemia and insulin resistance are as influential as hyperandrogenism in the disruption of the steroidogenesis pathway. Studies suggest that H_2S plays a role in regulating insulin secretion. When rat insulinoma cells are incubated with the CSE inhibitor PAG, an increase in insulin release is reported [200]. However, exogenous H_2S application has been found to reduce glucose-induced insulin secretion in rat insulinoma cells [200] and isolated mouse pancreatic islets [201]. Additionally, H_2S donors, such as NaHS and ACS67, are observed to decrease L-type Ca^{+2} currents through channels in mouse pancreatic β-cells. In $CSE^{-/-}$ mice, insulin secretion from pancreatic islets was higher compared to wild-type mice, and NaHS was found to dose-dependently inhibit glucose-induced insulin secretion [202] . Considering the regulatory effect of H_2S on insulin secretion, we speculate that NaHS may have a regulatory effect on hyperinsulinemia and insulin resistance in PCOS ovaries. NaHS may restore the impaired steroidogenesis mechanism by reducing insulin levels. However, it's important to note that this is only a hypothesis, and hyperinsulinemia and insulin resistance weren’t examined in this study. CBS, CSE (also known as CTH) and 3-MST are the

three main enzymes that produce H_2S. CBS and CSE reside in the cytosol, whereas 3-MST is present in both the mitochondria and cytosol [75,4]. In many tissues, CBS and CSE enzymes work in coordination to produce H_2S, but in some tissues, only one of the enzymes is necessary. CSE and CBS expression has been noted in the female reproductive systems of mice, rats and humans. In the uterus, placenta and fetal membranes of pregnant rats, both CSE and CBS enzymes are expressed, while in the non-pregnant rat uterus, only CBS and CSE enzymes are expressed [86,92]. In human tissues, both CBS and CSE expression have been illustrated in the myometrium, amnion, placenta and chorion [92]. In mice, CBS mRNA expression has been revealed in pregnant, non-pregnant uteri [87]. CBS enzyme activity is present in rat decidua and placental tissues [88]. The distribution of CBS and CSE were reported throughout the human fallopian tube [98]. CBS, CSE and 3-MST mRNA and protein expression have been demonstrated in pig oocytes. Inhibitors of these three enzymes suppress meiotic maturation when incubated with oocytes. However, incubating these oocytes with the H_2S donor NaHS accelerates meiotic maturation [94]. A decrease in CBS expression in rat granulosa cells has been associated with the inhibition of meiotic maturation in oocytes [203]. Liang et al. have shown that CBS is expressed in follicles at all stages in mouse ovaries [95]. The expression of CBS and CSE enzymes in the female reproductive system suggests that H_2S may have some functional roles in the reproductive system.

According to our research, we investigated the expression of CBS and CTH (also known as CSE) in rat ovaries. We assessed CBS and CTH enzymes in the ovaries of all groups both immunohistochemically and at the gene level. We found that CBS and CTH were situated in the cytoplasm of granulosa and theca cells of follicles at all stages, as well as in the cytoplasm of interstitial cells and luteal cells of the corpus luteum. This study reports, for the first time, the localization of CBS and CTH in the cytoplasm of oocytes. Additionally, In this study, we presented, for the first time, that CTH is localized in the cytoplasm of granulosa and theca cells of ovarian follicles, as well as in the cytoplasm of interstitial cells and luteal cells of the corpus luteum. We observed that CBS immunoreactivity was stronger in the cytoplasm of oocytes compared to CTH.

Li et al. reported remarkable decline in CBS mRNA expression in the liver tissues of rats with PCOS induced by the administration of DHEA along with a high-fat diet [204]. In a PCOS mouse model induced by letrozole, Bries et al. also demonstrated lower CBS mRNA expression [205]. Consistent with these studies, in our investigation

evaluating the expressions of CBS and CTH across groups, we found decreased immunoreactivity and mRNA expression of both enzymes in the PCOS group. Additionally, the PCOS+NaHS group, exogenous NaHS administration observed to increase the immunoreactivity and mRNA expression of CBS and CTH, promoting H_2S production. The application of DHEA inhibited H_2S production in the ovaries. However, the signaling pathways involved in this inhibition were not assessed in this study. Exogenous NaHS has restored H_2S production in the PCOS ovaries. Further studies on this topic are crucial for addressing the lack of information in the literature.

As a result, in the rats with PCOS induced by the administration of DHEA, the increase in serum E_2 and progesterone levels has contributed to hyperandrogenism, leading to disruption in the steroidogenesis pathway. The impaired steroidogenesis has resulted in increased expressions of StAR, 3β-HSD and CYP19A1 proteins. Disruption of the steroidogenesis pathway due to hyperandrogenism has led to insufficiency in the selection of dominant follicles, resulting in oligo/anovulation due to the consequent disruption of the HPG Axis.

In this study, it demonstrated that exogenous NaHS treatment in PCOS ovaries can increase the expression of H_2S-producing enzymes, thereby reducing the mRNA expression levels of the elevated StAR, 3β-HSD and CYP19A1 genes. Activation of the H_2S pathway has led to a decrease in estradiol and progesterone secretion in PCOS ovaries due to the inhibited production of increased StAR, 3β-HSD and CYP19A1 proteins. Our study has shown that the decrease in CYP19A1 protein and mRNA expression in PCOS ovaries in response to NaHS could result in a reduction in estradiol production. NaHS has restored impaired steroidogenesis, HPO axis, folliculogenesis and oligo/anovulation in PCOS ovaries. We attribute the protective effect of NaHS against DHEA-induced damage to its regulatory effects on endocrine system regulation, cytoprotective and anti-apoptotic properties. Further elucidating the mechanisms of H_2S effects could be important for identifying new Disease targets and devising all-encompassing treatment strategies for female reproductive disorders.

REFERENCES

1. Brassard M, AinMelk Y, Baillargeon JP. Basic Infertility Including Polycystic Ovary Syndrome. *Medical Clinics of North America*. 2008;92(5):1163-1192.
2. Wang R. *Two's Company, Three's a Crowd: Can H_2S Be the Third Endogenous Gaseous Transmitter? The FASEB Journal. 2002;16:13.*
3. Yang G, Wu L, Jiang B, et al. H2S as a physiologic vasorelaxant: Hypertension in mice with deletion of cystathionine γ-lyase. *Science*. 2008;322(5901):587-590.
4. Sugiura Y, Kashiba M, Maruyama K. Et. al. Cadmium Exposure Alter Metabolomics of Sulfur-Containing Amino Acids in Rat Testes. *Antioxidants&Redox Signaling.* 2005;7:5-6.
5. Li J, Li Y, Du Y, et al. Endogenous hydrogen sulfide as a mediator of vas deferens smooth muscle relaxation. *Fertil Steril*. 2011;95(5):1833-1835.
6. Magro-Lopez E, Muñoz-Fernández MÁ. The role of bmp signaling in female reproductive system development and function. *Int J Mol Sci*. 2021;22(21).
7. Moore KL, Torchia MG, Persaud TVNP. *The Developing Human: Clinically Oriented Embryology*. 11th ed. Philadelphia: Saunders; 2019.
8. Schuenke M, Schulte E, Schumacher U, Cass W. *Internal Organs (THIEME Atlas of Anatomy)*. Vol 2. 3rd ed. New York: THIEME; 2020.
9. Ross MH, Pawlina W. *Histology: A Text and Atlas: With Correlated Cell and Molecular Biology*. 6th ed. Philadelphia: Lippincott Williams & Wilkins; 2010.
10. Eroschenko VP. *DiFiore's Atlas of Histology With Functional Correlations*. 12th ed. Philadelphia: Lippincott Williams & Wilkins; 2012.
11. Mescher AL. *Junqueira's Basic Histology: Text and Atlas*. 16th ed. McGraw Hill Medical Books; 2021.
12. Baskind NE, Balen AH. Hypothalamic–pituitary, ovarian and adrenal contributions to polycystic ovary syndrome. *Best Pract Res Clin Obstet Gynaecol*. 2016;37:80-97.
13. Li H, Liu Y, Wang Y, Zhao X, Qi X. Hormone therapy for ovarian cancer: Emphasis on mechanisms and applications (Review). *Oncol Rep*. 2021;46(4).
14. Herbison AE. Control of puberty onset and fertility by gonadotropin-releasing hormone neurons. *Nat Rev Endocrinol*. 2016;12(8):452-466.
15. Richards JAS. The Ovarian Cycle. In: *Vitamins and Hormones*. Vol 107. Academic Press Inc.; 2018:1-25.

16. Miller WL. Steroidogenesis: Unanswered Questions. *Trends in Endocrinology and Metabolism*. 2017;28(11):771-793.
17. Fuentes N, Silveyra P. Estrogen receptor signaling mechanisms. In: *Advances in Protein Chemistry and Structural Biology*. Vol 116. Academic Press Inc.; 2019:135-170.
18. Barakat R, Oakley O, Kim H, Jin J, Ko CMJ. Extra-gonadal sites of estrogen biosynthesis and function. *BMB Rep*. 2016;49(9):488-496.
19. Cora MC, Kooistra L, Travlos G. Vaginal Cytology of the Laboratory Rat and Mouse:Review and Criteria for the Staging of the Estrous Cycle Using Stained Vaginal Smears. *Toxicol Pathol*. 2015;43(6):776-793.
20. Goldman JM, Murr AS, Cooper RL. The rodent estrous cycle: Characterization of vaginal cytology and its utility in toxicological studies. *Birth Defects Res B Dev Reprod Toxicol*. 2007;80(2):84-97.
21. Azziz R, Carmina E, Chen Z, et al. Polycystic ovary syndrome. *Nat Rev Dis Primers*. 2016;2.
22. Brettenthaler N, De Geyter C, Huber PR, Keller U. Effect of the insulin sensitizer pioglitazone on insulin resistance, hyperandrogenism, and ovulatory dysfunction in women with polycystic ovary syndrome. *Journal of Clinical Endocrinology and Metabolism*. 2004;89(8):3835-3840.
23. Dewailly D, Gronier H, Poncelet E, et al. Diagnosis of polycystic ovary syndrome (PCOS): Revisiting the threshold values of follicle count on ultrasound and of the serum AMH level for the definition of polycystic ovaries. *Human Reproduction*. 2011;26(11):3123-3129.
24. Mémoires pour servir à l'étude des maladies des ovaires : premier mémoire contenant : 1Les considérations anatomiques et physiologiques : 2L'agénésie et les vices de conformation des ovaires : 3L'inflammation aigue des ovaires (ovarite aigue) / par Achille Chereau. | Wellcome Collection. https://wellcomecollection.org/works/rdbh532x. Accessed January 4, 2024.
25. Stein IF, Leventhal ML. Amenorrhea associated with bilateral polycystic ovaries. *Am J Obstet Gynecol*. 1935;29(2):181-191.
26. Fauser BCJM, Tarlatzis, Fauser, et al. Revised 2003 consensus on diagnostic criteria and long-term health risks related to polycystic ovary syndrome (PCOS). *Hum Reprod*. 2004;19(1):41-47.

27. Lakhani K, Prelevic GM, Seifalian AM, Atiomo WU, Hardiman P. Polycystic ovary syndrome, diabetes and cardiovascular disease: risks and risk factors. *J Obstet Gynaecol*. 2004;24(6):613-621.
28. Dunaif A. Insulin resistance and the polycystic ovary syndrome: mechanism and implications for pathogenesis. *Endocr Rev*. 1997;18(6):774-800.
29. Blank SK, McCartney CR, Marshall JC. The origins and sequelae of abnormal neuroendocrine function in polycystic ovary syndrome. *Hum Reprod Update*. 2006;12(4):351-361.
30. Chang RJ, Cook-Andersen H. Disordered follicle development. *Mol Cell Endocrinol*. 2013;373(1-2):51-60.
31. Webber LJ, Stubbs S, Stark J, et al. Formation and early development of follicles in the polycystic ovary. *Lancet*. 2003;362(9389):1017-1021.
32. Teixeira Filho FL, Baracat EC, Lee TH, et al. Aberrant Expression of Growth Differentiation Factor-9 in Oocytes of Women with Polycystic Ovary Syndrome. *J Clin Endocrinol Metab*. 2002;87(3):1337-1344.
33. Weenen C, Laven JSE, von Bergh ARM, et al. Anti-Müllerian hormone expression pattern in the human ovary: potential implications for initial and cyclic follicle recruitment. *Mol Hum Reprod*. 2004;10(2):77-83.
34. Bhide P, Dilgil M, Gudi A, Shah A, Akwaa C, Homburg R. Each small antral follicle in ovaries of women with polycystic ovary syndrome produces more antimüllerian hormone than its counterpart in a normal ovary: an observational cross-sectional study. *Fertil Steril*. 2015;103(2):537-541.
35. Stubbs SA, Hardy K, Da Silva-Buttkus P, et al. Anti-müllerian hormone protein expression is reduced during the initial stages of follicle development in human polycystic ovaries. *J Clin Endocrinol Metab*. 2005;90(10):5536-5543.
36. Das M, Gillott DJ, Saridogan E, Djahanbakhch O. Anti-Mullerian hormone is increased in follicular fluid from unstimulated ovaries in women with polycystic ovary syndrome. *Hum Reprod*. 2008;23(9):2122-2126.
37. Pellatt L, Rice S, Dilaver N, et al. Anti-Müllerian hormone reduces follicle sensitivity to follicle-stimulating hormone in human granulosa cells. *Fertil Steril*. 2011;96(5).
38. Mason HD, Willis DS, Beard RW, Winston RM, Margara R, Franks S. Estradiol production by granulosa cells of normal and polycystic ovaries: relationship to

menstrual cycle history and concentrations of gonadotropins and sex steroids in follicular fluid. *J Clin Endocrinol Metab*. 1994;79(5):1355-1360.

39. Adashi EY, Hsueh AJW. Estrogens augment the stimulation of ovarian aromatase activity by follicle-stimulating hormone in cultured rat granulosa cells. *Journal of Biological Chemistry*. 1982;257(11):6077-6083.
40. Franks S, White D, Gilling-Smith C, Carey A, Waterworth D, Williamson R. Hypersecretion of androgens by polycystic ovaries: the role of genetic factors in the regulation of cytochrome P450c17 alpha. *Baillieres Clin Endocrinol Metab*. 1996;10(2):193-203.
41. Nelson VL, Legro RS, Strauss JF, McAllister JM. Augmented androgen production is a stable steroidogenic phenotype of propagated theca cells from polycystic ovaries. *Mol Endocrinol*. 1999;13(6):946-957.
42. Baillargeon JP, Carpentier A. Role of insulin in the hyperandrogenemia of lean women with polycystic ovary syndrome and normal insulin sensitivity. *Fertil Steril*. 2007;88(4):886-893.
43. Li H, Chen Y, Yan LY, Qiao J. Increased expression of P450scc and CYP17 in development of endogenous hyperandrogenism in a rat model of PCOS. *Endocrine*. 2013;43(1):184-190.
44. Wachs DS, Coffler MS, Malcom PJ, Chang RJ. Comparison of follicle-stimulating-hormone-stimulated dimeric inhibin and estradiol responses as indicators of granulosa cell function in polycystic ovary syndrome and normal women. *J Clin Endocrinol Metab*. 2006;91(8):2920-2925.
45. Dumont A, Robin G, Catteau-Jonard S, Dewailly D. Role of Anti-Müllerian Hormone in pathophysiology, diagnosis and treatment of Polycystic Ovary Syndrome: a review. *Reprod Biol Endocrinol*. 2015;13(1).
46. Wei LN, Huang R, Li LL, Fang C, Li Y, Liang XY. Reduced and delayed expression of GDF9 and BMP15 in ovarian tissues from women with polycystic ovary syndrome. *J Assist Reprod Genet*. 2014;31(11):1483-1490.
47. Balen AH, Conway G, Homburg R, Legro R, eds. Polycystic Ovary Syndrome : A Guide to Clinical Management. April 2005.
48. Artini PG, Monteleone P, Toldin MRP, et al. Growth factors and folliculogenesis in polycystic ovary patients. *Expert Rev Endocrinol Metab*. 2007;2(2):215-223.
49. Abd El Aal DEM, Mohamed SA, Amine AF, Meki ARMA. Vascular endothelial growth factor and insulin-like growth factor-1 in polycystic ovary syndrome and

their relation to ovarian blood flow. *European Journal of Obstetrics and Gynecology and Reproductive Biology*. 2005;118(2):219-224.

50. Peitsidis P, Agrawal R. Role of vascular endothelial growth factor in women with PCO and PCOS: A systematic review. *Reprod Biomed Online*. 2010;20(4):444-452.
51. Balen AH, Conway G, Homburg R, Legro R, eds. Polycystic Ovary Syndrome : A Guide to Clinical Management. April 2005.
52. Roland A V., Moenter SM. Prenatal androgenization of female mice programs an increase in firing activity of gonadotropin-releasing hormone (GnRH) neurons that is reversed by metformin treatment in adulthood. *Endocrinology*. 2011;152(2):618-628.
53. Soules MR, Steiner RA, Clifton DK, Cohen NL, Aksel S, Bremner WJ. Progesterone Modulation of Pulsatile Luteinizing Hormone Secretion in Normal Women*. *Journal of Clinical Endocrinology and Metabolism.* 1984;58:2.
54. Apterf D, Biitzow T, Laughlin GA, Yens SSC. Accelerated 24-Hour Luteinizing Hormone Pulsatile Activity in Adolescent Girls with Ovarian Hyperandrogenism: Relevance to the Developmental Phase of Polycystic Ovarian Syndrome*. *Journal of Clinical Endocrinology and Metabolism.* 1994;79:1.
55. Witchel SF, Tena-Sempere M. The Kiss1 system and polycystic ovary syndrome: Lessons from physiology and putative pathophysiologic implications. *Fertil Steril*. 2013;100(1):12-22.
56. van Houten ELAF, Visser JA. Mouse models to study polycystic ovary syndrome: a possible link between metabolism and ovarian function? *Reprod Biol*. 2014;14(1):32-43.
57. Shi D, Vine DF. Animal models of polycystic ovary syndrome: a focused review of rodent models in relationship to clinical phenotypes and cardiometabolic risk. *Fertil Steril*. 2012;98(1):185-193.
58. Edwards DA. Neonatal administration of androstenedione, testosterone or testosterone propionate: Effects on ovulation, sexual receptivity and aggressive behavior in female mice. *Physiol Behav*. 1971;6(3):223-228.
59. Loughlin T, Cunningham S, Moore A, Culliton M, Smyth PPA, Mc Kenna TJ. Adrenal abnormalities in polycystic ovary syndrome. *J Clin Endocrinol Metab*. 1986;62(1):142-147.

60. Abbott DH, Tarantal AF, Dumesic DA. Fetal, infant, adolescent and adult phenotypes of polycystic ovary syndrome in prenatally androgenized female rhesus monkeys. *Am J Primatol*. 2009;71(9):776.
61. Birch RA, Padmanabhan V, Foster DL, Unsworth WP, Robinson JE. Prenatal programming of reproductive neuroendocrine function: fetal androgen exposure produces progressive disruption of reproductive cycles in sheep. *Endocrinology*. 2003;144(4):1426-1434.
62. Unsworth WP, Taylor JA, Robinson JE. Prenatal Programming of Reproductive Neuroendocrine Function: The Effect of Prenatal Androgens on the Development of Estrogen Positive Feedback and Ovarian Cycles in the Ewe. *Biol Reprod*. 2005;72(3):619-627.
63. Elia E, Sander V, Luchetti CG, et al. The mechanisms involved in the action of metformin in regulating ovarian function in hyperandrogenized mice. *Mol Hum Reprod*. 2006;12(8):475-481.
64. Solano ME, Sander VA, Ho H, Motta AB, Arck PC. Systemic inflammation, cellular influx and up-regulation of ovarian VCAM-1 expression in a mouse model of polycystic ovary syndrome (PCOS). *J Reprod Immunol*. 2011;92(1-2):33-44.
65. Abe K, Kimura H. *The Possible Role of Hydrogen Sulfide as an Endogenous Neuromodulator*. 1996;76.
66. Cao X, Ding L, Xie ZZ, et al. A Review of Hydrogen Sulfide Synthesis, Metabolism, and Measurement: Is Modulation of Hydrogen Sulfide a Novel Therapeutic for Cancer? *Antioxid Redox Signal*. 2019;31(1):1.
67. Cirino G, Szabo C, Papapetropoulos A. Physiological roles of hydrogen sulfide in mammalian cells, tissues, and organs. *Physiol Rev*. 2023;103(1):31-276.
68. Kamoun P. Endogenous production of hydrogen sulfide in mammals. *Amino Acids*. 2004;26(3):243-254.
69. Li L, Moore PK. Putative biological roles of hydrogen sulfide in health and disease: a breath of not so fresh air? *Trends Pharmacol Sci*. 2008;29(2):84-90.
70. Kawabata A, Ishiki T, Nagasawa K, et al. Hydrogen sulfide as a novel nociceptive messenger. *Pain*. 2007;132(1-2):74-81.
71. Kimura H. Hydrogen sulfide induces cyclic AMP and modulates the NMDA receptor. *Biochem Biophys Res Commun*. 2000;267(1):129-133.

72. Yang G, Sun X, Wang R. Hydrogen sulfide-induced apoptosis of human aorta smooth muscle cells via the activation of mitogen-activated protein kinases and caspase-3. *The FASEB Journal*. 2004;18(14):1782-1784.
73. Zhao W, Wang R, Wang R. H 2 S-induced vasorelaxation and underlying cellular and molecular mechanisms. *Am J Physiol Heart Circ Physiol*. 2002;283:474-480.
74. Tang G, Wu L, Liang W, Wang R. Direct stimulation of KATP channels by exogenous and endogenous hydrogen sulfide in vascular smooth muscle cells. *Mol Pharmacol*. 2005;68(6):1757-1764.
75. Zhao W, Zhang J, Lu Y. et. al. The vasorelaxant effect of H_2S as a novel endogenous gaseous K_{ATP} channel opener. *The EMBO Journal*. 2001;20:21,6008-6016.
76. Yang G, Wu L, Jiang B, et al. H2S as a physiologic vasorelaxant: Hypertension in mice with deletion of cystathionine γ-lyase. *Science*. 2008;322(5901):587-590.
77. Kubo S, Doe I, Kurokawa Y, Kawabata A. Hydrogen sulfide causes relaxation in mouse bronchial smooth muscle. *J Pharmacol Sci*. 2007;104(4):392-396.
78. Castro-Piedras I, Perez-Zoghbi JF. Hydrogen sulphide inhibits Ca^{2+} release through InsP3 receptors and relaxes airway smooth muscle. *Journal of Physiology*. 2013;591(23):5999-6015.
79. D'emmanuele Di Villa Bianca R, Sorrentino R, Maffia P, et al. Hydrogen Sulfide as a Mediator of Human Corpus Cavernosum Smooth-Muscle Relaxation. *PNAS*. 2009,106:11.4513-4518.
80. Teague B, Asiedu S, Moore PK. The smooth muscle relaxant effect of hydrogen sulphide in vitro: Evidence for a physiological role to control intestinal contractility. *Br J Pharmacol*. 2002;137(2):139-145.
81. Srilatha B, Adaikan PG, Moore PK. Possible role for the novel gasotransmitter hydrogen sulphide in erectile dysfunction-A pilot study. *Eur J Pharmacol*. 2006;535(1-3):280-282.
82. Shukla N, Rossoni G, Hotston M, et al. Effect of hydrogen sulphide-donating sildenafil (ACS6) on erectile function and oxidative stress in rabbit isolated corpus cavernosum and in hypertensive rats. *BJU Int*. 2009;103(11):1522-1529.
83. Oi Y, Imafuku M, Shishido C, Kominato Y, Nishimura S, Iwai K. Garlic supplementation increases testicular testosterone and decreases plasma corticosterone in rats fed a high protein diet. *J Nutr*. 2001;131(8):2150-2156.

84. Azarbarz N, Shafiei Seifabadi Z, Moaiedi MZ, Mansouri E. Assessment of the effect of sodium hydrogen sulfide (hydrogen sulfide donor) on cisplatin-induced testicular toxicity in rats. *Environmental Science and Pollution Research*. 2020;27(8):8119-8128.
85. Wang J, Wang W, Li S, et al. Hydrogen Sulfide As a Potential Target in Preventing Spermatogenic Failure and Testicular Dysfunction. *Antioxid Redox Signal*. 2018;28(16):1447-1462.
86. Patel P, Vatish M, Heptinstall J, Wang R, Carson RJ. The endogenous production of hydrogen sulphide in intrauterine tissues. *Reproductive Biology and Endocrinology*. 2009;7.
87. Guzmán MA, Navarro MA, Carnicer R, et al. Cystathionine β-synthase is essential for female reproductive function. *Hum Mol Genet*. 2006;15(21):3168-3176.
88. G J M VanAerts LA, Poirot CM, Herberts CA, et al. Development of Methionine Synthase, Cystathionine-B-Synthase and S-Adenosyl-Homocysteine Hydrolase during Gestation in Rats. *Journal of Reproduction and Fertility.* 1995;103:227-232.
89. Hayden LJ, Goedent H, Roth SH. KeyWords: Growth, Development, Hydrogen Sulfide, Dystocia, Rat. *Toxicol Ind Health*. 1990;6(4):389-401.
90. Sidhu R, Singh M, Samir G, Carson RJ. L-Cysteine and Sodium Hydrosulphide Inhibit Spontaneous Contractility in Isolated Pregnant Rat Uterine Strips in vitro. *C Pharmacology & Toxicology*. 2001;88:198-203.
91. Pearson J R., Wilson R, Wang R. Endogenous hydrogen sulfide and the cardiovascular system-what's the smell all about? *Clin Invest Med*. 2006,29(3):146-50.
92. Srilatha B, Hu L, Adaikan GP, Moore PK. Initial characterization of hydrogen sulfide effects in female sexual function. *Journal of Sexual Medicine*. 2009;6(7):1875-1884.
93. Wray S, Kupittayanant S, Shmygol A, Smith R. D., Burdyga T. The physiological basis of uterine contractility: a short review. *Experimental Physiology.* 2001;86.2, 239–246.
94. Nevoral J, Žalmanová T, Zámostná K, et al. Endogenously produced hydrogen sulfide is involved in porcine oocyte maturation in vitro. *Nitric Oxide*. 2015;51:24-35.

95. Rong L, Wei-dong Y, Jun-bao D, Li-jun Y, Mei S, Jing-zhu G. Localization of Cystathionine-β Synthase in Mice Ovaries and Its Expression Profile during Follicular Development. *Chinese Medical Journal.* 2006;119(22):p1877-1883.
96. Liang R, Yu WD, Du JB, et al. Cystathionine β synthase participates in murine oocyte maturatione mediated by homocysteine. *Reproductive Toxicology*. 2007;24(1):89-96.
97. Liang R, Yu WD, Du JB, et al. Cystathionine β synthase participates in murine oocyte maturatione mediated by homocysteine. *Reproductive Toxicology*. 2007;24(1):89-96.
98. Ning N, Zhu J, Du Y, Gao X, Liu C, Li J. Dysregulation of hydrogen sulphide metabolism impairs oviductal transport of embryos. *Nat Commun*. 2014;5.
99. Estienne A, Portela VM, Choi Y, et al. The endogenous hydrogen sulfide generating system regulates ovulation. *Free Radic Biol Med*. 2019;138:43-52.
100. Brettenthaler N, De Geyter C, Huber PR, Keller U. Effect of the insulin sensitizer pioglitazone on insulin resistance, hyperandrogenism, and ovulatory dysfunction in women with polycystic ovary syndrome. *J Clin Endocrinol Metab*. 2004;89(8):3835-3840.
101. Azziz R, Carmina E, Chen Z, et al. Polycystic ovary syndrome. *Nat Rev Dis Primers*. 2016;2.
102. Motta AB. Dehydroepiandrosterone to induce murine models for the study of polycystic ovary syndrome. *Journal of Steroid Biochemistry and Molecular Biology*. 2010;119(3-5):105-111.
103. Dewailly D, Gronier H, Poncelet E, et al. Diagnosis of polycystic ovary syndrome (PCOS): Revisiting the threshold values of follicle count on ultrasound and of the serum AMH level for the definition of polycystic ovaries. *Human Reproduction*. 2011;26(11):3123-3129.
104. Walters KA, Allan CM, Handelsman DJ. Rodent models for human polycystic ovary syndrome. *Biol Reprod*. 2012;86(5).
105. Bakhshalizadeh S, Amidi F, Alleyassin A, Soleimani M, Shirazi R, Shabani Nashtaei M. Modulation of steroidogenesis by vitamin D3 in granulosa cells of the mouse model of polycystic ovarian syndrome. *Syst Biol Reprod Med*. 2017;63(3):150-161.

106. Myers M, Britt KL, Wreford NGM, Ebling FJP, Kerr JB. Methods for quantifying follicular numbers within the mouse ovary. *Reproduction*. 2004;127(5):569-580.
107. Furat Rencber S, Kurnaz Ozbek S, Eraldemlr C, et al. Effect of resveratrol and metformin on ovarian reserve and ultrastructure in PCOS: an experimental study. *J Ovarian Res*. 2018;11(1).
108. Güngör ND, Güngör K, Yurci A, Cil K, Hatırnaz Ş. Ovarian drilling down-regulates endometrial nuclear factor-κB p65 expression in women with PCOS: A prospective case-control study. *Turk J Obstet Gynecol*. 2022;19(1):45-50.
109. Maae E, Nielsen M, Steffensen KD, Jakobsen EH, Jakobsen A, Sørensen FB. Estimation of immunohistochemical expression of VEGF in ductal carcinomas of the breast. *Journal of Histochemistry and Cytochemistry*. 2011;59(8):750-760.
110. Stocco DM. *StAR* Proteın and the Regulatıon of Steroıd Hormone Bıosynthesıs. *Annual Review of Physiology*. 2001; 63:193-213.
111. Kim JY, Xue K, Cao M, et al. Chemerin suppresses ovarian follicular development and its potential involvement in follicular arrest in rats treated chronically with dihydrotestosterone. *Endocrinology*. 2013;154(8):2912-2923.
112. Lima PDA, Nivet AL, Wang Q, et al. Polycystic ovary syndrome: Possible involvement of androgen-induced, chemerin-mediated ovarian recruitment of monocytes/macrophages. *Biol Reprod*. 2018;99(4):838-852.
113. Wang Q, Kim JY, Xue K, Liu JY, Leader A, Tsang BK. Chemerin, a novel regulator of follicular steroidogenesis and its potential involvement in polycystic ovarian syndrome. *Endocrinology*. 2012;153(11):5600-5611.
114. McNeilly AS, Colin Duncan W. Rodent models of polycystic ovary syndrome. *Mol Cell Endocrinol*. 2013;373(1-2):2-7.
115. Henmi H, Endo T, Nagasawa K, et al. Lysyl Oxidase and MMP-2 Expression in Dehydroepiandrosterone-Induced Polycystic Ovary in Rats. *Bıology of Reproduction.* 2001;64,157–162.
116. Luchetti CG, Solano ME, Sander V, et al. Effects of dehydroepiandrosterone on ovarian cystogenesis and immune function. *J Reprod Immunol*. 2004;64(1-2):59-74.
117. Sander V, Luchetti CG, Solano ME, et al. Role of the N, N′-dimethylbiguanide metformin in the treatment of female prepuberal BALB/c mice

hyperandrogenized with dehydroepiandrosterone. *Reproduction*. 2006;131(3):591-602.

118. Azziz R, Carmina E, Dewailly D, et al. Position statement: Criteria for defining polycystic ovary syndrome as a predominantly hyperandrogenic syndrome: An androgen excess society guideline. *Journal of Clinical Endocrinology and Metabolism*. 2006;91(11):4237-4245.
119. Hirshfeld-Cytron J, Barnes RB, Ehrmann DA, Caruso A, Mortensen MM, Rosenfield RL. Characterization of Functionally Typical and Atypical Types of Polycystic Ovary Syndrome. *J Clin Endocrinol Metab*. 2009;94(5):1587.
120. Gilling-Smith C, Willis DS, Beard RW, Franks S. Hypersecretion of androstenedione by isolated thecal cells from polycystic ovaries. *J Clin Endocrinol Metab*. 1994;79(4):1158-1165.
121. Rebar R, Judd HL, Yen SSC, Rakoff J, Vandenberg G, Naftolin F. Characterization of the inappropriate gonadotropin secretion in polycystic ovary syndrome. *Journal of Clinical Investigation*. 1976;57(5):1320.
122. Ziegler D De, Steingold K, Cedars M, et al. Recovery of hormone secretion after chronic gonadotropin-releasing hormone agonist administration in women with polycystic ovarian disease. *J Clin Endocrinol Metab*. 1989;68(6):1111-1117.
123. Lee M -T, Anderson E, Lee GY. Changes in ovarian morphology and serum hormones in the rat after treatment with dehydroepiandrosterone. *Anat Rec*. 1991;231(2):185-192.
124. Wickenheisser JK, Quinn PG, Nelson VL, Legro RS, Strauss JF, McAllister. JM. Differential activity of the cytochrome P450 17alpha-hydroxylase and steroidogenic acute regulatory protein gene promoters in normal and polycystic ovary syndrome theca cells. *J Clin Endocrinol Metab*. 2000;85(6):2304-2311.
125. Fassnacht M, Schlenz N, Schneider SB, Wudy SA, Allolio B, Arlt W. Beyond adrenal and ovarian androgen generation: Increased peripheral 5 alpha-reductase activity in women with polycystic ovary syndrome. *J Clin Endocrinol Metab*. 2003;88(6):2760-2766.
126. Strauss JF. Some new thoughts on the pathophysiology and genetics of polycystic ovary syndrome. *Ann N Y Acad Sci*. 2003;997:42-48.
127. Eagleson CA, Gingrich MB, Pastor CL, et al. Polycystic ovarian syndrome: evidence that flutamide restores sensitivity of the gonadotropin-releasing

hormone pulse generator to inhibition by estradiol and progesterone. *J Clin Endocrinol Metab*. 2000;85(11):4047-4052.

128. Franks S, Gilling-Smith C, Watson H, Willis D. Insulin action in the normal and polycystic ovary. *Endocrinol Metab Clin North Am*. 1999;28(2):361-378.
129. Barbierit RL, Makris A, Randall RW, Daniels G, Kistner RW, Ryan KJ. Insulin stimulates androgen accumulation in incubations of ovarian stroma obtained from women with hyperandrogenism. *J Clin Endocrinol Metab*. 1986;62(5):904-910.
130. Bergh C, Carlsson B, Olsson JH, Selleskog U, Hillensjo T. Regulation of androgen production in cultured human thecal cells by insulin-like growth factor I and insulin. *Fertil Steril*. 1993;59(2):323-331.
131. Willis D, Mason H, Gilling-Smith C, Franks S . Modulation by insulin of follicle-stimulating hormone and luteinizing hormone actions in human granulosa cells of normal and polycystic ovaries. *J Clin Endocrinol Metab*. 1996;81(1):302-309.
132. Jakimiuk AJ, Weitsman SR, Navab A, Magoffin DA. Luteinizing hormone receptor, steroidogenesis acute regulatory protein, and steroidogenic enzyme messenger ribonucleic acids are overexpressed in thecal and granulosa cells from polycystic ovaries. *J Clin Endocrinol Metab*. 2001;86(3):1318-1323.
133. Willis DS, Watson H, Mason HD, Galea R, Brincat M, Franks S. Premature response to luteinizing hormone of granulosa cells from anovulatory women with polycystic ovary syndrome: relevance to mechanism of anovulation. *J Clin Endocrinol Metab*. 1998;83(11):3984-3991.
134. Kyei G, Sobhani A, Nekonam S, et al. Assessing the effect of MitoQ10 and Vitamin D3 on ovarian oxidative stress, steroidogenesis and histomorphology in DHEA induced PCOS mouse model. *Heliyon*. 2020;6(7).
135. Birch RA, Padmanabhan V, Foster DL, Unsworth WP, Robinson JE. Prenatal programming of reproductive neuroendocrine function: fetal androgen exposure produces progressive disruption of reproductive cycles in sheep. *Endocrinology*. 2003;144(4):1426-1434.
136. McNeilly AS, Colin Duncan W. Rodent models of polycystic ovary syndrome. *Mol Cell Endocrinol*. 2013;373(1-2):2-7.
137. Sander V, Solano ME, Elia E, et al. The influence of dehydroepiandrosterone on early pregnancy in mice. *Neuroimmunomodulation*. 2005;12(5):285-292.

138. Tessaro I, Modina SC, Franciosi F, et al. Effect of oral administration of low-dose follicle stimulating hormone on hyperandrogenized mice as a model of polycystic ovary syndrome. *J Ovarian Res*. 2015;8(1).
139. Eisner JR, Dumesic DA, Kemnitz JW, Abbott DH. Timing of prenatal androgen excess determines differential impairment in insulin secretion and action in adult female rhesus monkeys. *J Clin Endocrinol Metab*. 2000;85(3):1206-1210.
140. Familiari G, Toscano V, Motta PM. Morphological studies of polycystic mouse ovaries induced by dehydroepiandrosterone. *Cell Tissue Res*. 1985;240(3):519-528.
141. Sander V, Luchetti CG, Solano ME, et al. Role of the N, N'-dimethylbiguanide metformin in the treatment of female prepuberal BALB/c mice hyperandrogenized with dehydroepiandrosterone. *Reproduction*. 2006;131(3):591-602.
142. Jang M, Lee MJ, Lee JM, et al. Oriental medicine Kyung-Ok-Ko prevents and alleviates dehydroepiandrosterone-induced polycystic ovarian syndrome in rats. *PLoS One*. 2014;9(2).
143. Ghafurniyan H, Azarnia M, Nabiuni M, Karimzadeh L. The Effect of Green Tea Extract on Reproductive Improvement in Estradiol Valerate-Induced Polycystic Ovarian Syndrome in Rat. *Iranian Journal of Pharmaceutical Research*. 2015;14 (4):1215-1233.
144. Misugi T, Ozaki K, El Beltagy K, Tokuyama O, Honda KI, Ishiko O. Insulin-lowering agents inhibit synthesis of testosterone in ovaries of DHEA-induced PCOS rats. *Gynecol Obstet Invest*. 2006;61(4):208-215.
145. Gill A, Jamnongjit M, Hammes SR. Androgens promote maturation and signaling in mouse oocytes independent of transcription: a release of inhibition model for mammalian oocyte meiosis. *Mol Endocrinol*. 2004;18(1):97-104.
146. Jeelani H, Ganie MA, Masood A, et al. Assessment of PON1 activity and circulating TF levels in relation to BMI, testosterone, HOMA-IR, HDL-C, LDL-C, CHO, SOD activity and TAC in women with PCOS: An observational study. *Diabetes Metab Syndr*. 2019;13(5):2907-2915.
147. Sandhu JK, Waqar A, Jain A, et al. Oxidative Stress in Polycystic Ovarian Syndrome and the Effect of Antioxidant N-Acetylcysteine on Ovulation and Pregnancy Rate. *Cureus*. 2021;13(9).

148. González F, Rote NS, Minium J, Kirwan JP. Increased activation of nuclear factor kappaB triggers inflammation and insulin resistance in polycystic ovary syndrome. *J Clin Endocrinol Metab*. 2006;91(4):1508-1512.
149. González F. Inflammation in Polycystic Ovary Syndrome: underpinning of insulin resistance and ovarian dysfunction. *Steroids*. 2012;77(4):300-305.
150. Li L, Bhatia M, Moore PK. Hydrogen sulphide--a novel mediator of inflammation? *Curr Opin Pharmacol*. 2006;6(2):125-129.
151. Yusof M, Kamada K, Kalogeris T, Spencer Gaskin F, Korthuis RJ. Hydrogen sulfide triggers late-phase preconditioning in postischemic small intestine by an NO- and p38 MAPK-dependent mechanism. *Am J Physiol Heart Circ Physiol*. 2009;296(3):H868.
152. Guo R, Wu K, Chen J, et al. Exogenous hydrogen sulfide protects against doxorubicin-induced inflammation and cytotoxicity by inhibiting p38MAPK/NFκB pathway in H9c2 cardiac cells. *Cell Physiol Biochem*. 2013;32(6):1668-1680.
153. Ghafurniyan H, Azarnia M, Nabiuni M, et. al. The Effect of Green Tea Extract on Reproductive Improvement in Estradiol Valerate-Induced Polycystic Ovarian Syndrome in Rat. Iranian Journal of Pharmaceutical Research. 2015;14 (4):1215-1233.
154. De Felici M, Klinger FG. PI3K/PTEN/AKT Signaling Pathways in Germ Cell Development and Their Involvement in Germ Cell Tumors and Ovarian Dysfunctions. *Int J Mol Sci*. 2021;22(18):9838.
155. Zhang J, Liu W, Sun X, et al. Inhibition of mTOR Signaling Pathway Delays Follicle Formation in Mice. *J Cell Physiol*. 2017;232(3):585-595.
156. Chen X, Tang H, Liang Y, et al. Acupuncture regulates the autophagy of ovarian granulosa cells in polycystic ovarian syndrome ovulation disorder by inhibiting the PI3K/AKT/mTOR pathway through LncMEG3. *Biomedicine & Pharmacotherapy*. 2021;144:112288.
157. Guo Z, Yu Q. Role of mTOR Signaling in Female Reproduction. *Front Endocrinol (Lausanne)*. 2019;10:479357.
158. Cai Z, He S, Li T, Zhao L, Zhang K. Plumbagin inhibits proliferation and promotes apoptosis of ovarian granulosa cells in polycystic ovary syndrome by inactivating PI3K/Akt/mTOR pathway. *Anim Cells Syst (Seoul)*. 2020:197-204.

159. Restuccia DF, Hynx D, Hemmings BA. Loss of PKBβ/Akt2 predisposes mice to ovarian cyst formation and increases the severity of polycystic ovary formation in vivo. *DMM Disease Models and Mechanisms*. 2012;5(3):403-411.
160. Yu J, Yaba A, Kasiman C, Thomson T, Johnson J. Controls Ovarian Follicle Growth by Regulating Granulosa Cell Proliferation. *PLoS One*. 2011;6(7):21415.
161. Wu D, Zhong P, Wang Y, et al. Hydrogen Sulfide Attenuates High-Fat Diet-Induced Non-Alcoholic Fatty Liver Disease by Inhibiting Apoptosis and Promoting Autophagy via Reactive Oxygen Species/ Phosphatidylinositol 3-Kinase/AKT/ Mammalian Target of Rapamycin Signaling Pathway. *Frontiers in Pharmacology.* 2020;11:585860.
162. Xiao Q, Ying J, Qiao Z, et al. Exogenous hydrogen sulfide inhibits human melanoma cell development via suppression of the PI3K/AKT/ mTOR pathway. *J Dermatol Sci*. 2020;98(1):26-34.
163. Wang SS, Chen YH, Chen N, et al. Hydrogen sulfide promotes autophagy of hepatocellular carcinoma cells through the PI3K/Akt/mTOR signaling pathway. *Cell Death Dis*. 2017;8(3).
164. Xu K, Wu F, Xu K, et al. NaHS restores mitochondrial function and inhibits autophagy by activating the PI3K/Akt/mTOR signalling pathway to improve functional recovery after traumatic brain injury. *Chem Biol Interact*. 2018;286:96-105.
165. Xu X, Li H, Gong Y, Zheng H, Zhao D. Hydrogen sulfide ameliorated lipopolysaccharide-induced acute lung injury by inhibiting autophagy through PI3K/Akt/mTOR pathway in mice. *Biochem Biophys Res Commun*. 2018;507(1-4):514-518.
166. NIE L, LIU M, CHEN J, et al. Hydrogen sulfide ameliorates doxorubicin-induced myocardial fibrosis in rats via the PI3K/AKT/mTOR pathway. *Mol Med Rep*. 2021;23(4).
167. Yi S, Zheng B, Zhu Y, Cai Y, Sun H, Zhou J. Melatonin ameliorates excessive PINK1/Parkin-mediated mitophagy by enhancing SIRT1 expression in granulosa cells of PCOS. *Am J Physiol Endocrinol Metab*. 2020;319(1):E91-E101.
168. Zheng Q, Li Y, Zhang D, et al. Anp promotes proliferation and inhibits apoptosis of ovarian granulosa cells by NPRA/PGRMC1/EGFR complex and improves ovary functions of pcos rats. *Cell Death Dis*. 2017;8(10).

169. Pan JX, Liu Y, Ke ZH, et al. Successive and cyclic oral contraceptive pill pretreatment improves IVF/ICSI outcomes of PCOS patients and ameliorates hyperandrogenism and antral follicle excess. *Gynecol Endocrinol*. 2015;31(4):332-336.
170. Shen H, Wang Y. Activation of TGF-β1/Smad3 signaling pathway inhibits the development of ovarian follicle in polycystic ovary syndrome by promoting apoptosis of granulosa cells. *J Cell Physiol*. 2019;234(7):11976-11985.
171. Anderson E, Lee GY. The polycystic ovarian (PCO) condition: apoptosis and epithelialization of the ovarian antral follicles are aspects of cystogenesis in the dehydroepiandrosterone (DHEA)-treated rat model. *Tissue Cell*. 1997;29(2):171-189.
172. Honnma H, Endo T, Henmi H, et al. Altered expression of Fas/Fas ligand/caspase 8 and membrane type 1-matrix metalloproteinase in atretic follicles within dehydroepiandrosterone-induced polycystic ovaries in rats. *Apoptosis*. 2006;11(9):1525-1533.
173. Yang G, Zhao K, Ju Y, et al. Hydrogen sulfide protects against cellular senescence via S-sulfhydration of Keap1 and activation of Nrf2. *Antioxid Redox Signal*. 2013;18(15):1906-1919.
174. Zhao K, Ju Y, Li S, Altaany Z, Wang R, Yang G. S-sulfhydration of MEK1 leads to PARP-1 activation and DNA damage repair. *EMBO Rep*. 2014;15(7):792-800.
175. Hellmich MR, Coletta C, Chao C, Szabo C. The therapeutic potential of cystathionine β-synthetase/hydrogen sulfide inhibition in cancer. *Antioxid Redox Signal*. 2015;22(5):424-448.
176. Hellmich MR, Szabo C. Hydrogen Sulfide and Cancer. *Handb Exp Pharmacol*. 2015;230:233-241.
177. Tay AS, Hu LF, Lu M, Wong PTH, Bian JS. Hydrogen sulfide protects neurons against hypoxic injury via stimulation of ATP-sensitive potassium channel/protein kinase C/extracellular signal-regulated kinase/heat shock protein 90 pathway. *Neuroscience*. 2010;167(2):277-286.
178. Yin J, Tu C, Zhao J, et al. Exogenous hydrogen sulfide protects against global cerebral ischemia/reperfusion injury via its anti-oxidative, anti-inflammatory and anti-apoptotic effects in rats. *Brain Res*. 2013;1491:188-196.

179. Zhang LM, Jiang CX, Liu DW. Hydrogen sulfide attenuates neuronal injury induced by vascular dementia via inhibiting apoptosis in rats. *Neurochem Res*. 2009;34(11):1984-1992.
180. Shi S, Li Q song, Li H, et al. Anti-apoptotic action of hydrogen sulfide is associated with early JNK inhibition. *Cell Biol Int*. 2009;33(10):1095-1101.
181. Li Y, Chandra TP, Song X, et al. H2S improves doxorubicin-induced myocardial fibrosis by inhibiting oxidative stress and apoptosis via Keap1-Nrf2. *Technol Health Care*. 2021;29(S1):S195-S209.
182. Diamanti-Kandarakis E. Polycystic ovarian syndrome: pathophysiology, molecular aspects and clinical implications. *Expert Rev Mol Med*. 2008;10(3):1-21.
183. Catteau-Jonard S, Dewailly D. Pathophysiology of polycystic ovary syndrome: the role of hyperandrogenism. *Front Horm Res*. 2013;40:22-27.
184. Mason HD, Willis DS, Beard RW, Winston RM, Margara R, Franks S. Estradiol production by granulosa cells of normal and polycystic ovaries: relationship to menstrual cycle history and concentrations of gonadotropins and sex steroids in follicular fluid. *J Clin Endocrinol Metab*. 1994;79(5):1355-1360.
185. Minegishi T, Tsuchiya M, Hirakawa T, et al. Expression of steroidogenic acute regulatory protein (StAR) in rat granulosa cells. *Life Sci*. 2000;67(9):1015-1024.
186. Miller WL. Steroidogenic acute regulatory protein (StAR), a novel mitochondrial cholesterol transporter. *Biochim Biophys Acta*. 2007;1771(6):663-676.
187. Taira H, Beck MM. Activity of three-beta-hydroxysteroid dehydrogenase in granulosa cells treated in vitro with luteinizing hormone, follicle-stimulating hormone, prolactin, or a combination. *Poult Sci*. 2006;85(10):1769-1774.
188. Rasmussen MK, Ekstr B, Zamaratskaia G. Regulation of 3β-hydroxysteroid dehydrogenase/Δ5-Δ4 isomerase: A review. *Int J Mol Sci*. 2013;14(9):17926-17942.
189. Motta AB. Dehydroepiandrosterone to induce murine models for the study of polycystic ovary syndrome. *J Steroid Biochem Mol Biol*. 2010;119(3-5):105-111.
190. La Marca A, Morgante G, Palumbo M, Cianci A, Petraglia F, De Leo V. Insulin-lowering treatment reduces aromatase activity in response to follicle-stimulating hormone in women with polycystic ovary syndrome. *Fertil Steril*. 2002;78(6):1234-1239.

191. Rodrigues JK, Navarro PA, Zelinski MB, Stouffer RL, Xu J. Direct actions of androgens on the survival, growth and secretion of steroids and anti-Müllerian hormone by individual macaque follicles during three-dimensional culture. *Hum Reprod*. 2015;30(3):664-674.
192. Sander V, Luchetti CG, Solano ME, et al. Role of the N, N'-dimethylbiguanide metformin in the treatment of female prepuberal BALB/c mice hyperandrogenized with dehydroepiandrosterone. *Reproduction*. 2006;131(3):591-602.
193. Luchetti CG, Solano ME, Sander V, et al. Effects of dehydroepiandrosterone on ovarian cystogenesis and immune function. *J Reprod Immunol*. 2004;64(1-2):59-74.
194. Huang Y, Gao JM, Zhang CM, et al. Assessment of growth and metabolism characteristics in offspring of dehydroepiandrosterone-induced polycystic ovary syndrome adults. *Reproduction*. 2016;152(6):705.
195. Bakhshalizadeh S, Amidi F, Alleyassin A, Soleimani M, Shirazi R, Shabani Nashtaei M. Modulation of steroidogenesis by vitamin D3 in granulosa cells of the mouse model of polycystic ovarian syndrome. *Syst Biol Reprod Med*. 2017;63(3):150-161.
196. Wu YG, Bennett J, Talla D, Stocco C. Testosterone, not 5α-dihydrotestosterone, stimulates LRH-1 leading to FSH-independent expression of Cyp19 and P450scc in granulosa cells. *Mol Endocrinol*. 2011;25(4):656-668.
197. Hatler TB, Hayes SH, Laranja da Fonseca LF, Silvia WJ. Relationship between endogenous progesterone and follicular dynamics in lactating dairy cows with ovarian follicular cysts. *Biol Reprod*. 2003;69(1):218-223.
198. Teshome E, Kebede A, Abdela N, Ahmed WM. Ovarian Cyst and its Economic Impact in Dairy Farms: A Review. *Glob Vet*. 2016;16(5):461-471.
199. Wu L Ming, Wang Y xue, Zhan Y, et al. Dulaglutide, a long-acting GLP-1 receptor agonist, can improve hyperandrogenemia and ovarian function in DHEA-induced PCOS rats. *Peptides (NY)*. 2021;145.
200. Yang W, Yang G, Jia X, Wu L, Wang R. Activation of KATP channels by H2S in rat insulin-secreting cells and the underlying mechanisms. *J Physiol*. 2005;569(Pt 2):519-531.

201. Kaneko Y, Kimura T, Taniguchi S, et al. Glucose-induced production of hydrogen sulfide may protect the pancreatic beta-cells from apoptotic cell death by high glucose. *FEBS Lett*. 2009;583(2):377-382.
202. Tang G, Zhang L, Yang G, Wu L, Wang R. Hydrogen sulfide-induced inhibition of L-type Ca2+ channels and insulin secretion in mouse pancreatic beta cells. *Diabetologia*. 2013;56(3):533-541.
203. Liang R, Yu WD, Du JB, et al. Cystathionine β synthase participates in murine oocyte maturatione mediated by homocysteine. *Reproductive Toxicology*. 2007;24(1):89-96.
204. Li D, Liu HX, Fang YY, et al. Hyperhomocysteinemia in polycystic ovary syndrome: decreased betaine-homocysteine methyltransferase and cystathionine β-synthase-mediated homocysteine metabolism. *Reprod Biomed Online*. 2018;37(2):234-241.
205. Bries AE, Webb JL, Vogel B, et al. Letrozole-Induced Polycystic Ovary Syndrome Attenuates Cystathionine-β Synthase mRNA and Protein Abundance in the Ovaries of Female Sprague Dawley Rats. *Journal of Nutrition*. 2021;151(6):1407-1415.

6. APPENDICES

6.1. EHICAL APPROVAL

T.C.
YEDİTEPE ÜNİVERSİTESİ
Hayvan Deneyleri Yerel Etik Kurulu (HADYEK)

ETİK KURUL KARARI

Protokol No	Toplantı Tarihi	Toplantı Sayısı	Karar No	Proje Yürütücüsü
2022-017	28.04.2022	2022/04	2022/04-2	Dr. Öğr. Üyesi Alev Cumbul Aysun Özbay Önal
"Dehidroepiandrosteron ile İndüklenen Polikistik Over Sendromu Sıçan Modelinde Hidrojen Sülfit'in Steroidogenez ve Histomorfoloji Üzerine Etkisinin Histolojik ve Biyokimyasal Yöntemler ile Araştırılması" isimli proje oy birliğiyle etik açıdan uygun görülmüştür.				

Hayvan Türü / Irkı	Toplam Hayvan Sayısı	Hayvanın Cinsiyeti
Sıçan / Spraque Dawley	30	Dişi

Görevi	Adı Soyadı	Katılım Durumu
Başkan	Prof. Dr. Bayram YILMAZ	
Başkan Vekili	Prof. Dr. Erdem YEŞİLADA	
Üye	Dr. Engin SÜMER	
Üye	Prof. Dr. M. Ece GENÇ	
Üye	Prof. Dr. Rukset ATTAR	
Üye	Prof. Dr. Gamze TORUN KÖSE	
Üye	Prof. Dr. Özlem MALKONDU	
Üye	Doç. Dr. Aylin YABA UÇAR	
Üye	Doç. Dr. Burcu GEMİCİ BAŞOL	
Üye	Atakan Mücahit YAVUZ	
Üye	Ahmet ŞENKARDEŞLER	

6.2. CIRRICULUM VITAE

Name	AYSUN	**Surname**	ÖZBAY ÖNAL

Personal Information

Education

Degree	Department	The name of the Institution Graduated from	Graduation Year
Master	Institute of Health Science/	Reproductive Biology and Clinical Embryology	2017
University	Faculty of Science and Letters/Biology	Bursa Uludag University	2015
High School	Science Branch	Füsun Yönder Anatolian High School	2011

#All the grades must be listed if there is more than one (KPDS, ÜDS, TOEFL, EELTS vs)

Languages	**Grades (#)**
English (YOKDİL)	

Work Experience (Sort from present to past)

Position	Institute	**Duration (Year - Year)**
Research Assistant-Department of Histology and Embryology	Istanbul Aydin University, Faculty of Medicine	2019-

Computer Skills

Program	**Level**
Microsoft Office (Word, Excel, Powerpoint)	Good
GraphPad Prism	Good

****Excellent, good, average or basic**

Scientific works

The article publishes in the journals indexed by SCI, SSCI, AHCI

Berrin Avci, Isil Kasapoglu, Cihan Cakir, **Aysun Ozbay**, Baris Ata & Gurkan Uncu (2020): Fertilisation and early embryonic development of immature and rescue in vitro- matured sibling oocytes, Human Fertility,

Articles published in other journals

Aysun ÖZBAY, Berrin AVCI. Doksorubisin ile İndüklenmiş Ovaryan Toksisitede Visnaginin Koruyucu Etkisi. Uludağ Üniversitesi Tıp Fakültesi Dergisi 44 (3) 143-151, 2018
Esra ŞEN, Seda SARIBAL SAYGI, **Aysun ÖNAL,** Ayşe AKBAŞ, Berrin AVCI, Zeynep KAHVECİ. Sıçan Ovaryum Dokusunda Doksorubisin ile İndüklenmiş Folliküler Apoptotik Aktivasyonda Dialil Disülfit'in Koruyucu Etkisi. Uludağ Üniversitesi Tıp Fakültesi Dergisi 46 (1) 1-8, 2020.

Proceedings presented in international scientific meetings and published in proceedings book.

Aysun Ozbay and Berrin Avci. Protective effect of visnagin on doxorubicin-induced follicular apoptotic activation in ovarian tissue of rat. Poster presentation. 34th Annual Meeting of ESHRE. Barcelona, Spain. 1 to 4 July 2018.

Journals in the proceedings book of the refereed conference / symposium

Esra Şen, Işıl Kasapoğlu, **Aysun Özbay**, İlknur Yavaş, Gürkan Uncu, Berrin Avcı. Dentrimental Effects of Endometriosis on Embryo Development in ICSI Cycles; A Retrospective Cohort Study. Poster Bildirimi. Klinik Embriyoloji Derneği, 4. Klinik Embriyoloji Derneği Kongresi, Bodrum 2017.
Esra Şen, Işıl Kasapoğlu, **Aysun Özbay**, İlknur Yavaş, Gürkan Uncu, Berrin Avcı. Dentrimental Effects of Endometriosis on Embryo Development in ICSI Cycles; A Retrospective Cohort Study. Oral presentation. Turkish Society of Reproductive Medicine Izmir Symposium, 2017.
Aysun Özbay, Berrin Avcı. Sıçan Ovaryum Dokusunda Doksorubisin ile İndüklenmiş Folliküler Apoptotik Aktivasyonda Visnaginin Koruyucu Etkisi. Poster Bildirimi. 7. Jinekolojik Endoskopi Sempozyum ve Çalıştayı/ 2. Üreme Endokrinolojisi ve İnfertilite Akademisi, Uludağ 2018.
Aysun Özbay, Berrin Avcı. Sıçan Ovaryum Dokusunda Doksorubisin ile İndüklenmiş Folliküler Apoptotik Aktivasyonda Visnaginin Koruyucu Etkisi. Sözlü Bildiri. 14. Ulusal Histoloji ve Embriyoloji Kongresi, Antalya 2018.
Cansu Cebiroğlu, **Aysun Özbay,** Berrin Avcı, Hakan Ozan. Sıçan Endometriozis Modelinde Antioksidan Tedavinin Endometriotik Ocak Hacmi ve DNA Hasarı Üzerine Etkisi. Poster Bildirimi. Üreme Sağlığı ve İnfertilite Kongresi, Antalya 2018.

Others (Projects / Certificates / Rewards)

Dehidroepiandrosteron ile İndüklenen Polikistik Over Sendromu Sıçan Modelinde Hidrojen Sülfit'in Steroidogenez ve Histomorfoloji Üzerine Etkisinin Histolojik ve Biyokimyasal Yöntemler ile Araştırılması, **TÜBİTAK** #222S748, Proje Yürütücüsü.
Deney Hayvanları Kullanım Kursu- Uludağ Üniversitesi/BURSA, 2016.
Frontiers in Reproduction and Stem Cells- Koç Üniversitesi Tıp Fakültesi/İSTANBUL, 11-17 Kasım, 2018.
Kanser ve Kök Hücre Konusunda Temel Bilgiler, Yenilikçi Yaklaşımlar- Maltepe Üniversitesi/İSTANBUL. 1-5 Nisan, 2019.
Bilimsel Araştırmanın Planlanması ve Proje Yazma Online Eğitimi-Ankara Yıldırım Beyazıt Üniversitesi. 7 Mart, 2021.
Yaşam Bilimlerinde Bilimsel Araştırma Makalesi Yazma Eğitimi -ACT Biyoteknoloji&Danışmanlık. 15-16 Aralık, 2022.
DNA ve RNA Analiz Yöntemleri Eğitimi- ACT Biyoteknoloji&Danışmanlık, 7 Ocak 2023.
Hücre ve Doku Analiz Yöntemleri Eğitimi- ACT Biyoteknoloji&Danışmanlık, 25 Kasım 2023.